

Development of a Probabilistic Dynamic Synthesis Method for the Analysis of Nondeterministic Structures

A.M. Brown

Marshall Space Flight Center, Marshall Space Flight Center, Alabama

The NASA STI Program Office...in Profile

Since its founding, NASA has been dedicated to the advancement of aeronautics and space science. The NASA Scientific and Technical Information (STI) Program Office plays a key part in helping NASA maintain this important role.

The NASA STI Program Office is operated by Langley Research Center, the lead center for NASA's scientific and technical information. The NASA STI Program Office provides access to the NASA STI Database, the largest collection of aeronautical and space science STI in the world. The Program Office is also NASA's institutional mechanism for disseminating the results of its research and development activities. These results are published by NASA in the NASA STI Report Series, which includes the following report types:

- **TECHNICAL PUBLICATION.** Reports of completed research or a major significant phase of research that present the results of NASA programs and include extensive data or theoretical analysis. Includes compilations of significant scientific and technical data and information deemed to be of continuing reference value. NASA's counterpart of peer-reviewed formal professional papers but has less stringent limitations on manuscript length and extent of graphic presentations.
- **TECHNICAL MEMORANDUM.** Scientific and technical findings that are preliminary or of specialized interest, e.g., quick release reports, working papers, and bibliographies that contain minimal annotation. Does not contain extensive analysis.
- **CONTRACTOR REPORT.** Scientific and technical findings by NASA-sponsored contractors and grantees.

- **CONFERENCE PUBLICATION.** Collected papers from scientific and technical conferences, symposia, seminars, or other meetings sponsored or cosponsored by NASA.
- **SPECIAL PUBLICATION.** Scientific, technical, or historical information from NASA programs, projects, and mission, often concerned with subjects having substantial public interest.
- **TECHNICAL TRANSLATION.** English-language translations of foreign scientific and technical material pertinent to NASA's mission.

Specialized services that complement the STI Program Office's diverse offerings include creating custom thesauri, building customized databases, organizing and publishing research results...even providing videos.

For more information about the NASA STI Program Office, see the following:

- Access the NASA STI Program Home Page at <http://www.sti.nasa.gov>
- E-mail your question via the Internet to help@sti.nasa.gov
- Fax your question to the NASA Access Help Desk at (301) 621-0134
- Telephone the NASA Access Help Desk at (301) 621-0390
- Write to:
NASA Access Help Desk
NASA Center for AeroSpace Information
800 Elkridge Landing Road
Linthicum Heights, MD 21090-2934



Development of a Probabilistic Dynamic Synthesis Method for the Analysis of Nondeterministic Structures

A.M. Brown

Marshall Space Flight Center, Marshall Space Flight Center, Alabama

National Aeronautics and
Space Administration

Marshall Space Flight Center

Acknowledgments

I would like to thank NASA/Marshall Space Flight Center for their support of this research and my doctorate education. I would particularly like to thank my managers Larry Kiefling, Wayne Holland, Jim McBride, and Joe Brunty for their patience with this long project, and my colleagues John Admire, Jeff Peck, John Townsend, Dave McGhee, and Mike Tinker for the tremendous amount of assistance they gave me with aspects of the research.

I also thank my advisor, Dr. Aldo Ferri, for his patience and many helpful comments throughout the research and for his extensive review of the dissertation. The helpful and insightful comments of the reading committee are also appreciated.

Finally, I would like to thank my wife, Maria, for helping me persevere during the less encouraging moments of this project.

Available from:

NASA Center for AeroSpace Information
800 Elkridge Landing Road
Linthicum Heights, MD 21090-2934
(301) 621-0390

National Technical Information Service
5285 Port Royal Road
Springfield, VA 22161
(703) 487-4650

TABLE OF CONTENTS

1. INTRODUCTION	1
1.1 Motivation	1
1.2 Scope of Dissertation	3
2. THEORETICAL BACKGROUND AND LITERATURE SURVEY—COMPONENT MODE SYNTHESIS.	4
3. THEORETICAL BACKGROUND AND LITERATURE SURVEY—PROBABILISTIC ANALYSIS OF ENGINEERING QUANTITIES	13
3.1 Exact Methods	13
3.2 Approximate Methods—Monte Carlo	15
3.3 Approximate Methods—Reliability	16
3.4 Comparison of Reliability Methods	27
3.5 Approximate Methods—Perturbation	32
3.6 Comparison of Probabilistic Methods	36
4. DEVELOPMENT OF PROBABILISTIC DYNAMIC SYNTHESIS THEORY AND SIMPLE TEST CASE	39
4.1 Development of Probabilistic Dynamic Synthesis Methodology	39
4.2 Test Case	42
4.3 Additional Studies of Seven Mass/Spring Problem	48
5. FREE-AND FORCED-RESPONSE ANALYSIS OF REALISTIC SYSTEM	55
5.1 Problem Definition	55
5.2 System Description	56
5.3 Monte Carlo Analysis	58
5.4 PDS Methodology—Simulation of Statistics from Modal Test	59
5.5 Use of Dynamic Random Variables for PDS	63
5.6 Forced Response—Deterministic Case	69
5.7 Forced Response—Probabilistic Case Using PDS	73

TABLE OF CONTENTS (Continued)

6. FREE-AND FORCED-RESPONSE ANALYSIS OF REALISTIC BLADED-DISK SYSTEMS	76
6.1 Introduction and Literature Survey	76
6.2 Comparison of Previous Techniques for Mistuning Analysis With PDS	79
6.3 Application of PDS for Nine-Bladed Disk	81
7. CONCLUSIONS AND FUTURE RESEARCH	88
7.1 Conclusions	88
7.2 Directions for Future Research and Application	90
REFERENCES	93

LIST OF FIGURES

1.	Joint probability volume of two standard normal rv's	15
2.	Reduction of two-dimensional joint PDF to one-dimension	20
3.	Reliability space for two standard, normal rv's	21
4.	Matching actual and "equivalent" normal distributions	24
5.	Plots of exact response function $g_{\text{exact}}(x_1, x_2)$	29
6.	Plots of linear approximation of response $g_{\text{lin}}(x_1, x_2)$	30
7.	Obtaining MPP's for FORM, AMV	31
8.	Obtaining MPP's for AFORM	33
9.	Comparison of methods for obtaining CDF of explicit nonlinear limit state	34
10.	Test case system	43
11.	Comparison of PDS FORM and AMV CDF's for seven spring/mass test case.....	46
12.	Comparison of CDF's using PDS FORM and AMV with MC	47
13.	Linearity of fundamental eigenvalue w.r.t. independent rv's	49
14.	FORM and AMV CDF's versus MC; cov=10 percent	49
15.	Comparison of AFORM with FORM, AMV; cov=10 percent.....	51
16.	Comparison of CDF'S for different MC; approaches cov=10 percent	51
17.	Verification of NESSUS/FPI AFORM	52
18.	CDF using quadratic "approx. stats," cov=10 percent	52
19.	Comparison of CDF's of seven mass/spring system, cov=15 percent	54
20.	Two-bladed disk	57
21.	Two-bladed disk, mode 3 natural frequency comparison of PDS MC baseline with MC baseline	64
22.	Two-bladed disk, mode 3 natural frequency comparison of MC baseline with PDS Form using mean	66
23.	Two-bladed disk, mode 3 natural frequency comparing FORM using median versus mean	66
24.	Two-bladed disk, mode 3 frequency as a function of u16, using medians and mean values of dynamic rv's dynamic	68
25.	Two-bladed disk, mode 3 natural frequency comparing MC versus PDS	68
26.	Two-bladed disk, mode 3 at 456 Hz.....	72

LIST OF FIGURES (Continued)

27.	Two-bladed disk frequency response: MC versus PDS	75
28.	Variation of first three first-stage turbine blade frequencies for P&W SSME fuel pump.....	77
29.	Finite element model of SSME turbine blade	80
30.	Nine-bladed disk, mode 6 at 444.6 Hz (using CMS)	81
31.	Nine-bladed disk, mode 6 PDS evaluation	83
32.	Maximum frequency response using PDS andMC	86
33.	Frequency response of maximum blade to 3ND input for 50 Hz frequency range at mode 6 of median system; comparison of tuned system variations versus mistuned system.....	86
34.	Nonlinear dependence of mode 6 and maximum response as a function of independency rv's 23 and 89	87

LIST OF TABLES

1.	Comparison of reliability methods	28
2.	Statistics of dynamic characteristics	44
3.	Partial results of distribution types routine	45
4.	Sample MPP output	46
5.	Dispersion error of PDS versus full MC model	48
6.	Three-substructure system (“two-bladed disk”) information	58
7.	Comparison of methods for analysis of structures with probabilistic substructures	91

NOMENCLATURE

Chapter 1

CMS	component mode synthesis
CDF	cumulative distribution function
dof	degree of freedom
FEM	finite element method
MC	Monte Carlo
PDS	probabilistic dynamic synthesis
PDF	probability density function
rv	random variable
RF	residual flexibility

Chapter 2

[.]	designates a matrix
[.] ^T	transpose of a matrix
[α]	transformation matrix
b	subscript denoting boundary degrees of freedom
CB	Craig-Bampton method of Component Mode Synthesis
[cb]	Craig-Bampton transformation matrix
{F}	nodal force vector
Φ	modal matrix
G _{res-bb}	boundary-boundary partition of residual flexibility matrix
G _{res-ib}	internal-boundary partition of residual flexibility matrix
[G _{residual}]	residual flexibility matrix
[G _{retained}]	flexibility matrix obtained using retained modes only
[G]	flexibility matrix
i	subscript denoting internal degrees of freedom
I	Identity matrix
K ⁻¹	matrix inverse
[K.E.]	kinetic energy matrix
[K]	stiffness matrix
Λ^N	diagonal matrix partition of N retained eigenvalues λ

M_{bb}, K_{bb}	boundary-boundary partiton of matrices
M_{ib}, K_{ib}	internal-boundary partiton of matrices
M_{ii}, K_{ii}	internal degree of freedom partiton of mass, stiffness matrix
$[M]$	mass matrix
$[M]^{RF}, [K]^{RF}$	residual flexibility mass and stiffness matrices
$[M]_{sys}, [K]_{sys}$	system mass, stiffness matrices
N	superscript denoting number of retained modes
$[\psi]$	constrained transformation modal matrix
$[P.E.]$	potential energy matrix
q	generalized coordinates
q^N	generalized coordinate using N retained modes
si	superscript denoting substructure i
$[T]$	general transformation matrix
$[T^{RF}]$	residual flexibility transformation matrix
$\{.\}$	designates a vector
$\{x\}$	displacement vector
	acceleration vector

Chapter 3

$ \cdot $	absolute value
$[A]$	system matrix
AFORM	advanced first order reliability method
a_i	coefficients of first order terms of Taylor Series
α_i^*	gradient unit vector component i
AMV	advanced mean value method
β	safety index
b_i	coefficients of second order terms of Taylor Series
C	confidence interval
c_o	constant resulting from transformation of a_i and b_i
cov	coefficient of variation
$[cov]$	covariance matrix
δ	distance from most probable point to origin
$\delta(.)$	small change in quantity
	matrix equal to the partial derivative of each element in matrix K with respect to each random variable r_i
Δx	numerically calculated change in x

$E(.)$	statistical expectation function of a random variable
$\Phi(.)$	Gaussian cumulative distribution function of a value
FORM	first order reliability method
FPI	fast probability integration
$\varphi(.)$	Gaussian probability density function of a value
$\{\phi\}^i$	i'th modal vector
f_{XY}	joint probability density function of continuous random variables X and Y
F_{XY}	joint cumulative distribution function of random variables X and Y
γ	scaling factor
$g(\mathbf{X})$	limit state function of vector of input random variables
$g(x,y)$	a function of two random variables x and y
g_{exact}	exact limit state function
g_{lin}	linear approximation of limit state function
g_{pquad}	partial quadratic approximation of limit state function
$H(x)$	some function of x
$ J $	Jacobian
λ^i	i'th eigenvalue
$[\Lambda]$	diagonal matrix of system eigenvalues
μ_x	mean of a random variable x
MPP	most probable point
N	sample size for Monte Carlo simulation
o	subscript denoting original, unperturbed value
p	subscript denoting perturbed value
Ω	failure region of integration
$P(.)$	probability of an occurrence
$\Pi(.)$	product of terms
P_f	probability of failure
\mathbf{r}	vector of random variables r_i
SORM	second order reliability method
σ_x	standard deviation of a random variable x
	median of random variable X
\mathbf{X}	vector of input random variables
\mathbf{X}^*	design point
$Y(\mathbf{X})$	performance function of input random variables
z,u	standard normal random variable
\mathbf{Z},\mathbf{U}	vector of standard normal random variables

$\{X\} \sim U(\mu, \sigma)$	continuous random variable X has a uniform distribution with mean μ and standard deviation σ
$\{Y\} \sim N(\mu, \sigma)$	continuous random variable Y has a normal distribution with mean μ and standard deviation σ

Chapter 4

$\{.\}^{m,i}$	i 'th sample, m 'th substructure
$[C]$	correlation matrix
$\text{Cov}(x,y)$	covariance of two random variables x and y
FORMA	Fortran Matrix Analysis set of subroutines
G_{11}, \dots, G_{bb}	elements of boundary partition of residual flexibility matrix
k	number of retained modes
$[L]_c$	Cholesky Decomposition lower triangular matrix
$\lambda_{\text{sys}}^1(\mathbf{X})$	performance function for first system eigenvalue
λ_{sys}^1	first system eigenvalue
m	superscript denoting substructure
N	dimension of \mathbf{X} , total number of random variables
N_m	dimension of original dynamic random variables $\{x\}$
ρ	correlation coefficient
$\{U\}$	vector of individual vectors $\{u\}^m$
$\{u\}^m$	set of independent normal random variables for substructure m
$\{x\}$	vector of standard normally distributed random variables
$\{x\}$	vector of original dynamic random variables
$\{X\}$	vector of individual vectors $\{x\}^m$

Chapter 5

α_n	relative phase of the excitation force
$[C]$	system damping matrix
CPU	central processing unit
Φ_c	eigenvectors of correlation matrix
f_{gen}	complex excitation vector including relative phase information
$\{f\}$	excitation vector
F_n	complex excitation vector
Φ_R	matrix containing rigid body modes
G_{elastic}	residual flexibility matrix for elastic modes only
G^S	residual flexibility matrix associated with K_{EE}

K_{EE}	partition of stiffness matrix for statically determinate subset
λ_c	eigenvalues of correlation matrix
$[M]_1, [C]_1, [K]_1$	transformed set of system matrices
v	amplitude of harmonic solution for q_2
Ω	excitation frequency
P	inertia-relief transformation matrix
p_n	amplitude of excitation
Ψ_j	output phase of the j 'th generalized degree of freedom
$\{q\}_1$	transformed set of generalized coordinates
$\{q\}_2$	transformed set of generalized coordinates
θ_x	global rotational axis
x_b	boundary dof's which may or may not have external load applied
x_i, q_i	internal dof's with an external load applied
x_o, q_o	internal dof's with no external load applied
ζ	damping coefficient

Chapter 6

$[R]$	rigid body transformation matrix
ROM	reduced order method
SSME	Space Shuttle Main Engine
θ_z	angle about the z axis

SUMMARY

Accounting for the statistical geometric and material variability of structures in analysis has been a topic of considerable research for the last 30 years. The determination of quantifiable measures of statistical probability of a desired response variable, such as natural frequency, maximum displacement, or stress, to replace experience-based “safety factors” has been a primary goal of these studies. There are, however, several problems associated with their satisfactory application to realistic structures, such as bladed disks in turbomachinery. These include the accurate definition of the input random variables (rv’s), the large size of the finite element models frequently used to simulate these structures, which makes even a single deterministic analysis expensive, and accurate generation of the cumulative distribution function (CDF) necessary to obtain the probability of the desired response variables.

The research presented here applies a methodology called probabilistic dynamic synthesis (PDS) to solve these problems. The PDS method uses dynamic characteristics of substructures measured from modal test as the input rv’s, rather than “primitive” rv’s such as material or geometric uncertainties. These dynamic characteristics, which are the free-free eigenvalues, eigenvectors, and residual flexibility (RF), are readily measured and for many substructures, a reasonable sample set of these measurements can be obtained. The statistics for these rv’s accurately account for the entire random character of the substructure. Using the RF method of component mode synthesis, these dynamic characteristics are used to generate reduced-size sample models of the substructures, which are then coupled to form system models. These sample models are used to obtain the CDF of the response variable by either applying Monte Carlo simulation or by generating datapoints for use in the response surface reliability method, which can perform the probabilistic analysis with an order of magnitude less computational effort. Both free- and forced-response analyses have been performed, and the results indicate that, while there is considerable room for improvement, the method produces usable and more representative solutions for the design of realistic structures with a substantial savings in computer time.

TECHNICAL MEMORANDUM

DEVELOPMENT OF A PROBABILISTIC DYNAMIC SYNTHESIS METHOD FOR THE ANALYSIS OF NONDETERMINISTIC STRUCTURES

1. INTRODUCTION

1.1 Motivation

The primary assumption for the basic analysis of structures has always been knowledge of the material properties and of the geometric layout. Once an initial analysis is performed, uncertainties in the above inputs, as well as uncertainties in the analysis method used, computer accuracy, and many other factors are addressed by the use of somewhat arbitrary experience-based “safety” factors. Some attempt has been made over the last several decades to account for the variation in material properties by using “3- σ ” curves from material handbooks, but in general, the statistical variability of structures has not been quantitatively accounted for in structural analysis.

This problem has been well recognized and therefore a significant amount of research has been performed over the last 30 years to develop methods of dealing with the statistical variability of structures. The goal of these methods is that given statistically characterized input quantities, a desired output response quantity can also be characterized statistically. Examples of the varied input quantities, which can be defined as random variables (rv's), are Young's modulus, density, thickness, length, and width. Output rv's could be, for example, stress, load, or natural frequency. There are various levels of statistical characterization for these rv's; the most complete is the cumulative distribution function (CDF), which defines the probability of occurrence of a specific value of an rv over its entire range of possibility.

For very small problems of one or two input rv's, an exact solution for the response rv can be obtained. The first step is to obtain the joint probability distribution function, which is the multidimensional integral defined by the probability distribution function (PDF) of the input rv's. This surface (or curve for one rv) must then be integrated from negative infinity to the domain defined by the function relating the input to response variables. For multiple degree-of-freedom (dof) structures, however, this integration often becomes intractable. For these multi-dof structures, the most straightforward method of obtaining these results is to use the Monte Carlo (MC) method. In this method, a complete sample set of each input rv fitting a desired distribution is created. A variety of methods are available for generating these sample sets.¹ Once a set for each input rv is created, an analogous solution sample set is calculated using a numerical method capable of analyzing large structures, such as the finite element method (FEM) or boundary element method. The statistical parameters of the desired response value is obtained from this solution set and a distribution type can be fit to it using commercially available software.² The drawback to this method is the large number of runs required to obtain a response CDF and the even

larger number required to obtain an accurate PDF. Although the capability for performing these calculations for realistic multi-dof structures is improving dramatically and will be discussed in this dissertation, the process is still extremely computer-intensive and expensive, especially if multiple runs are required for parametric design studies.

The thrust, therefore, of the published research has been to develop approximate methods, frequently called reliability methods, to obtain response statistics of complex structural components using an order of magnitude less calculations than MC techniques. Initial methods assumed Gaussian input rv's and obtained only the mean and standard deviation of the response rv. Further development has resulted in advanced, commercially available computer codes, such as Southwest Research Institute's NESSUS code,³ that allow input rv's of any distribution type and produce entire distributions of response variables along with accurate statistical parameters from finite element structural models. These codes incorporate a number of reliability methods that reduce the number of runs to as few as the number of input rv's plus one, down from the several thousand runs required for MC.

There are still many limitations to the direct application of the above codes to complex structural components. One main problem is determination of the statistical characteristics of the input rv's. A great deal of data are available characterizing material property variability, but accurately defining geometric variation in a structure is extremely difficult. In addition, because the structure is typically represented by spatial coordinates of finite element grids, using the location of each of the grids as an rv would make the probabilistic problem intractable. The method of random fields can be used to describe the spatial variation using correlation techniques, but obtaining accurate correlation for a manufactured part is frequently not possible.

Another problem is that many of these structural components require finite element models of so many dof's that substructuring reduction techniques are required to decrease the size of the model just to perform a single, deterministic analysis. These techniques separate the model into groups of elements called substructures; frequently these substructure models are composed of similar groups, such as turbine blades on an engine turbine bladed-disk, or are required because different companies build the substructures, such as the booster, external tank, and orbiter of the space shuttle system. The mass and stiffness matrices of these substructures are then mathematically reduced to a smaller set; one group of reduction techniques called component mode synthesis (CMS) methods represent the substructures by a set of interface dof's and generalized modal coordinates. The combination of CMS methods and reliability probabilistic techniques is one of the topics explored in this thesis.

One possible solution to the above problems is the direct use of statistics generated by modal testing of a population of the substructures. One example of such a population is turbine blades for a specific stage in a turbopump. For many engine development programs, the experimental determination

a hundred blades each, the population can therefore number in the thousands. The measured values from this testing, which include the structural eigenvalues, eigenvectors, and residual flexibility of the boundaries, would be established as the "dynamic" rv's of the system, rather than "primitive" rv's like variable thickness or length. These dynamic rv's can be used directly in the residual flexibility (RF) method of CMS to create the substructure mass and stiffness matrices.

The objective of the research presented here is to apply the RF CMS method to the probabilistic analysis of complex structural systems using this set of statistically accurate “dynamic” rv’s as input. The method developed is called probabilistic dynamic synthesis (PDS). Application of this new method would enable accurate probabilistic analyses to be performed on a variety of realistic, complex structural components that presently are not performed due to enormous computer requirements and limited result accuracy. One type of structure particularly applicable to the PDS method is the mistuned bladed disk; the size of blade finite element models is so large that realistically modeling even a single sample of such a disk, with every blade slightly different, has not been attempted even with CMS techniques. Only recently have studies using reduced order methods on bladed disks been initiated.⁴ The use of PDS allows a complete probabilistic analysis to be performed of the mistuned bladed disk to generate both free- and forced-response solutions.

1.2 Scope of Dissertation

Because one of the major objectives of this research is to combine several different disciplines together to form a new analytical tool, extensive theoretical and literature background will be presented on each of these aspects. The first topic to be examined is the CMS procedure, which is presented in chapter 2. The emphasis in this chapter is the comparison between the CB and residual flexibility methods of CMS and why residual flexibility is more applicable to this research.

Chapter 3 is an extensive study of probabilistic analysis as applied to structures. This study is divided into six parts: (1) theoretical basis and exact methods, (2) MC approximate method, (3) reliability approximate methods, (4) comparison of reliability methods, (5) perturbation methods, and (6) comparison of methods and their areas of applicability.

Chapter 4 presents the application of PDS to a simple test case consisting of two substructures represented by masses and springs. Some of the remaining aspects of the theoretical background of PDS will be completed as part of the examination, including examining the effects of correlation of the input rv’s.

Chapter 5 examines the application of the PDS method to a realistic three substructure system modeled using the finite element method. Both free- and forced-response solutions are presented, along with examinations of many aspects of the problem that are only encountered because of the realistic aspect of the models. In addition, an MC analysis of the system is described; this type of analysis on a structure with this level of complexity has not previously been reported in the literature.

Chapter 6 applies the PDS method to realistically modeled tuned and mistuned bladed disks. A literature survey of bladed disk research will be presented, and the results from chapter 3 will be used to show the advantages and disadvantages of using PDS for this application. Improvements in the methodology resulting from the work presented in chapters 4 and 5 are applied, and both free- and forced-response solutions are produced.

Chapter 7 discusses the applicability of the method to general problems in structural analysis. A detailed chart is presented that lists the methods used in this field of research and summarizes the advantages and disadvantages of each. Some specific directions for future research are examined, and final conclusions of the research are presented.

2. THEORETICAL BACKGROUND AND LITERATURE SURVEY—COMPONENT MODE SYNTHESIS

CMS is a very well developed topic in structural dynamics. An extensive literature survey will not be presented here; rather, the applicability of the various methods to PDS will be discussed and the theoretical background behind those procedures will be presented. CMS is extensively used in the automotive and aerospace fields, and was initially discussed by Hurty in 1965.⁵ In 1968, Craig and Bampton developed the concept into a readily usable methodology and it became widely used by industry.⁶ The CB method uses fixed-interface modes and “constraint” modes to represent each substructure. An alternative method, initially investigated by MacNeil, uses free-interface modes and residual flexibility of the interface to represent the substructure instead.⁷ In 1984, Martinez altered the method into a representation similar to the CB method for ready use by industry.⁸

The CB method was initially evaluated for its applicability to the PDS method. In this method, a structure is divided into substructures a,b,...,n, which are denoted with superscripts sa through sn. The physical displacement vectors of each substructure, which have either a subscript i denoting internal dof or a subscript b denoting boundary dof, can be written as

$$\begin{Bmatrix} x_i \\ x_b \end{Bmatrix}^{sa}, \begin{Bmatrix} x_i \\ x_b \end{Bmatrix}^{sb}, \dots, \begin{Bmatrix} x_i \\ x_b \end{Bmatrix}^{sn} . \quad (1)$$

Similarly, the substructure mass and stiffness matrices can be written in partitioned form as

$$\begin{bmatrix} M_{ii} & M_{ib} \\ M_{bi} & M_{bb} \end{bmatrix}^{sa}, \begin{bmatrix} K_{ii} & K_{ib} \\ K_{bi} & K_{bb} \end{bmatrix}^{sa}, \dots, \begin{bmatrix} M_{ii} & M_{ib} \\ M_{bi} & M_{bb} \end{bmatrix}^{sn}, \begin{bmatrix} K_{ii} & K_{ib} \\ K_{bi} & K_{bb} \end{bmatrix}^{sn} . \quad (2)$$

The CB transformation between the physical coordinates and a reduced vector of generalized and physical coordinates is

$$\begin{Bmatrix} x_i \\ x_b \end{Bmatrix}^{sa} = [cb]^{sa} \begin{Bmatrix} q \\ x_b \end{Bmatrix}^{sa} \quad (3)$$

The partitioned transformation matrix $[cb]^{sa}$ is defined as

$$[cb]^{sa} = \begin{bmatrix} \Phi^N & \Psi \\ 0 & I \end{bmatrix} , \quad (4)$$

where the “constrained transformation modes” matrix is defined as

$$[\Psi] = -[K_{ii}]^{sa-1} [K_{ib}]^{sa} , \quad (5)$$

and Φ^N is the truncated matrix of N cantilevered modes of the substructure (the CB method uses clamped boundary conditions, as mentioned previously). The vector of generalized coordinates in equation (3) is composed of q , a truncated set of generalized coordinates that describe, approximately, the internal displacement field, and x_b , the physical coordinates of the substructure boundary that are retained throughout the analysis. The size of q is equal to the number of modes retained for the analysis. The number of retained modes depends on a variety of factors including the desired accuracy, the frequency range over which the model is intended for use, the frequency range of the input excitation, etc. Generally the number of retained modes is much smaller than the number of physical dof's of the system and is the source of the reduction in the size of the problem.

The transformation between each substructure's reduced vector and the total structure's reduced vector is then calculated. For substructure a , this transformation will be

$$\begin{Bmatrix} q \\ x_b \end{Bmatrix}^{sa} = [T]^{sa} \begin{Bmatrix} q^{sa} \\ \vdots \\ q^{sn} \\ x_b^{sa} \\ \vdots \\ x_b^{sn} \end{Bmatrix} \quad (6)$$

where

$$[T]^{sa} = \begin{bmatrix} I & \cdots & 0 & 0 & \cdots & 0 \\ 0 & \cdots & 0 & I & \cdots & 0 \end{bmatrix} . \quad (7)$$

Using equation (3), the transformation between the system-reduced vector and the substructure physical vector is therefore

$$\begin{Bmatrix} x_i \\ x_b \end{Bmatrix}^{sa} = [\alpha]^{sa} \begin{Bmatrix} q^{sa} \\ \vdots \\ q^{sn} \\ x_b^{sa} \\ \vdots \\ x_b^{sn} \end{Bmatrix}, \quad (8)$$

where

$$[\alpha]^{sa} = [cb]^{sa} [T]^{sa}. \quad (9)$$

A conservation of energy approach is used to synthesize the system mass and stiffness matrices for the system undamped equations of motion. A complete derivation is given in the textbook by Craig.⁹ Essentially, the kinetic and potential energy of substructures are defined as

$$\begin{aligned} [K.E.]^{sa} &= \frac{1}{2} \begin{Bmatrix} \dot{x}_i \\ \dot{x}_b \end{Bmatrix}^{saT} [M]^{sa} \begin{Bmatrix} \dot{x}_i \\ \dot{x}_b \end{Bmatrix}^{sa} \\ [P.E.]^{sa} &= \frac{1}{2} \begin{Bmatrix} x_i \\ x_b \end{Bmatrix}^{sa} [K]^{sa} \begin{Bmatrix} x_i \\ x_b \end{Bmatrix}^{sa}. \end{aligned} \quad (10)$$

The energy terms for each substructure are then added together to form the total kinetic and potential energies of the system, which can be expressed in terms of the system coordinates using equation (8):

$$[\text{K.E.}]^{\text{sys}} = \frac{1}{2} \begin{Bmatrix} \dot{\mathbf{q}}^{\text{sa}} \\ \vdots \\ \dot{\mathbf{q}}^{\text{sn}} \\ \dot{\mathbf{x}}_{\text{b}}^{\text{sa}} \\ \vdots \\ \dot{\mathbf{x}}_{\text{b}}^{\text{sn}} \end{Bmatrix}^T [\boldsymbol{\alpha}]^{\text{sa}^T} [\mathbf{M}]^{\text{sa}} [\boldsymbol{\alpha}]^{\text{sa}} \begin{Bmatrix} \dot{\mathbf{q}}^{\text{sa}} \\ \vdots \\ \dot{\mathbf{q}}^{\text{sn}} \\ \dot{\mathbf{x}}_{\text{b}}^{\text{sa}} \\ \vdots \\ \dot{\mathbf{x}}_{\text{b}}^{\text{sn}} \end{Bmatrix} + \dots + \frac{1}{2} \begin{Bmatrix} \dot{\mathbf{q}}^{\text{sa}} \\ \vdots \\ \dot{\mathbf{q}}^{\text{sn}} \\ \dot{\mathbf{x}}_{\text{b}}^{\text{sa}} \\ \vdots \\ \dot{\mathbf{x}}_{\text{b}}^{\text{sn}} \end{Bmatrix}^T [\boldsymbol{\alpha}]^{\text{sn}^T} [\mathbf{M}]^{\text{sn}} [\boldsymbol{\alpha}]^{\text{sn}} \begin{Bmatrix} \dot{\mathbf{q}}^{\text{sa}} \\ \vdots \\ \dot{\mathbf{q}}^{\text{sn}} \\ \dot{\mathbf{x}}_{\text{b}}^{\text{sa}} \\ \vdots \\ \dot{\mathbf{x}}_{\text{b}}^{\text{sn}} \end{Bmatrix}$$

$$= \frac{1}{2} \begin{Bmatrix} \dot{\mathbf{q}}^{\text{sa}} \\ \vdots \\ \dot{\mathbf{q}}^{\text{sn}} \\ \dot{\mathbf{x}}_{\text{b}}^{\text{sa}} \\ \vdots \\ \dot{\mathbf{x}}_{\text{b}}^{\text{sn}} \end{Bmatrix}^T [\mathbf{M}]^{\text{sys}} \begin{Bmatrix} \dot{\mathbf{q}}^{\text{sa}} \\ \vdots \\ \dot{\mathbf{q}}^{\text{sn}} \\ \dot{\mathbf{x}}_{\text{b}}^{\text{sa}} \\ \vdots \\ \dot{\mathbf{x}}_{\text{b}}^{\text{sn}} \end{Bmatrix}^{\text{sa}}$$

$$[\text{P.E.}]^{\text{sys}} = \frac{1}{2} \begin{Bmatrix} \mathbf{q}^{\text{sa}} \\ \vdots \\ \mathbf{q}^{\text{sn}} \\ \mathbf{x}_{\text{b}}^{\text{sa}} \\ \vdots \\ \mathbf{x}_{\text{b}}^{\text{sn}} \end{Bmatrix}^T [\boldsymbol{\alpha}]^{\text{sa}^T} [\mathbf{K}]^{\text{sa}} [\boldsymbol{\alpha}]^{\text{sa}} \begin{Bmatrix} \mathbf{q}^{\text{sa}} \\ \vdots \\ \mathbf{q}^{\text{sn}} \\ \mathbf{x}_{\text{b}}^{\text{sa}} \\ \vdots \\ \mathbf{x}_{\text{b}}^{\text{sn}} \end{Bmatrix} + \dots + \frac{1}{2} \begin{Bmatrix} \mathbf{q}^{\text{sa}} \\ \vdots \\ \mathbf{q}^{\text{sn}} \\ \mathbf{x}_{\text{b}}^{\text{sa}} \\ \vdots \\ \mathbf{x}_{\text{b}}^{\text{sn}} \end{Bmatrix}^T [\boldsymbol{\alpha}]^{\text{sn}^T} [\mathbf{K}]^{\text{sn}} [\boldsymbol{\alpha}]^{\text{sn}} \begin{Bmatrix} \mathbf{q}^{\text{sa}} \\ \vdots \\ \mathbf{q}^{\text{sn}} \\ \mathbf{x}_{\text{b}}^{\text{sa}} \\ \vdots \\ \mathbf{x}_{\text{b}}^{\text{sn}} \end{Bmatrix} \quad (11)$$

$$= \frac{1}{2} \begin{Bmatrix} \mathbf{q}^{\text{sa}} \\ \vdots \\ \mathbf{q}^{\text{sn}} \\ \mathbf{x}_{\text{b}}^{\text{sa}} \\ \vdots \\ \mathbf{x}_{\text{b}}^{\text{sn}} \end{Bmatrix}^T [\mathbf{K}]^{\text{sys}} \begin{Bmatrix} \mathbf{q}^{\text{sa}} \\ \vdots \\ \mathbf{q}^{\text{sn}} \\ \mathbf{x}_{\text{b}}^{\text{sa}} \\ \vdots \\ \mathbf{x}_{\text{b}}^{\text{sn}} \end{Bmatrix}^{\text{sa}},$$

where

$$[\mathbf{M}]_{\text{sys}} = [\alpha]^{saT} [\mathbf{M}]^{sa} [\alpha]^{sa} + \dots + [\alpha]^{snT} [\mathbf{M}]^{sn} [\alpha]^{sn} \quad (12)$$

$$[\mathbf{K}]_{\text{sys}} = [\alpha]^{saT} [\mathbf{K}]^{sa} [\alpha]^{sa} + \dots + [\alpha]^{snT} [\mathbf{K}]^{sn} [\alpha]^{sn} . \quad (13)$$

These matrices can now be used to form the system equation of motion,

$$[\mathbf{M}]_{\text{sys}} \begin{Bmatrix} \ddot{\mathbf{q}}^{sa} \\ \vdots \\ \ddot{\mathbf{q}}^{sn} \\ \ddot{\mathbf{x}}_b \end{Bmatrix} + [\mathbf{K}]_{\text{sys}} \begin{Bmatrix} \mathbf{q}^{sa} \\ \vdots \\ \mathbf{q}^{sn} \\ \mathbf{x}_b \end{Bmatrix} = \mathbf{0} , \quad (14)$$

from which the system eigenvalues and eigenvectors can be obtained.

The CB procedure is a straightforward and time-tested method of substructure synthesis. However, upon closer examination, it was determined that the CB method relies upon data that are not easily obtained through experimental tests. This can be seen if one applies the CB transformation as defined in equation (4) to a single substructure:¹⁰

$$[\mathbf{M}^{sa}]^{cb} = [\mathbf{c}^{sa}]^T [\mathbf{M}^{sa}] [\mathbf{c}^{sa}] = \begin{bmatrix} \mathbf{I} & \Phi^N (\mathbf{M}_{ii} \Psi + \mathbf{M}_{ib}) \\ \text{sym} & \Psi^T (\mathbf{M}_{ii} \Psi + \mathbf{M}_{ib}) + \mathbf{M}_{ib} \Psi + \mathbf{M}_{bb} \end{bmatrix} \quad (15)$$

$$[\mathbf{K}^{sa}]^{cb} = [\mathbf{c}^{sa}]^T [\mathbf{K}^{sa}] [\mathbf{c}^{sa}] = \begin{bmatrix} \Lambda^N & 0 \\ 0 & \mathbf{K}_{bb} - \mathbf{K}_{bi} \mathbf{K}_{ii}^{-1} \mathbf{K}_{bi} \end{bmatrix} . \quad (16)$$

The Λ^N partition is the diagonal of N retained substructure eigenvalues (squares of the natural frequencies) and the other variables and subscripts refer to equations (2), (4), and (5). It is clear that significant portions of the matrices are derived directly from the original mass and stiffness matrices and cannot be obtained from test (unlike Λ^N and Φ^N). Recall that a major goal of this work is to incorporate randomness into the model using information that can be measured solely from test. This information is not fully accounted for in the above transformed mass and stiffness matrices. However, since the method is fairly simple to use, it does suggest that it would be the CMS method of choice for a purely analytical PDS methodology, or possibly a hybrid that would use some test information and other analytical information. This might be useful for parametric mistuning studies, for instance.

In order to circumvent the limitations of the CB method, the RF method was investigated. One of the fundamental concepts used to reduce the dof's in CMS is the truncation of substructure modes at

some level, thus assuming that the higher modes will not have a major effect on the combined system modes. The RF method partially accounts for the higher modes by determining their flexibility. A side benefit is that all the elements of the system stiffness matrix can be obtained from test and that the mass matrix can be closely approximated by a unity matrix in the nonboundary partition (equal in size to the number of kept modes N). Since all the substructure information can be obtained from test, probabilistic data can be completely incorporated into the system matrices to obtain the system modes.

The derivation of the free response of substructures using the RF method is presented below. The presentation, which is similar to that of Admire and Tinker,¹¹ begins with the statics equation for the structure:

$$[K]\{x\} = \{F\} \quad (17)$$

where $[K]$ is the stiffness matrix and $\{x\}$ and $\{F\}$ are the nodal displacement and force vectors, respectively. Solving for $\{x\}$, the flexibility formulation is obtained:

$$\{x\} = [G]\{F\} \quad \text{where} \quad [G] = [K]^{-1} . \quad (18)$$

At this point, a modal analysis is performed and the lower N modes are retained for future use. The vector $\{x\}$ can be partially represented by a transformation to the generalized coordinates $\{q^N\}$ using these N retained modes of the substructure

$$\{x_{\text{partial}}\} = [\Phi^N]\{q^N\} . \quad (19)$$

Substitution of equation (19) into equation (17) and premultiplication by $[\Phi^N]^T$ yields

$$[\Phi^N]^T [K^N] [\Phi^N] \{q^N\} = [\Phi^N]^T \{F\} . \quad (20)$$

If the retained modes Φ^N are mass-normalized,¹² this is equivalent to

$$[\Lambda^N] \{q^N\} = [\Phi^N]^T \{F\} . \quad (21)$$

Now, using equations (19) and (21), the following result is obtained for $\{x\}_{\text{partial}}$:

$$\{x_{\text{partial}}\} = [\Phi^N] [\Lambda^N]^{-1} [\Phi^N]^T \{F\} = [G_{\text{retained}}] \{F\} . \quad (22)$$

The total residual flexibility $[G]$ can therefore be split into two parts, the first resulting from the retained modes (shown in equation (22) and the second from the deleted modes, which is defined as the residual flexibility $[G_{\text{residual}}]$;

$$\{x\} = ([G_{\text{retained}}] + [G_{\text{residual}}])\{F\} \quad (23)$$

and $[G_{\text{residual}}]$ can be solved for as

$$[G_{\text{residual}}] = [G] - [\Phi^N][\Lambda^N]^{-1}[\Phi^N]^T. \quad (24)$$

Therefore, the physical displacement set can be completely represented by two terms:

$$\{x\} = [\Phi^N]\{q^N\} + [G_{\text{residual}}]\{F\}. \quad (25)$$

As with the CB method, the substructure is now divided into internal dof's and boundary dof's:

$$\{x\} = \begin{Bmatrix} x_i \\ x_b \end{Bmatrix}. \quad (26)$$

For a free-response analysis of a structure, the only forces that must be accounted for are the internal forces that act at the interfaces of the substructures. Therefore, the equation of motion for the free-response analysis of the substructure is

$$\begin{bmatrix} M_{ii} & M_{ib} \\ M_{bi} & M_{bb} \end{bmatrix} \begin{Bmatrix} \ddot{x}_i \\ \ddot{x}_b \end{Bmatrix} + \begin{bmatrix} K_{ii} & K_{ib} \\ K_{bi} & K_{bb} \end{bmatrix} \begin{Bmatrix} x_i \\ x_b \end{Bmatrix} = \begin{Bmatrix} 0 \\ F_b \end{Bmatrix}. \quad (27)$$

Since the applied forces at the internal dof's of each substructure are zero, only the boundary columns of the residual flexibility matrix are needed, which is beneficial for coupling with the other substructures. Equation (25) therefore reduces to

$$\begin{Bmatrix} x_i \\ x_b \end{Bmatrix} = \begin{bmatrix} \Phi_i^N & G_{\text{res-ib}} \\ \Phi_b^N & G_{\text{res-bb}} \end{bmatrix} \begin{Bmatrix} q^N \\ F_b \end{Bmatrix}. \quad (28)$$

Using the lower partition to solve for $\{F_b\}$ yields

$$\{F_b\} = G_{\text{res-bb}}^{-1}x_b - G_{\text{res-bb}}^{-1}\Phi_b^N q^N. \quad (29)$$

Substituting equation (29) into the top partition of (28) yields

$$\begin{aligned} x_i &= \Phi_i^N q^N + G_{\text{res-ib}} \left(G_{\text{res-bb}}^{-1}x_b - G_{\text{res-bb}}^{-1}\Phi_b^N q^N \right) \\ &= \left(\Phi_i^N - G_{\text{res-ib}} G_{\text{res-bb}}^{-1}\Phi_b^N \right) q^N + G_{\text{res-ib}} G_{\text{res-bb}}^{-1}x_b. \end{aligned} \quad (30)$$

Substituting this result into equation (28) yields the RF transformation matrix $[T^{RF}]$

$$\begin{Bmatrix} x_i \\ x_b \end{Bmatrix} = \begin{bmatrix} \Phi_i^N - G_{res-ib} G_{res-bb}^{-1} \Phi_b^N & G_{res-ib} G_{res-bb}^{-1} \\ 0 & I \end{bmatrix} \begin{Bmatrix} q_i^N \\ x_b \end{Bmatrix} = [T^{RF}] \{q_1\} . \quad (31)$$

Applying this transformation to the undamped equation of motion (24) to obtain the equation in the reduced coordinates $\{q_1\}$ yields

$$[M^{RF}] \begin{Bmatrix} \ddot{q}_i \\ \ddot{x}_b \end{Bmatrix} + [K^{RF}] \begin{Bmatrix} q_i \\ x_b \end{Bmatrix} = [T^{RF}]^T \begin{Bmatrix} 0 \\ F_b \end{Bmatrix} , \quad (32)$$

where

$$[M^{RF}] = [T^{RF}]^T [M] [T^{RF}] \approx \begin{bmatrix} I & 0 \\ 0 & 0 \end{bmatrix} , \quad (33)$$

and

$$[K^{RF}] = [T^{RF}]^T [K] [T^{RF}] = \begin{bmatrix} \Lambda^N + \Phi_b^{NT} G_{res-bb}^{-1} \Phi_b^N & -\Phi_b^{NT} G_{res-bb}^{-1} \\ \text{sym} & G_{res-bb}^{-1} \end{bmatrix} . \quad (34)$$

and $[M]$ and $[K]$ are the partitioned mass and stiffness matrices from equation (27). The symbol Φ_b^N refers to the partition of the modal matrix consisting of N retained modes on the boundary of the substructure. These substructure matrices are then coupled together to form the system mass and stiffness matrices in an identical manner as used in the CB method.

To facilitate ease of implementation, the approximation shown in equation (34) is used in this method. The “residual mass” terms on the off-diagonals have been neglected, which makes the creation of the substructure mass matrix considerably simpler; this assumption is discussed in detail by Admire and Tinker¹³ and is shown to be acceptable. In addition, the boundary partition terms on the diagonal in the mass matrix that are equal to zero are instead set to very small numbers in the analysis to provide numerical stability for eigensolution routines.

The applicability of the RF method to probabilistic dynamic synthesis can now be seen by examining the substructure matrices. All of the elements of the substructure stiffness matrix can be obtained directly from modal tests. The free-free modes and mode shapes are generally readily available; if it is difficult to obtain them (for very small structures like turbine blades, for instance), recent studies by Han, Chen and others have identified a method for obtaining the free-free modes using constrained modal test data.^{14,15} The residual flexibility partitions are obtained by measuring the slope of the stiffness line for drive point frequency response function measurements. The determination of this value has been the subject of considerable research in the last few years.¹⁶

An assumption in this application of the RF CMS method is that the modal test measurements are accurate. There has only been limited success in synthesizing mass and stiffness matrices from test, and one reason may be that there are inherent errors in the measurements themselves. The fact that an entire sample set of these measurements is required for use in the PDS method, as will be discussed in chapter 4, may mitigate this error. This subject will be discussed further in areas for future research in chapter 7.

3. THEORETICAL BACKGROUND AND LITERATURE SURVEY—PROBABILISTIC ANALYSIS OF ENGINEERING QUANTITIES

For most engineering problems, a desired response variable is a function of some given input variables. As discussed previously, if the inputs can be expressed as rv's, then the response will possess a probability density function, cumulative distribution function, the statistical moments of mean and standard deviation, and possibly other characterizing parameters. This chapter includes a brief basic theoretical background of the subject including “exact” methods for obtaining the statistics of the response variable and discussions of various approximate methods for this determination. These approximate methods include the MC method; reliability methods, which have grown out of civil engineering applications of strength versus load; and the perturbation method, which has been used extensively in research, particularly in the vibration analysis of bladed disks in turbomachinery. Two detailed examples are presented to illustrate these various techniques. Finally, a detailed comparison of the reliability and perturbation methods will be presented. A thorough understanding of this information is necessary to determine which method would be best applicable for use in the PDS technique.

3.1 Exact Methods

Given two continuous rv's X and Y , the joint probability density function f_{XY} is defined such that the following integral can be evaluated to determine the probability that X will take on a value between two limits “a” and “b” and that Y will take on a value between two limits “c” and “d:”

$$P(a < X < b, c < Y < d) = \int_c^d \int_a^b f_{XY}(x, y) dx dy, \quad (35)$$

where x and y are the variables of integration. The probability that both X is below the variable x and Y is below the variable y is defined as F_{XY} , the joint CDF of X and Y . The integration of f_{XY} from negative infinity to x and y will result in F_{XY} as a function of x and y :

$$F_{XY}(x, y) = P(X < x, Y < y) = \int_{-\infty}^x \int_{-\infty}^y f_{XY}(x, y) dx dy. \quad (36)$$

Like the functions of one variable, the joint CDF varies between 0 and 1, where 1 is the total volume under the joint PDF f_{XY} .¹⁷

In most engineering applications, a desired response variable is some function of the rv's. This response variable can also be described by either its PDF or CDF. For a single input rv where g is a function $H(x)$, the probability density function of the continuous rv G can be shown to be¹⁸

$$f_G(g) = f_x(x) \left| \frac{dx}{dg} \right|. \quad (37)$$

For two input rv's an exact methodology has been formulated called the auxiliary variable technique.¹⁹ It is beyond the scope of this thesis to describe the technique in detail, but the final expression for the probability density function of g requires the creation of an auxiliary dependent variable so that the number of dependent variables equals the number of input rv's. This allows the following relationship to be expressed:

$$f_{G1G2}(g_1, g_2) = \frac{f_{XY}(x, y)}{|J|}, \quad (38)$$

where $|J|$ denotes the determinant of the Jacobian matrix,

$$[J] = \begin{bmatrix} \frac{\partial g_1}{\partial x} & \frac{\partial g_1}{\partial y} \\ \frac{\partial g_2}{\partial x} & \frac{\partial g_2}{\partial y} \end{bmatrix}.$$

The PDF of g_1 can therefore be isolated by integrating out g_2 over a region R bounded by the solution of g_2 in terms of x and y , which are, in turn, in terms of g_1 . This results in

$$f_{G1}(g_1) = \int_R \frac{f_{XY}(x, y)}{|J|} dg_2. \quad (39)$$

This can only be solved analytically for a few simple functions $g=H(x,y)$ combined with simple PDF's for x and y , such as a uniform distribution. Any other combination requires numerical solutions, even for just two rv's.

The CDF of the response variable can be obtained directly by integrating the volume under the probability density function bounded by the curvilinear plane defining a specific value of the function $g=H(x,y)$:

$$F_G(g) = P(G < g) = \iiint_R f_{XY}(x, y) dx dy. \quad (40)$$

This volume is shown in figure 1. To perform the calculation, y must be expressed in terms of x and then x expressed in terms of g to create the region R forming the integration bounds. Again, for any but the most simple functions combined with uniform distributions, the exact determination of the integral even for just two input rv's is not possible; defining the domains for a nonlinear function is very difficult and typical bivariate distributions like the binormal distribution are not readily integrable.

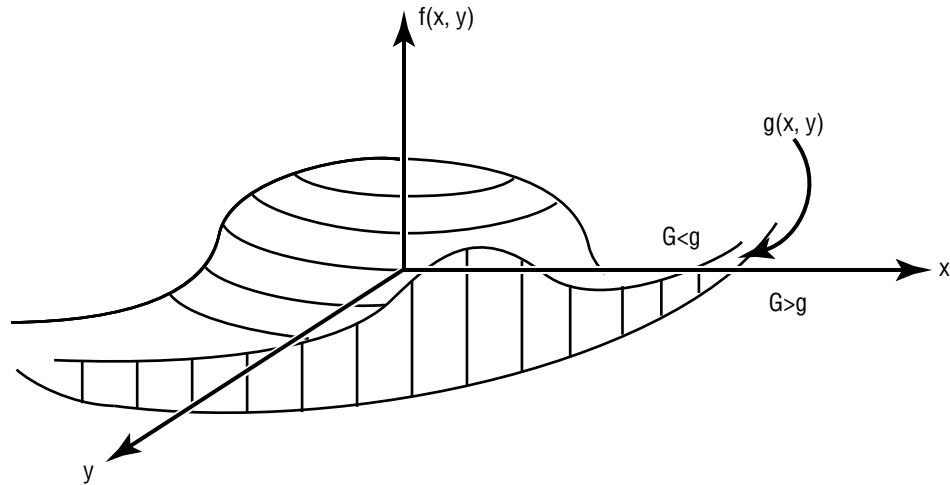


Figure 1. Joint probability volume of two normal rv's.

It is clear from the above discussion that these methods are infeasible for determining the CDF of an rv that is a function of many input rv's. For applications to structural systems, in which the entire geometry as well as material characteristics can be random, this limitation makes the integration intractable. However, the theoretical development above has been used to develop more practical methods which are discussed next.

3.2 Approximate Methods—Monte Carlo

The MC method is an approximate numerical method for calculating the PDF and CDF of a function of rv's. It is frequently used as a baseline against which other approximate methods are measured. The method essentially takes a sample from each of the input rv's and uses them to generate a solution for the response variable of interest. A large number of these solutions are produced and a PDF and CDF are calculated from these results. This “brute-force” method is very straightforward, but it is extremely computationally intensive since a large number of solutions are required for accurate results.

The first step in the MC method is to create a set or ensemble of input variables having the same statistics as the input rv's of the problem in question. A digital computer is used to generate a large number of uniformly distributed “pseudo-random” numbers (the vector is not completely random because it is repeatable for the same given “seed” value). An algorithm to generate an analogous vector of random numbers that fall into a desired statistical distribution type is then applied. For example, the “Box-Muller Algorithm” is used to obtain a vector of two statistically independent normally distributed rv's from a uniform set.²⁰ If

$$\{X\} \sim U(0,1) \quad (41)$$

denotes a vector X that has a uniform distribution between 0 and 1, then

$$y_1 = (-2 \ln x_i)^{.5} \cos (2\pi x_{i+1}) \quad (42)$$

$$y_2 = (-2 \ln x_i)^{.5} \sin (2\pi x_{i+1}) , \quad (43)$$

with

$$y_1 \text{ and } y_2 \sim N(0,1) ,$$

denoting that y_1 and y_2 are two independent rv's with standard normal (or Gaussian) distributions (mean 0 and standard deviation 1). These can be converted to nonstandard normal distributions z with given mean μ_z and standard deviation σ_z using

$$z = \mu_z + \sigma_z y . \quad (44)$$

Once the desired distributions are created, the function of interest (e.g., $t=t(z_1, z_2)$) is simply calculated for each set of input rv's z_1 and z_2 and a histogram of t is created to obtain its PDF and CDF. The size of the sample required depends on the CDF value of interest, which is the probability that t will be less than some given constant value T , denoted $P(t < T)$. The sample size is also a function of the required confidence interval C , which is a measure of the percentage of the time that a sample of size N will yield a CDF value at $P(t < T)$ that is accurate. One estimate of this value is

$$N > \frac{-\ln(1-C)}{P(t < T)} . \quad (45)$$

This necessitates a large number of samples required to obtain accurate CDF's at small probability levels.²¹

3.3 Approximate Methods—Reliability

The PDS method described in this dissertation employs the reliability method approach for determining the statistical structural response characteristics of interest. This methodology grew out of approximate techniques developed to obtain the moments of the response variable g directly from the moments of the input rv's.²² For clarity, the theory will be first presented for a response variable g that is a function of two input rv's, x and y . The first two moments of each rv are defined as the means μ_x and μ_y and the standard deviations σ_x and σ_y . These response moments can be used to determine the approximate probability density function of g , and by themselves are useful for design and analysis. The first step is to expand g as a Taylor's series about the means of the input rv's.

$$\begin{aligned}
g(x,y) = & g(\mu_x, \mu_y) + \frac{\partial g(\mu_x, \mu_y)}{\partial x}(x - \mu_x) + \frac{\partial g(\mu_x, \mu_y)}{\partial y}(y - \mu_y) \\
& + \frac{1}{2} \left(\frac{\partial^2 g(\mu_x, \mu_y)}{\partial x^2}(x - \mu_x)^2 + \frac{\partial^2 g(\mu_x, \mu_y)}{\partial y^2}(y - \mu_y)^2 + 2 \frac{\partial^2 g}{\partial x \partial y}(x - \mu_x)(y - \mu_y) \right) + \dots \quad (46)
\end{aligned}$$

Now, the mean of g can be obtained by taking the expectation of both sides

$$\begin{aligned}
\mu_g = & g(\mu_x, \mu_y) + \frac{1}{2} \left(\frac{\partial^2 g(\mu_x, \mu_y)}{\partial x^2} [E(x^2) - \mu_x^2] + \frac{\partial^2 g(\mu_x, \mu_y)}{\partial y^2} [E(y^2) - \mu_y^2] \right. \\
& \left. + 2 \frac{\partial^2 g}{\partial x \partial y} E[(x - \mu_x)(y - \mu_y)] \right) + \dots \quad (47)
\end{aligned}$$

and the standard deviation of g is

$$\begin{aligned}
\sigma_g^2 = & \left(\frac{\partial g(\mu_x, \mu_y)}{\partial x} \right)^2 [E(x^2) - \mu_x^2] + \left(\frac{\partial g(\mu_x, \mu_y)}{\partial y} \right)^2 [E(y^2) - \mu_y^2] \\
& + \text{products of cross partials} + \text{higher order terms} + \dots \quad (48)
\end{aligned}$$

These expansions obviously have to be truncated at some point for tractability. Wirshing performed detailed studies in 1975 of the errors in the mean and standard deviation resulting from using only first order, second order, and other selected terms from the series for selected linear and nonlinear functions of the rv's.²³ As can be seen from equation (47) and (48), the error in the mean is directly related to the degree of nonlinearity, indicated by the second partial term, and the size of the standard deviations of the input rv's, as indicated by the other term in the product. A relative measure of the size of the standard deviation is the coefficient of variation (cov), which is defined as the standard deviation divided by the mean. For some simple nonlinear functions of two rv's, Wirshing found that the error can be up to 20 percent using only the first order terms for high levels of the coefficients of variation such as 0.2. It is therefore clear that first order methods can result in significant errors for evaluating the mean and standard deviation in the case of nonlinear functions of rv's.

“Reliability” methods were developed by initially adapting the terminology discussed above to the analysis of structures. The goal of reliability analysis is to determine an expression for the probability of failure of a structure, which is one minus the probability of reliability. The exact value is obtained

by calculating the volume of the joint probability function of the vector of multiple input rv's \mathbf{X} that influence the structural characteristics over the failure region Ω :

$$P_f = \int_{\Omega} f(\mathbf{X}) d\Omega \quad , \quad (49)$$

where P_f is the probability of failure and $f(\mathbf{X})$ is the joint probability distribution function for \mathbf{X} . Due to the difficulty of evaluating this integral, the following approximate procedures have been developed to determine P_f . For these methods, the function of input rv's g is defined as the “limit state function” $g(\mathbf{X})$:

$$g = \text{strength} - \text{load} \quad . \quad (50)$$

For this definition, the probability of failure is the probability that $g < 0$. Cornell,²⁴ using the reliability approach, developed the “first order, second moment” method by truncating the higher order terms from the Taylor series derived in the previous section:

$$g(\mathbf{X}) \cong g(\mu_x) + \sum_{i=1}^N \frac{\partial g}{\partial x_i} (x_i - \mu_i) \quad . \quad (51)$$

This resulted in the following simple approximations for μ and σ of g :

$$\mu_g \cong g(\mu_x) \quad ; \quad (52)$$

$$\sigma_g \approx \sqrt{\sum \left(\frac{\partial g}{\partial x_i} \right)^2 \sigma_{x_i}^2} \quad (53)$$

Hasofer and Lind²⁵ further refined and expanded this method, now entitled the first order reliability method (FORM). They redefined g as

$$g(\mathbf{X}) = Y(\mathbf{X}) - y \quad , \quad (54)$$

where y is a specific value and the performance function (or response surface) $Y(\mathbf{X})$ is a function of the rv's. The plot of $g(\mathbf{X})=0$ will be a line on the \mathbf{X} plane, dividing it into two parts, $g < 0$ ($Y < y$) and $g > 0$ ($Y > y$). The probability that the function Y not exceed the value y is the probability that $g < 0$. For example, if $Y(\mathbf{X})$ is a specific eigenvalue of interest, and we wish to know the probability that $Y(\mathbf{X})$ is less than a particular value y , then that probability is equivalent to $P(g < 0)$. There will therefore be a limit state function g for every value of y possible over some range of interest. If the distributions of the rv's are normal and the resulting distribution of g is normal, then the following steps can be performed to obtain the probability that $g < 0$ ($Y < y$). First, a transformation of g to standard normal coordinates Z is made as follows:

$$Z = \frac{g(\mathbf{X}) - \mu_g}{\sigma_g} , \quad (55)$$

and if β , which Cornell had termed the safety index, is defined as

$$\beta = \frac{\mu_g}{\sigma_g} , \quad (56)$$

then

$$P(g(\mathbf{X}) < 0) = p(Z < -\beta) = \Phi(-\beta) , \quad (57)$$

where Φ is the CDF of the standard normal distribution function found in handbooks. Since negative values for β are not tabulated, the relationship

$$\Phi(-\beta) = 1 - \Phi(\beta) \quad (58)$$

is used instead to calculate this probability. The complete CDF for $Y(\mathbf{X})$ is formed by finding the β 's for all the specific values of y in the probability range of interest. One problem with this method is that g can be formulated differently for some cases, thereby yielding different probabilities. To provide invariance with respect to the formulation of g , Hasofer and Lind introduced an initial reduction of each of the primitive normal rv's x_i into standard normal rv's u_i using

$$u_i = \frac{x_i - \mu_{x_i}}{\sigma_{x_i}} . \quad (59)$$

This transformation allows the new limit states $g(\mathbf{U}) = Y(\mathbf{U}) - y = 0$ to be plotted in standard normal joint probability space for every possible y . An essential point of the reliability methods becomes evident at this point. For a linear limit state function of normally distributed rv's, the multidimensional bell-shaped volume under the joint probability density function bounded by the planar limit state function is exactly equivalent to a one-dimensional probability density function up to the point β (see fig. 2). The joint probability of $g < 0$ will be the volume under the joint PDF over the area where $g < 0$. β can be shown to be the shortest distance from the origin to the line $g(\mathbf{U}) = 0$; the point on the line $g=0$ having the shortest distance (β) to the origin is termed the most probable point (MPP) because that point will have the highest probability of occurrence of any point along the line $g(\mathbf{U})=0$. The MPP is also called the *design point* \mathbf{X}^* , because it is the vector of input rv's that will generate the probability level obtained from $\Phi(-\beta)$. For a nonlinear limit state, as shown in figure 1, one source of error for this probability value is the degree to which the volume bounded by the curved plane is different than that bounded by the linear plane. Because the volume rapidly drops off away from the MPP, this error is usually small.

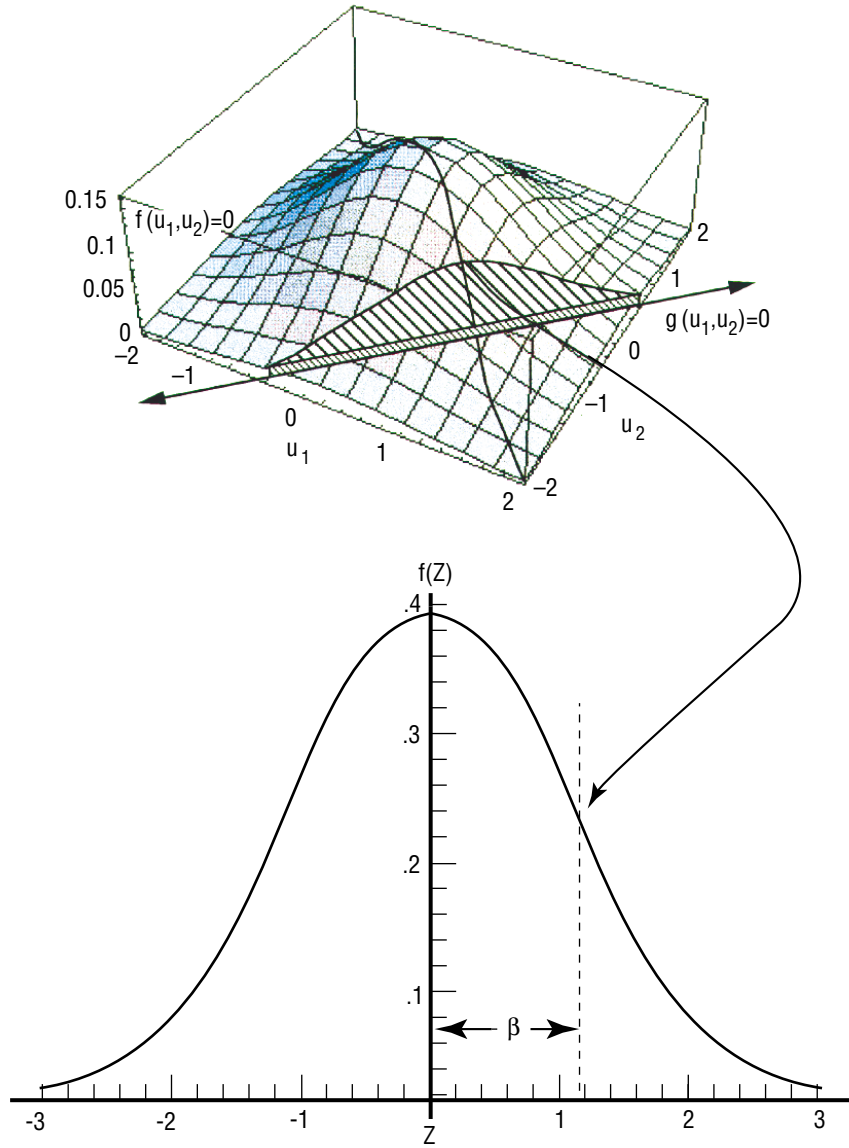


Figure 2. Reduction of two-dimensional joint PDF to one-dimension.

The derivation above is used in the case when the origin is in the “success” region (i.e., $g(\mathbf{U}=0) > 0$) and will yield probability levels < 0.5 . If the origin is in the “failure” region ($g(\mathbf{U}=0) < 0$), then β is defined to be the negative of the distance from the origin to the MPP.²⁶ Applying the Gaussian CDF function for this value will therefore yield probabilities > 0.5 ; if the distance δ is defined such that $(\delta \equiv -\beta) > 0$, then

$$\Phi(-\beta) = \Phi(\delta) > 0.5 \quad . \quad (60)$$

An example of a closed-form limit state function is shown below to illustrate this method. Consider a cantilever beam of length $L = 1$ and with statistically characterized input rv's load P and plastic moment strength M (see fig. 3). P is normally distributed with mean of 12 and standard deviation of 1,

and M is normally distributed with mean of 40 and standard deviation of 3. Failure can be defined as $M < P \cdot L$, so a limit state function in M and P is formulated as

$$g(M, P) = M - PL \quad , \quad (61)$$

where $g < 0$ corresponds to failure. The primitive rv's M and P are now converted to standard normal variables m and p ,

$$m = \frac{(M - 40)}{3}; \quad p = P - 12 \quad . \quad (62)$$

In terms of m and p , the limit state function is

$$g = (3m + 40) - (p + 12) \quad (63)$$

Setting $g=0$ results in an equation for m as a function of p , which can be plotted in the reliability space as shown in figure 3. The design point, or MPP, is located at the shortest distance from the limit state g to the origin. The distance β can then be calculated using the distance equation from the origin to a line and substituted into equation (58) to obtain the probability of failure for this system.

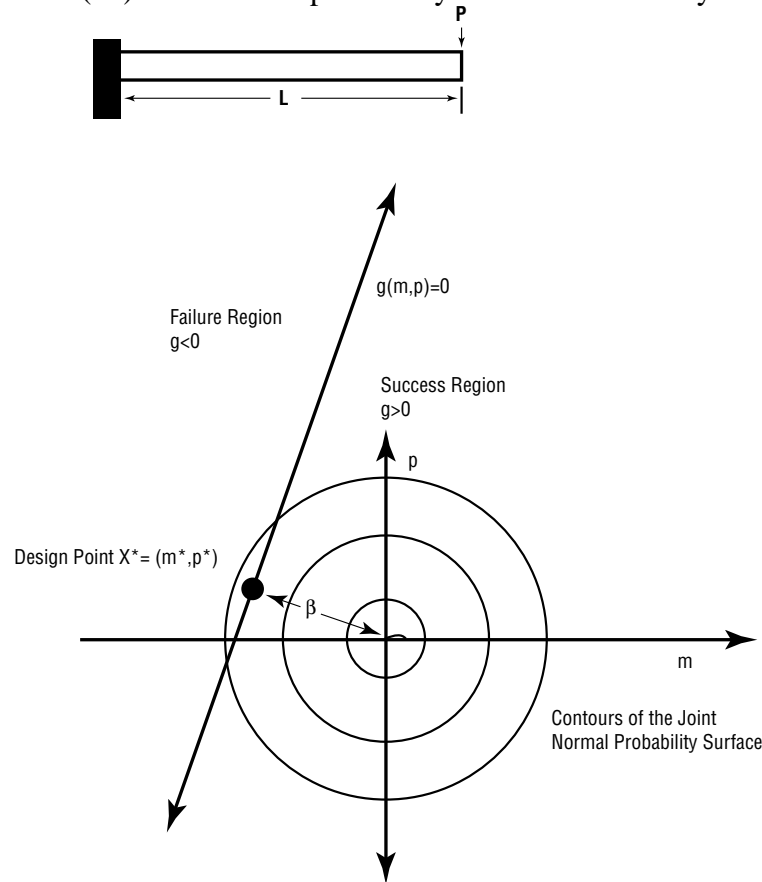


Figure 3. Reliability space for two standard, normal rv's.

In the general case, the FORM contains several sources of error for the prediction of P_f , especially if the actual response function is nonlinear. First, it assumes that the original input distributions are Gaussian, although this assumption is addressed.

later in this section. Second, it approximates the slice between the failure and safe regions of the volume under the joint probability surface by a straight plane, as opposed to the curved surface that would arise from a nonlinear g function. Finally, one of the main sources of error is the inaccuracy in the calculated location of the MPP's. Errors in the location of an MPP can arise due to a number of reasons, some of which are identified in examples described in section 3.4.

The reliability method was expanded by Rackwitz in 1976 to multidimensional problems for which the limit state curve $g=0$ is an explicit, nonlinear function of the rv's.²⁷ This, of course, makes the determination of β much more difficult. The method makes use of an iterative algorithm to find β . Initially, an assumed value of the design point \mathbf{X}^* is chosen. The rv's are then converted to standard normal variables u_i using equation (59). Lagrange techniques are used to minimize the distance β from the limit state curve $g=0$ to the origin, resulting in the following set of expressions for each of the standard normal rv's:

$$u_i = -\alpha_i^* \beta, \quad i = 1, 2, \dots, n, \quad (64)$$

where the gradient unit vector components α_i^* are defined as

$$\alpha_i^* \equiv \frac{\frac{\partial g}{\partial u_i}}{\sqrt{\sum_{j=1}^n \left(\frac{\partial g}{\partial u_j} \right)^2}}. \quad (65)$$

The substitution of equation (64) into equation (59) yields the expression

$$x_i^* = \mu_{x_i} - \alpha_i^* \sigma_{x_i} \beta. \quad (66)$$

Using the assumed values for each primitive rv, these expressions are substituted into the limit state function $g=0$, yielding a single equation for β . An updated design point u_i^{*1} is then obtained by evaluating equation (64) using the new value of β . The process is iterated until convergence of β is reached. An entire CDF is obtained by using equation (54) to define limit states for the entire range of possible response values, and obtaining β for each of these limit states.

Rackwitz and Feissler continued the development of this method by examining how to develop an "equivalent normal rv" for nonnormal rv's.²⁸ The starting point of this procedure is to obtain \mathbf{X}^* using the algorithm discussed above for each rv in \mathbf{X} and then determine the actual CDF values, $F(x^*)$,

and PDF values, $f(x^*)$, for that point. An equivalent rv z^* is then defined as a function of the design point x^* and the unknown equivalent normal mean and standard deviation parameters, denoted by μ_x^n and σ_x^n , respectively,

$$z^* = \frac{x^* - \mu_x^n}{\sigma_x^n} . \quad (67)$$

At this point, $F(x^*)$ and $f(x^*)$ are set equal to a normal CDF and PDF, which are identified by Φ and ϕ respectively, at the same value of x^*

$$\Phi(z^*) = F(x^*) , \quad (68)$$

$$\frac{\phi(z^*)}{\sigma_x^n} = f(x^*) . \quad (69)$$

The simultaneous solution of the two equations yields μ_x^n and σ_x^n and is shown graphically in figure 4. The new rv with parameters μ_x^n and σ_x^n is used in the iteration procedure described previously until convergence on β is obtained.

Chen and Lind further modified this method by adding a scaling factor γ to the matching process, calling the overall procedure “fast probability integration” (FPI).²⁹ This factor is used to multiply the normal distribution in order to match not only the CDF and PDF values but also the slope of the PDF with that of the actual distribution at the design point, which is usually near the tails. This results in a “three-parameter approximation,” where the three equations used to find the equivalent normal distributions are:

$$\gamma \Phi(z^*) = F(x^*) \quad (70)$$

$$\frac{\gamma}{\sigma_x^n} \phi(z^*) = f(x^*) \quad (71)$$

$$-\frac{\gamma z^*}{\sigma_x^n} \phi(z^*) = \frac{\partial f(x^*)}{\partial x} . \quad (72)$$

Of course, the new “normal distribution” is not mathematically feasible since the final CDF value will equal γ_i instead of unity, but the shape of the distribution in the vicinity of the design point will be very accurate, which is the primary use of this three-parameter distribution.

Second order reliability methods (SORM), which approximate the limit state with a higher order series expansion, have also been examined. The goal of these methods is to describe nonlinear g functions more accurately to obtain better determinations of the location of the MPP. Rackwitz and Fiessler introduced a parameter for measuring reliability in addition to β by examining the effect of keeping the

second order terms in the Taylor series expansion and considered the different quadratic forms that could be used in the analysis.³⁰ They concluded that FORM was adequate for most engineering problems, especially if the rv's were not too far away from normal.

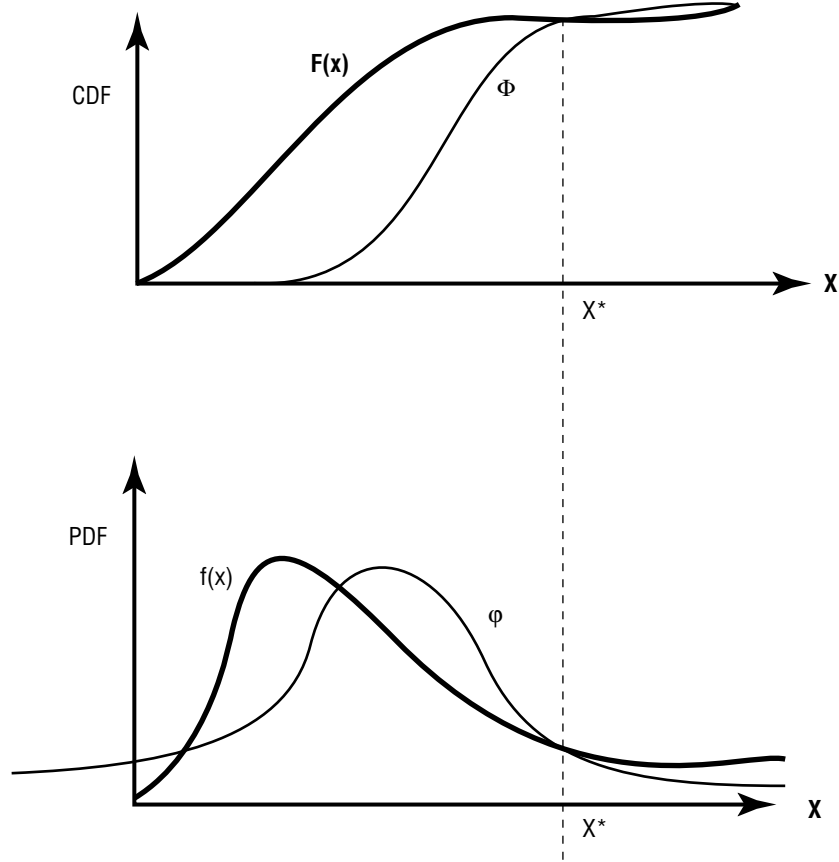


Figure 4. Matching actual and “equivalent” normal distribution.

The application of FORM and its extensions for nonexplicit limit state functions, as is the case for large structural finite element models, requires the use of numerical differentiation to obtain a first order approximation of the performance function $Y(\mathbf{X})$, as defined in equation (54).³¹ The module FPI of the general probabilistic structural analysis code NESSUS implements this differentiation, which is defined by the following equation:

$$Y(\mathbf{X}) = a_0 + \sum_{i=1}^N a_i (x_i - \mu_{xi}) , \quad (73)$$

where

$$\begin{aligned} a_0 &= Y(\mu_x) \\ N &= \text{number of rv's} . \end{aligned} \quad (74)$$

$$a_i \approx \frac{\Delta Y}{\Delta x_i}$$

The expansion point a_0 is about the mean value μ_{x_i} of each of the rv's. The range of response values for a desired probability range is estimated based on the approximate mean and standard deviation as calculated using equations (52) and (53). These specific values of y are then substituted in equation (54) to generate a limit state equation $g(X)$ for each value. This limit state is used to obtain β and the most probable point for each desired response value as outlined in the preceding discussion. In addition to the errors discussed previously, since the limit state curves are all based upon the expansion at the mean, there will be some error for the probability levels obtained if the curvature of the function changes away from the mean.

Alternatively, a CDF can be constructed directly from the approximate mean and standard deviation if the distribution is assumed to be Gaussian. This is essentially the original "first order, second moment" method as defined by Cornell. For linear functions of normal rv's, this CDF will be identical to that obtained using the MPP iterative search contained in the FORM procedure described above. Although it is more direct, implementation of this procedure actually requires an additional step since NESSUS/FPI automatically assumes that the input rv's might be nonnormal and therefore always calculates the CDF using the MPP search procedure. Nevertheless, calculation of this CDF outside of the NESSUS program using the Gaussian CDF function can prove illustrative in some cases.

In 1987, Wu and Wirshing developed a procedure for improving the accuracy of probability levels obtained by FORM for nonexplicit limit states by using a partial second order expansion.³² This procedure is called the advanced FORM (AFORM). Initially, the FORM is performed and MPP's obtained. The limit state is then expanded about each MPP using only the first order and the pure (no mixed variable terms) second order terms of equation (47). This is accomplished by performing the numerical calculation of g at the mean of the rv's and at two other points (at least) for every input rv x_i , resulting in the following new approximation for the limit state:

$$g(x) = \sum_{i=1}^n a_i (x_i - x_i^*) + b_i (x_i - x_i^*)^2, \quad (75)$$

where the coefficients a_i of the first order terms and b_i of the quadratic only terms are obtained by a least-squares curve fit of these points. Rather than continue to use this partial second order approximation, the quadratic is transformed using algebraic manipulation to a linear function of a set of new rv's r_i :

$$g(\mathbf{r}) = c_0 + \sum_{i=1}^n b_i r_i, \quad (76)$$

in which

$$c_0 = -\frac{1}{4} \sum_{i=1}^n \frac{a_i^2}{b_i} \quad (77)$$

and

$$r_i = \left(x_i - \left(x_i^* - \frac{a_i}{2b_i} \right) \right)^2 . \quad (78)$$

The probability transformation rules discussed in Section 3.1 are then applied to x_i to obtain the distributions of r_i , which will no longer be Gaussian. Therefore, the three parameter normal fit developed by Chen and Lind is used to find equivalent normal distributions for r_i . Using the equivalent normal rv's, the Rackwitz-Feissler algorithm is applied to generate new MPP's and associated β 's. The new probability value for this β is calculated by multiplying the probability obtained using the normal cumulative distribution function of β times the product of the γ_i scale factor for each transformed rv:

$$p_f = \Phi(\beta) \prod_{i=1}^n P(\gamma_i) . \quad (79)$$

These probabilities have been found to be an improvement over the original values using FORM for slightly nonlinear functions. However, for some nonnormal distributions of the input rv's or for substantially nonlinear functions, the Rackwitz-Feissler algorithm may not converge to a β and so AFORM is not as "robust" as the FORM method.³³

In cases where the AFORM does not converge or yield realistic answers, use of the "approximate statistics" generated at the first stage of the procedure can provide a useful CDF. These statistics are generated directly from the partial quadratic form of equations (47) and (48). In addition to the approximate mean the approximate median, which is the first term in equation (47) (and which is equal to the approximate mean for the first order approximation) is output. These three parameters can be used to generate a lognormal distribution X , which is defined as the antilog of a normal distribution Y , with the mean μ_X , median \tilde{X} , and standard deviation σ_X related to the mean μ_Y and standard deviation σ_Y in the following manner:³⁴

$$\mu_Y = \ln \tilde{X} \quad (80)$$

$$\sigma_Y^2 = \ln \left(1 + \left(\frac{\sigma_X}{\mu_X} \right)^2 \right) . \quad (81)$$

This method is accurate for slightly nonlinear functions of normal rv's, which generally transform to lognormal distributions of the new rv's.

Wu also developed the advanced mean value (AMV) method, a procedure for updating the FORM or AFORM solution by using the original, exact solution for g .³⁵ Initially, equivalent normal rv's are obtained for any nonnormal rv using the Chen-Lind method. Values of β and \mathbf{X}^* are then obtained for each desired limit state. Each resulting design point is inaccurate, though, for a nonlinear (for

FORM) or nonquadratic (for AFORM) limit state, because the approximate limit state function cannot track the actual MPP accurately, or if the curvature of the response surface varies away from the mean. This will be illustrated in the example in section 3.4. A relatively simple improvement can be obtained by transforming the values of the MPP's to the original nonstandard normal space, and substituting them into the exact equation for the limit state, which for structural analysis is usually a finite element model, to obtain new response levels associated with the original probability values. Mahadevan explains that this incorporates some of the nonlinearity of the actual limit state without having to resort to the complexities of using a complete second order approximation.³⁶ This method has been shown to be very accurate for several examples given in the literature.

Further iterations, which are called AMV+, can be performed by expanding the limit state about each most probable point instead of about the means as was performed in equation (73). This is a very tedious process, and has not been implemented to a significant extent in this research. Both AMV and AMV+ have been incorporated in NESSUS, but these automated features were not used in this research due to the use of independent FORTRAN codes outside of NESSUS. The incorporation of the automated implementation of these methods is one avenue for future work.

3.4 Comparison of Reliability Methods

In this section, some of the reliability concepts discussed in section 3.3 are compared and illustrated. Table 1 summarizes the basic premises and areas of applicability of each method. These methods are demonstrated with an example. Consider a simple nonlinear limit state function of two rv's, X_1 and X_2 , with means μ_{X_1} and μ_{X_2} and standard deviations σ_{X_1} and σ_{X_2} , respectively. These rv's are transformed to standard normal variables x_1 and x_2 using equation (59). Assume that the exact function of a desired response variable Y in terms of the standard normal rv's, defined as the response surface $Y(x_1, x_2)$, is

$$Y(x_1, x_2) = 6 + x_1 + x_2 + 0.25x_1^2 - 0.25x_2^2 + 0.25x_1x_2 \quad (82)$$

as plotted in figure 5(a). The limit state function is therefore formulated according to equation (54) in terms of the transformed rv's, the response function (or surface) Y , and specific response values y :

$$g(x_1, x_2) = Y(x_1, x_2) - y. \quad (83)$$

A plot of the function $g(x_1, x_2) = 0$ can be obtained for several different values of y by creating a contour plot of the response surface Y , shown in figure 5(b), where the legend identifies the values of y associated with the different curves $g=0$. For a response level of $y = 8$, the exact CDF probability level can be determined using the program "Mathematica." First, the variable x_1 is expressed as a function of x_2 , requiring the solution for the roots of the polynomial $g = 0$ formulated using equation (83). The root corresponding to the $g=0$ curve at $y=8$ is

$$x_1(x_2) = -2 - 0.5x_2 - 1.11803\sqrt{9.6 - 1.6x_2 + x_2^2}. \quad (84)$$

Table 1. Comparison of reliability methods.

Method	Method of Approximation of Limit State Function	Method for Obtaining CDF	Types of rv's Allowed	Accuracy for Linearity of Limit State
FORM (first order reliability method)	Linear approximation	MPP iterative search	All types of rv's	Robust, medium level of accuracy for all levels of linearity
Linear Approx. Statistics	Linear approximation	Gaussian Distribution using μ and σ	Normal rv's only	Accurate for linear functions
AFORM (advanced FORM)	Linear approximation	MPP iterative search, linear transformation of rv's, improved β	All types of rv's	Accurate for slightly nonlinear functions
Partial Quadratic Approx. Stats	Partial quadratic approximation	Lognormal Distribution using μ, σ , and $\tilde{\chi}$	Normal rv's	Accurate for quadratic functions
AMV Update of FORM or AFORM	Linear or partial quadratic	Update response value associated with MPP using exact limit state calculation	All types of rv's	Improved results for nonlinear functions using FORM or AFORM

The double integral of the Gaussian probability density function bounded by the limit state is then calculated numerically over the domain $-\infty < x_1 < x_1(x_2)$, $-\infty < x_2 < \infty$:

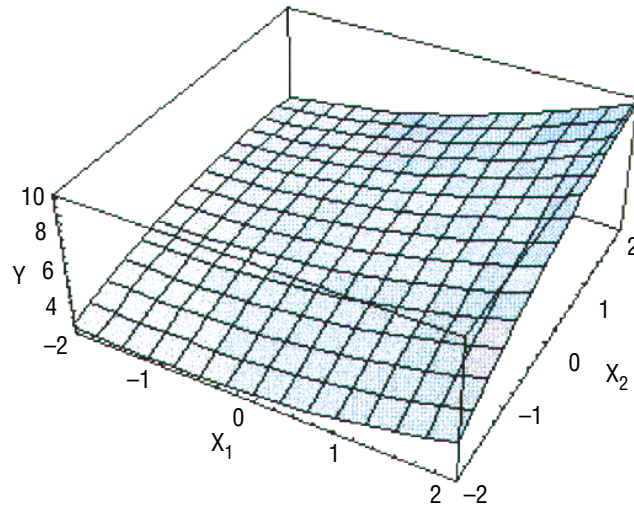
$$P(Y < 8) = \int_{-\infty}^{\infty} \left(\int_{-\infty}^{x_1(x_2)} \frac{\exp\{\frac{1}{2}(-x_1^2 - x_2^2)\}}{2\pi} dx_1 \right) dx_2 \quad (85)$$

This yields an exact probability of 0.90605.

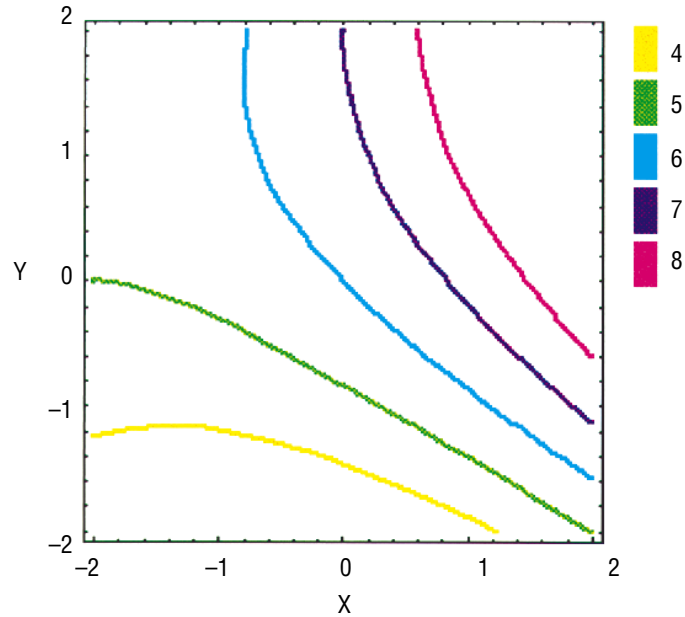
The FORM method is applied by initially generating a linear approximation g_{lin} of the function Y by expanding about the mean, resulting in

$$g_{lin} = 6 + x_1 + x_2 - y \quad (86)$$

A plot of this surface is shown in figure 6(a). As with the exact function, now termed g_{exact} , plots of $g_{lin} = 0$ for various values of y can be made using a contour plot of the linear response surface $Y_{lin} = 6 + x_1 + x_2$, as shown in figure 6(b). To illustrate the MPP searching procedure in FORM and some of the errors involved with the linear approximation, the plot of the Gaussian PDF and its contour plot are generated (see fig. 7(a)–7(b)). The values of the PDF are identified on the contours. The MPP searching algorithm is performed graphically by superimposing all three contour plots in figure 7(c). The MPP on $g_{lin} = 0$ at a specific value of $y = 8$ is first determined by locating the point on the linear contours closest to the origin, specified at point “A.” The value of the CDF is obtained by graphically determining the coordinates of the MPP to be (1,1), calculating the distance β to the origin, and using the Gaussian CDF function to calculate a probability level of 0.92135 for $y=8$, an error of +1.7 percent from



(a) Plot of exact response surface $Y(x_1, x_2)$.

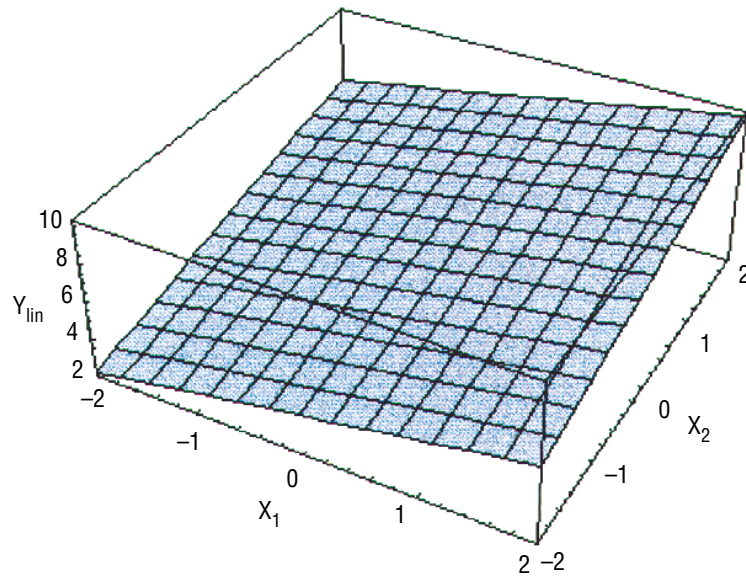


(b) Contour plot of response surface showing $g=0$ curves.

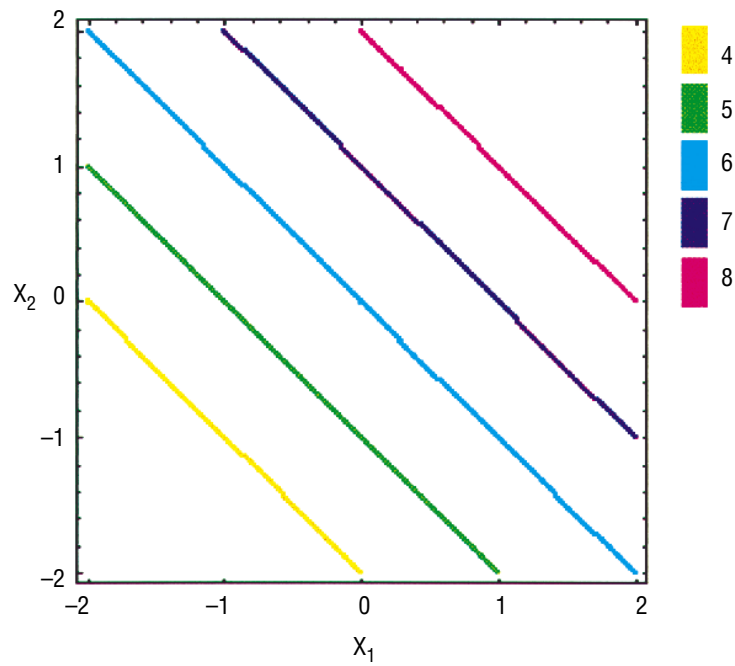
Figure 5. Plots of exact response function $g_{\text{exact}}(x_1, x_2)$.

the exact value calculated above. This example illustrates the error due to the inability of the linear response surface to track the MPP's accurately, which, for the exact limit state, is approximately at point "B."

The AMV method is applied by substituting x_1 and x_2 at the MPP "A" into $Y_{\text{exact}}(x_1, x_2)$ and obtaining an updated response value of 8.75. This is still associated with the original probability value obtained using FORM of 0.92135. For comparison with the exact formulation, the AMV procedure can be iterated to find the point on the FORM MPP locus (the gradient of the linear response surface) that has an exact y value of 8. Since x_1 and x_2 are equal along this locus, the MPP is solved for in the equation $0 = 2x_1 + 0.25x_1^2 - 2$ to obtain point "C" at (0.899, 0.899). This results in a probability value of 0.8982, which has an error of -0.87 percent from the exact value for $y=8$, an improvement over the original FORM result.

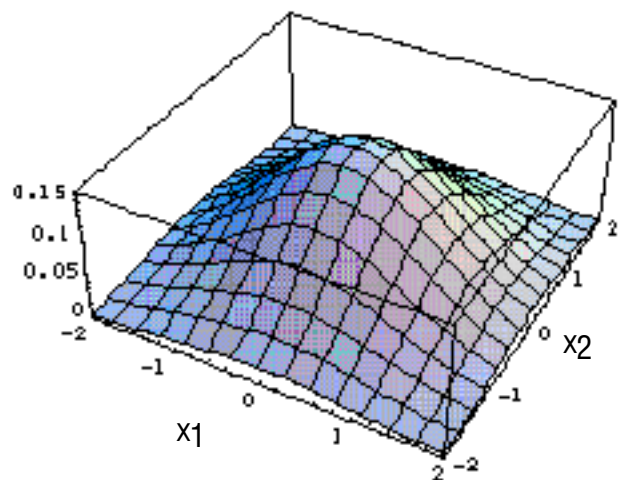


(a) Plot of linear response surface Y_{lin}

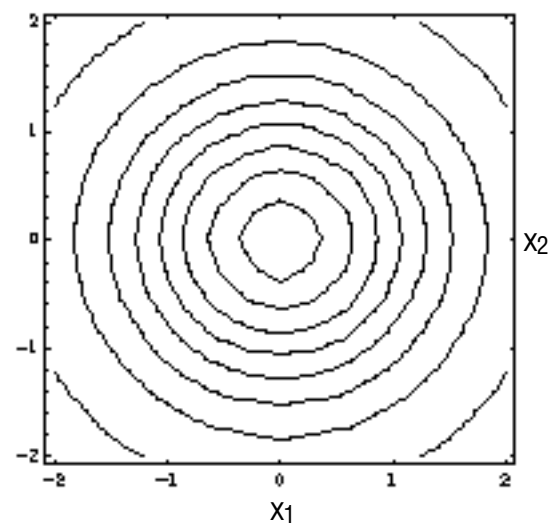


(b) Contour Plot of response surface showing $g=0$ curves

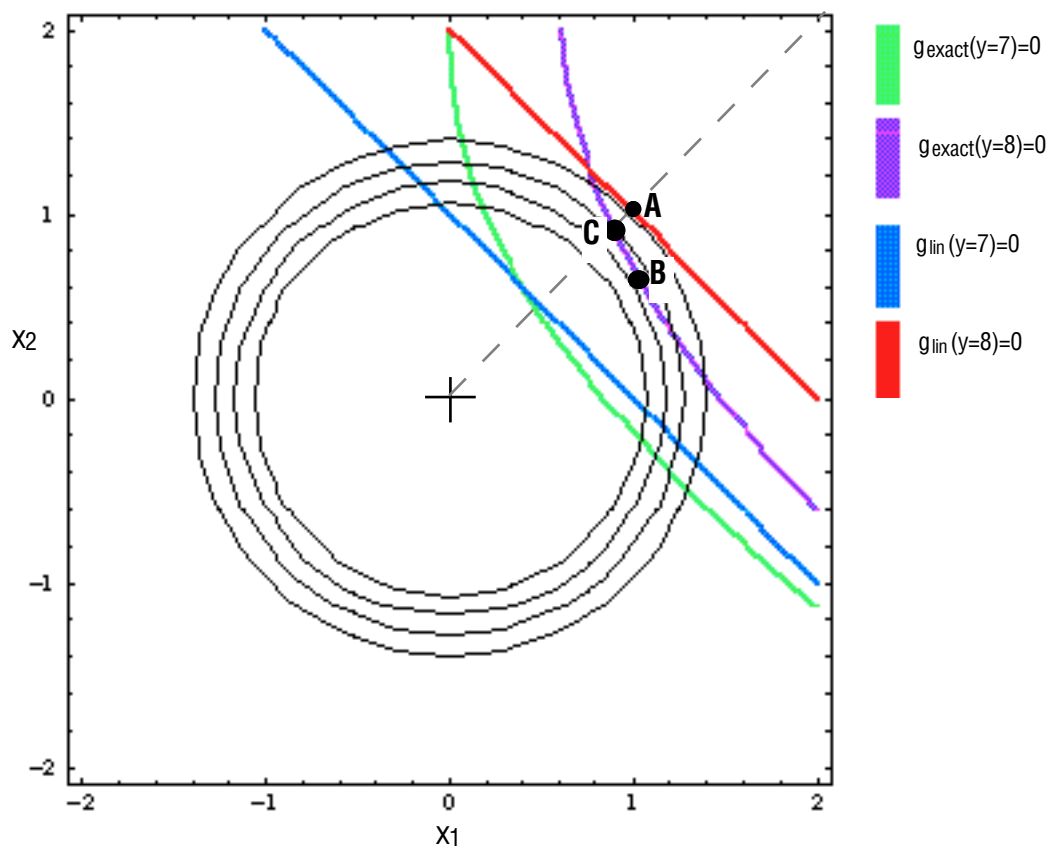
Figure 6. Plots of linear approximation of response $(g_{lin}x_1, x_2)$.



(a) Gaussian PDF of two standard normal rv's.



(b) Contour plot of PDF.



(c) Superposition of contour plots to obtain MPP's and probability.

Figure 7. Obtaining MPPs for FORM, AMV.

The AFORM method is illustrated by representing the limit state in a partial quadratic form defined as g_{pquad} :

$$g_{pquad} = 6 + x_1 + x_2 + 0.25x_1^2 - 0.25x_2^2 - y \quad (87)$$

Plots of the partial quadratic response surface and its contour graph are shown in figure 8 (a) and (b), respectively. The MPP for $y = 8$ is estimated graphically to be point A at (1.163,0.584), and a CDF value of 0.9035 is calculated using the Gaussian CDF function, an error of -0.3 percent from the exact value. The exact determination of the MPP point for nonlinear limit state functions is performed using the Rackwitz-Feissler algorithm described earlier. The contour plot of the exact equation and its estimated MPP at point “B” is superimposed for reference. This result shows a considerable improvement using AFORM compared with FORM.

For illustrative purposes, the MPP technique for determining the CDF, which is equivalent to integrating the probability volume bounded by a linear slice tangent to the $g=0$ curve at the MPP, is applied for the exact function $g_{exact}=0$ for $y=8$. Using the estimated MPP at point “B” of (1.7232, 0.5514), the distance to the origin is calculated and the Gaussian CDF function yields a probability value of 0.88605. This value is less than the exact number obtained previously since the contour $g_{exact}=0$ for $y=8$ curves away from the mean, yielding a larger probability volume than the linear slice method. Since this function is substantially nonlinear, this error is -2.2 percent, which although small, is of the same magnitude as the errors due to tracking of the MPP.

The entire CDF for this function was then examined. The distribution for the exact limit state was performed using the “Mathematica” integration methodology described above and verified using a 40,000 sample MC run in NESSUS, which can accept user-supplied explicit limit state equations as input. These results are compared with NESSUS applications of FORM and AFORM in figure 9. Calculating the error based on the exact CDF value, the AFORM varies from -0.4 percent error at $y=9$ to -7.5 percent error at $y=6$, while the FORM errors are all slightly larger.

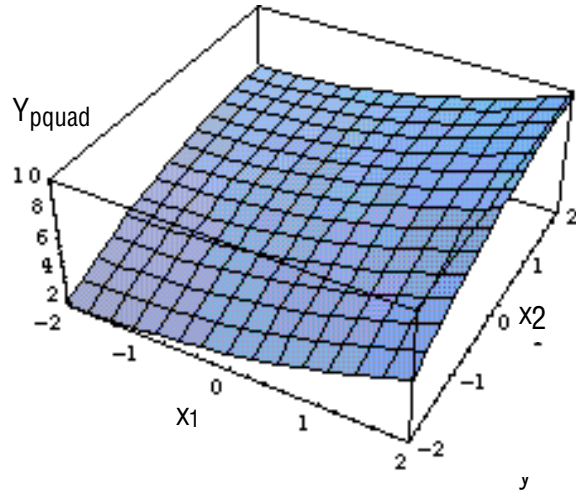
3.5 Approximate Methods—Perturbation

The perturbation method is a method for deriving an analytical expression for the change in value of a desired response variable as a direct function of the perturbation of the system matrix. For the eigenvalue problem, as explained in detail by Meirovitch,³⁷ it is seen to be a method of obtaining the variation in the eigenvalues and eigenvectors of a system due to a change in the mass and stiffness matrices without having to resolve the characteristic polynomial. Consider the N dof structural free-response problem, which can be expressed as an eigenvalue problem in the form of

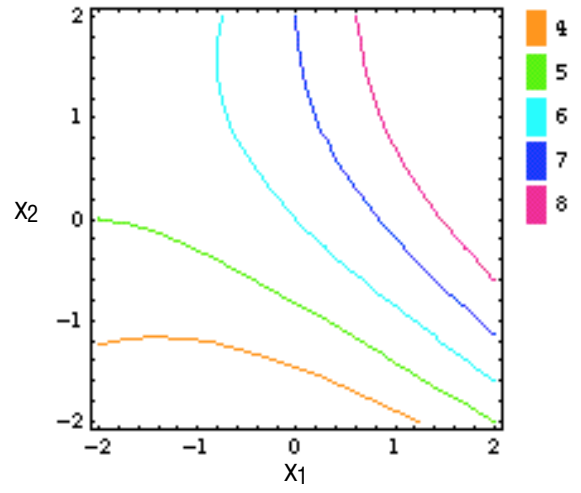
$$[K]\{\phi\}^i = \lambda^i [M]\{\phi\}^i \quad (88)$$

where $\{\phi\}^i$ is the i 'th modal vector. Usually, this can be converted to the standard eigenvalue problem by inverting $[M]$ and premultiplying both sides to obtain

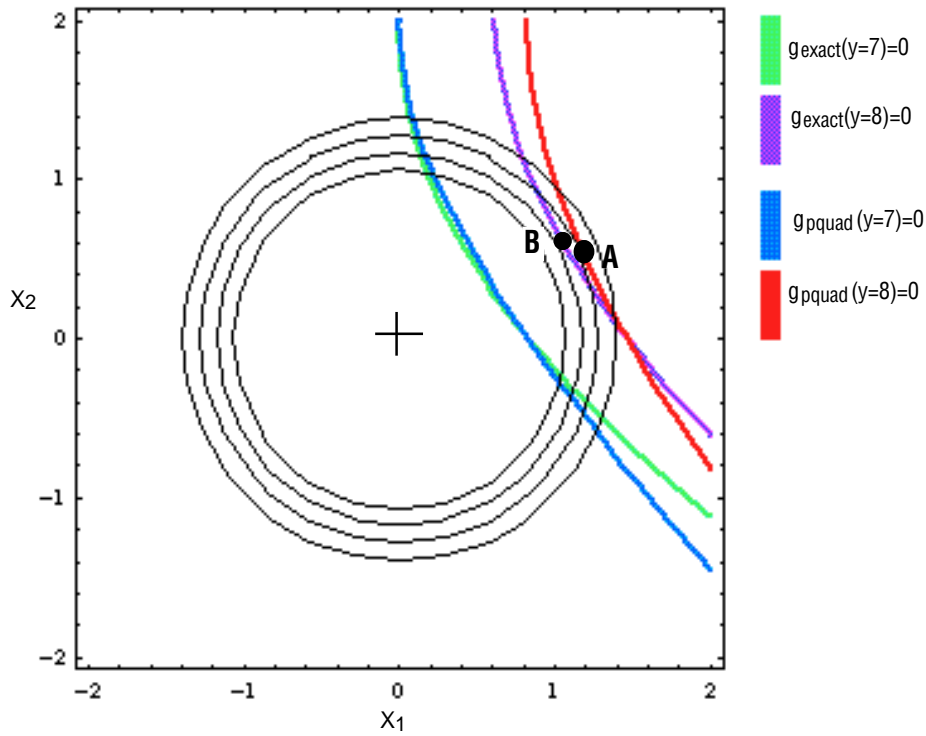
$$[A]\{\phi\}^i = \lambda^i \{\phi\}^i \quad (89)$$



(a) Plot of partial quadratic approximation response surface Y_{pquad} .



(b) Contour plot of response surface



(c) Superposition of contour plots to obtain MPP's and probability.

Figure 8. Obtaining MPPs for AFORM.

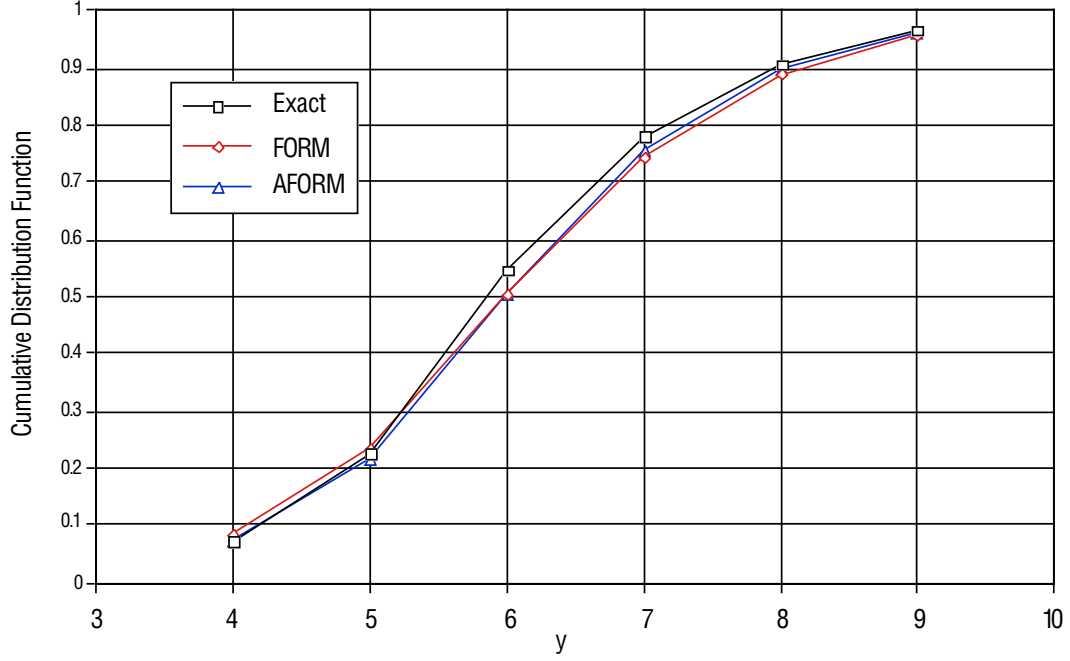


Figure 9. Comparison of methods for obtaining CDF of explicit nonlinear limit state.

where

$$[A] = [M]^{-1} [K] \quad (90)$$

Now, let $[A]$ be perturbed by a small variation such that

$$[A]_p = [A]_o + [\delta A] \quad (91)$$

where

$$\begin{aligned} [A]_o &= [M]^{-1} [K] = \text{original unperturbed system matrix} \\ [\delta A] &= \text{small change in } A \text{ (matrix quantity)} \\ [A]_p &= \text{perturbed matrix} \end{aligned}$$

The eigenvalues and eigenvectors can be expressed in a perturbed form similar to that used above for $[A]$:

$$\lambda_p^i = \lambda_o^i + \delta \lambda^i \quad (92)$$

$$\{\phi\}_p^i = \{\phi\}_o^i + \delta \{\phi\}^i \quad (93)$$

where the subscript “o” represents the original, unperturbed value.

The expressions for the perturbed matrices are now substituted into equation (89):

$$([A]_o + [\delta A])\left(\{\phi\}_o^i + \{\delta\phi\}^i\right) = \left(\lambda_o^i + \delta\lambda^i\right)\left(\{\phi\}_o^i + \{\delta\phi\}^i\right) . \quad (94)$$

This set of N equations in $N+1$ unknowns can be solved for in terms of the known original quantities $([A]_o, \lambda_o, \{\phi\}_o)$, and the size of the perturbation of the elements in $[A]$ and $[\delta A]$, by multiplying out equation (94) and assuming the effect of the second order terms is negligible. This enables a direct expression for the perturbation of λ and ϕ without resolving the eigenvalue problem. These results are

$$\delta\lambda^i = \{\phi\}_o^i{}^T ([\delta A]) \{\phi\}_o^i \quad (95)$$

$$\delta[\Phi]^i = \sum_{k=1}^n \frac{\{\phi\}_o^k{}^T ([\delta A]) \{\phi\}_o^i}{\lambda_o^i - \lambda_o^k} (\{\phi\}_o^k) , \quad i, k = 1, \dots, n ; i \neq k , \quad (96)$$

where $[\Phi]^i$ is the complete modal matrix. These first order correction terms can be substituted into equations (92) and (93) to obtain the new eigenvalues and eigenvectors.

In the late 1960's, this method was applied by Collins and Thomson,³⁸ Kiefling,³⁹ and Collins, Kennedy and Hart,⁴⁰ to probabilistic structural dynamics. Initially, they substituted $[K]$ and $[M]$ back into the perturbation equations to obtain the derivative of λ with respect to each rv r_u :

$$\frac{\partial\lambda^j}{\partial r_u} = \frac{\{\phi^j\}^T \left(\frac{\partial[K]}{\partial r_u} - \frac{\lambda^j \partial[M]}{\partial r_u} \right) \{\phi^j\}}{\{\phi^j\}^T [M] \{\phi^j\}} . \quad (97)$$

The standard deviation of λ is then obtained by substituting λ^j for g and using these eigenvalue sensitivities in equation (53), which resulted from a first order Taylor series expansion. The mean was obtained by directly applying equation (52) for λ equal to g (i.e., calculating the eigenvalue for the mean mass and stiffness matrices). The partial derivatives of the elements of the stiffness and mass matrices can be obtained by taking the derivative of the analytical expression for each element of the matrix with respect to each random property. This method does not take into account nonnormal rv's, nor does it try to describe the eigenvalue distribution at the tails of the cumulative distribution functions since it assumes a small perturbation about the mean value. Hart and Hasselman⁴¹ incorporated modal truncation into equation (97) so that the entire modal matrix would not have to be obtained a priori. They used component mode synthesis to derive similar analytical expressions for the system eigenvalue matrix $[\Lambda]$ as a function of the modally reduced substructure stiffness and mass matrices.

In 1985, Pierre performed an extensive study of the analysis of structural systems with parameter uncertainties.⁴² He formulated the "statistical perturbation method," which incorporates the correlation between input rv's and response variables (in this case, the eigenvalues), with the perturbation method. An expression is derived for the covariance matrix of λ as a function of the covariance matrix of $\{r\}$,

which are the perturbed parameters or input rv's, using a first order Taylor series approximation:

$$[\text{cov}_\lambda] = \left[\frac{\partial \lambda}{\partial \mathbf{A}} \right] \left[\frac{\partial \mathbf{A}}{\partial \mathbf{r}} \right] [\text{cov}_\mathbf{r}] \left\{ \left[\frac{\partial \lambda}{\partial \mathbf{A}} \right] \left[\frac{\partial \mathbf{A}}{\partial \mathbf{r}} \right] \right\}^T . \quad (98)$$

For an uncorrelated system, the diagonal elements of $[\text{cov}_\lambda]$, which are the standard deviations of the response variable, will be identical to the results obtained using equation (53).

If the chain differentiation for the first two terms in the righthand side of equation (98) is carried out, the result will be equal to the eigenvalue sensitivity obtained in equation (97). As with the above methods, the mean of λ is simply the eigenvalue of the unperturbed system. Pierre also was able to improve upon the method described in Meirovitch's textbook for deriving the partial derivative of λ with respect to the elements of the system matrix $[\mathbf{A}]$ by applying the method developed previously by Collins, et al., shown in equation (97):

$$\frac{\partial \lambda}{\partial [\mathbf{A}]} = \frac{\delta \lambda^i}{\delta \mathbf{A}_{rs}} = \frac{\phi_r^i \phi_s^i}{\{\phi^i\}^T \{\phi^i\}} , \quad (99)$$

where r and s denote the row number and column number of the element in $[\mathbf{A}]$, respectively. Obtaining the covariance matrix is quite tedious; calculating the partial derivatives of λ with respect to each element of $[\mathbf{A}]$ is made easier by using the analytical expression of equation (99), but the calculation of the partial derivative of each element in $[\mathbf{A}]$ with respect to every input rv may have to be performed numerically, which would be extremely intensive both in terms of central processing unit (CPU) and memory requirements. Pierre also derived the covariance matrix using the second order expansion of the Taylor series shown in equation (48), but shows that it is "unsuitable for a large number of parameter variations."

3.6 Comparison of Probabilistic Methods

Mahadevan has written an excellent unpublished book for NASA/Marshall Space Flight Center that reviews and contrasts the various techniques used in the engineering community for evaluating probabilistic structures.⁴³ In this reference, he outlines several approaches for obtaining the limit state function defined in section 3.3 for realistic structures modeled using the finite element method. The first is the MC method, and it is applied by literally running the finite element model for each sample set of input rv's. This has actually only been made possible in 1997 by an addition to the NESSUS code that allows automatic variation of input rv's in the commercially established finite element code NASTRAN, submission of the sample runstream, and statistical processing of the desired response variable. One of the achievements of this research was performing a substantial amount of debugging and testing necessary for using this capability. Even with the new code, a 500-sample run of a realistic bladed-disk structure still takes 24 hours to run on a CRAY supercomputer.

Another method outlined by Mahadevan is "perturbation-sensitivity analysis," in which an approximate closed-form limit state function is obtained. This is done in two ways. The first is the finite

difference approach as performed in FORM by equation (73). Mahadevan refers to this method as the “brute-force” method because the response variable is solved directly for a change in every input rv. For example, if the response variable is a system eigenvalue for a N-dof system, the steps are as follows:

1(a) Vary input rv r_i by Δr_i , where $i=1, \dots, d$

1(b) Calculate new matrix $[A]=[M]^{-1}[K]$, which has N^2 elements (100)

1(c) Solve new eigenvalue problem, yielding new λ

1(d) Estimate $\frac{\partial \lambda}{\partial r} = \frac{\lambda_{\text{new}} - \lambda_{\text{old}}}{r_{\text{new}} - r_{\text{old}}}$ (101)

1(e) Substitute directly into equation (73).

The second technique for “perturbation-sensitivity analysis” is the “classical perturbation” approach, which uses the chain rule to calculate the partial derivative in equation (101). The steps are as follows:

2(a) and 2(b) Same as 1(a) and 1(b) above

2(c) Calculate the partial derivative of each element in $[A]$ with respect to each input rv r , $\frac{\partial [A]}{\partial \{r\}}$, either numerically or analytically if a closed form expression is available

2(d) Using equation (99), calculate the partial derivative of λ with respect to each element in the system matrix $[A]$

2(e) Carry out the chain rule to obtain $\frac{\partial \lambda}{\partial r_i} = \sum_{r=1}^N \sum_{s=1}^N \frac{\partial \lambda}{\partial A_{rs}} \frac{\partial A_{rs}}{\partial r_i}$. (102)

2(f) Substitute directly into equation (73).

Steps 2(d) and 2(e) are equivalent to carrying out equation (97). As mentioned previously, repeated eigensolutions are not necessary for the classical perturbation method; however, the number of calculations required is substantially greater than for the direct finite difference approach because of step 2(c). However, if a closed-form solution for the partial derivatives of the elements $[A]$ with respect to the input rv's is available, this approach would be advantageous. This is why the method has been chosen for simplified models of mistuned bladed disks, as will be discussed in chapter 5, where the matrix elements have all been expressed explicitly in terms of the input rv's. For a finite element model, these partial derivatives would have to be estimated numerically, so the far fewer number of calculations required for FORM would be preferable even though each calculation is more complex.

This chapter has reviewed the necessary probabilistic groundwork for development of the PDS method for analyzing the dynamics of structures. As seen in the next chapter, applying the PDS method required a step-by-step implementation of the methodologies presented since no preexisting code could accommodate the combination of component mode synthesis with probabilistics. In addition, knowledge of the limits of the methodology and ways to extend those limits are essential in evaluating the success of the PDS method and identifying sources of improvement.

4. DEVELOPMENT OF PROBABILISTIC DYNAMIC SYNTHESIS THEORY AND SIMPLE TEST CASE

4.1 Development of Probabilistic Dynamic Synthesis Methodology

Enough background material has now been covered to allow a derivation of the PDS methodology. This procedure is a unique combination of the CMS techniques discussed in chapter 2, probabilistic reliability methods from section 3.3, and other advanced topics in dynamics and probabilistics, such as correlation theory and application of complex loads onto structures. The chapter concludes with a test case applying the PDS method to a simple two substructure probabilistic spring-mass system. Much of this work appears in reference.⁴⁴

Consider a structure represented by $m=1,...,p$ substructures. Similar to equation (1), the displacement coordinates for each substructure can be arranged in vectors containing internal and boundary dof's:

$$\begin{Bmatrix} x_i \\ x_b \end{Bmatrix}^a, \begin{Bmatrix} x_i \\ x_b \end{Bmatrix}^b, \dots, \begin{Bmatrix} x_i \\ x_b \end{Bmatrix}^p. \quad (103)$$

Assume that there exists a set of samples of size s for each substructure. Each sample is modally tested individually in a configuration such that the interface locations with other substructures are in a free condition. For substructure m , sample i , the test will yield eigenvalues $\{\lambda\}^{m,i}$ and the eigenvector matrix $[\Phi]^{m,i}$. In addition, the boundary partition of the residual flexibility matrix $[G_{bb}]^{m,i}$ is obtained from the measured boundary drive point frequency response functions of the boundary coordinates, as mentioned previously. For simplicity, the notation G in this section will refer to only the boundary partition of the residual flexibility matrix. These measurements are used to create the stiffness matrix for that substructure as shown in equation (34); for free response, only the kept eigenvalues and the boundary partition of the kept eigenvectors along with G are required. For ease of analysis, these values are expressed as a single vector $\{x\}^{m,i}$ of dimension N_m defined as

$$\{x\}^{m,i} = \begin{Bmatrix} \lambda_1 \\ \vdots \\ \lambda_k \\ \{\phi_b\}_1 \\ \vdots \\ \{\phi_b\}_k \\ G_{11} \\ \vdots \\ G_{bb} \end{Bmatrix}^{m,i}, \quad (104)$$

where λ_j is the j 'th eigenvalue of substructure m and $\{\phi_b\}_j$ is a vector that contains the elements from the j 'th mass-normalized eigenvector that pertains to the boundary dof's. If the entire sample $i=1,s$ of substructure m is tested, $\{x\}^m$ can therefore be defined as a vector composed of elements that are each an rv with measured mean and standard deviation. For this research, they have been defined as the set of “dynamic” rv's, in contrast to “primitive” rv's like material or geometric properties.

The distribution for these rv's is assumed to be Gaussian. This assumption is made both because it is the most likely distribution for an rv set resulting from manufacturing variations, as is the case for structures, and because it is the most convenient for analysis. Techniques for verifying this assumption are used in the test case to be discussed below, and a normal distribution did fit the data fairly well. If a nonnormal distribution is assumed, the PDS method can still be used, but the rv's must be transformed to equivalent normal distributions using the Chen-Lind procedure described in section 3.3. Because of this assumption of normality, equation (59) can now be used to convert $\{x\}^m$ to $\{x^|\}^m$, a vector of standard normally distributed rv's ($\mu=0$, $\sigma=1$).

There is clearly a large degree of correlation between these dynamic rv's. This correlation can be quantitatively defined by the correlation coefficient ρ . For two correlated rv's x and y ,

$$\rho = \frac{\text{Cov}(x,y)}{\sigma_x \sigma_y} , \quad (105)$$

where the covariance of x and y is

$$\text{Cov}(x,y) = E[(x - \mu_x)(y - \mu_y)] = E(xy) - \mu_x \mu_y . \quad (106)$$

The value of the correlation coefficient ranges from -1 to $+1$, and can be easily calculated from the measured data using the above equations. A value of -1 or $+1$ means the rv's are fully inversely correlated or fully directly correlated, respectively. A value of 0 means the rv's are uncorrelated. For the standard normal variables $\{x^|\}$, it can be seen that the correlation coefficient is equal to the covariance. The correlation coefficients of all the dynamic rv's to each other can be expressed by creating a symmetric correlation matrix $[C]$, where the first row is the correlation coefficient of the first variable with all of the other variables, etc.

The correlation matrix is used directly to form a set of independent standard normal rv's $\{u\}^m$, which is required for the application of the reliability methods. The method chosen initially was to invoke an orthogonal transformation of $\{x^|\}^m$ using the Cholesky decomposition of $[C]$, which is the lower triangular matrix $[L]_c^m$, to uncouple the $\{x^|\}^m$ coordinates, thereby creating $\{u\}^m$.⁴⁵ This can be expressed for substructure m as

$$\{x^|\}^m = [L]_c^m \{u\}^m . \quad (107)$$

This transformation results in a set of rv's $\{u\}^m$ that have a mean of zero, as with the set $\{x^|\}^m$, but a standard deviation equal to the eigenvalues of the correlation matrix $[C]$. Further discussions of the role of the correlation matrix will be presented in later chapters.

As described in equation (73), a numerical differentiation of the limit state with respect to each rv must be performed. This differentiation is performed about the mean value of the limit state. As described in section 3.3, an entire CDF of the response variable is obtained by creating a limit state function for various response values in the range. If the response variable is chosen to be the first system eigenvalue λ_{sys}^1 , the limit state function is therefore

$$g(X) = \lambda_{\text{sys}}^1(X) - y, \quad (108)$$

where the performance function $Y(X)$ is equal to $\lambda_{\text{sys}}^1(X)$, formed from the collection of $\{x\}^m$ vectors

and having length $N = \sum_{m=1}^p N_m$, and y is a specific eigenvalue in the response probability range. This

eigenvalue problem is solved for the mass and stiffness matrices formulated according to the residual flexibility CMS method as shown in equations (33) and (34).

The numerical differentiation requires the formulation of the substructure system matrices for the mean value of each of the elements of $\{u\}^m$ and a formulation for a variation by some small amount of each element of $\{u\}^m$ while all the other elements are left at their mean. For the test case discussed in the next section, the variation of the rv's was chosen to be 50 percent of a standard deviation. Since the elements of u are standard normal variables, this results in a series of "load" cases, with the first case being

$$\{u\}^a = \begin{Bmatrix} .5 \\ 0 \\ \vdots \\ 0 \end{Bmatrix}, \quad \{u\}^m = \begin{Bmatrix} 0 \\ 0 \\ \vdots \\ 0 \end{Bmatrix}, \quad m = 2, \dots, p, \quad (109)$$

where $\{u\}^m$ is of dimension N_m . As can be seen, N_m vectors $\{u\}$ are required for $m=1,2,\dots,p$ substructures in the total structure. This set of $\{u\}^a, \{u\}^b, \dots, \{u\}^p$ is then back-transformed, first to the correlated standard normal set $\{x^l\}^m$ using the transpose of $[L]_c^m$, then to the correlated, nonstandard normal, original rv's $\{x\}^m$ using equation (59). The new vectors $\{\lambda\}$, $[\Phi_b]$, and $[G]$ are extracted from the vector $\{x\}$ for each substructure and used to calculate a stiffness matrix for that substructure using equation (34). As shown in equation (33), the mass matrix is generated by simply placing an identity matrix in the generalized coordinate partition on the upper left of the complete system matrix. Rather than using zero partitions for the rest of the matrix as specified, small dummy values are instead used on the diagonal of the boundary partition on the lower right of the mass matrix to provide numerical stability for the eigensolution routine. The global system mass and stiffness matrices are now assembled by directly coupling the substructure mass and stiffness matrices. This is accomplished by ordering the "kept" dof's of each substructure sequentially in the system matrices and adding the boundary partitions together. The system eigenvalues are then obtained, and the chosen response variable, in this case the first system eigenvalue, is isolated. This process is then repeated, with a "load" case for every rv in substructures 1 through p . For example, the second load case will be identical to the first except that the first element of $\{u\}^a$ will be zero and the second element will be 0.5. After the response variable λ_{sys}^1 is obtained for

every input rv variation, the numerical partial differentiation of the eigenvalue with respect to each of the rv's in the complete vector of independent rv's $\{U\}$, defined as:

$$\{U\} = \begin{Bmatrix} \{u\}^a \\ \{u\}^b \\ \vdots \\ \{u\}^p \end{Bmatrix} \quad (110)$$

can now be estimated by the first order finite difference technique.

The actual generation of the limit state function of λ_{sys}^1 with respect to each element of $\{u\}$ is performed within the code NESSUS. Each “datapoint,” consisting of a “load” case $\{U\}$ and its corresponding value of λ_{sys}^1 , is copied into the NESSUS/FPI module. In addition, several other parameters are established for the NESSUS run. The first parameter specifies whether a linear or quadratic curve fit will be used for the limit state function. The next instruction determines whether the FORM, AFORM, or another reliability methodology will be used to obtain the most probable points, β 's, and CDF of the response variable. Finally, either the set of response values for which a probability level will be obtained or the set of desired probability levels for which a corresponding response value is obtained is input. In this case, since each element of $\{u\}$ is only varied by a single value, only a linear approximate limit state function can be obtained, so only the FORM can be used.

The output for this computer run consists of a CDF, β values, and the values of $\{u\}$ that locate the most probable point X^* in N-dimensional space for each β value. This solution is also called the “mean value” solution because it results from an expansion about the mean of the limit state. The solution can now be updated by applying the AMV method explained in section 3.3, which should correct some of the inaccuracies due to nonlinearity of the limit state. For this method, each element of the most probable point vector $\{U^*\}$ is back-transformed to an original set of rv's similar to the back transformation of the load cases performed earlier. Each of these original sets $\{x^*\}$ is then used in the residual flexibility formulation of the substructure stiffness matrices, the substructures are coupled, and a new λ_{sys}^1 is calculated. This value is now associated with the previously calculated β value for that most probable point. A new CDF is therefore created by shifting the response levels for each of the probability levels from the value originally obtained using FORM to the new, updated value.

4.2 Test Case

A test case was formulated to further develop and validate the proposed technique. The test case consisted of a two substructure, 7-dof spring-mass system (fig. 10).

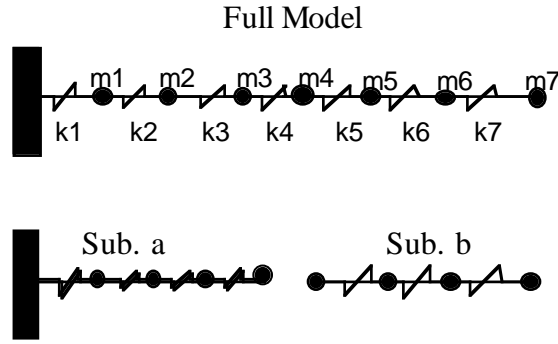


Figure 10. Test case system.

To simulate the modal test phase of the procedure, an MC simulation was performed of each substructure using 5,000 samples. To achieve complete probabilistic generality, each spring in the system was assigned a normal distribution with a μ_k of 200 and σ_k of 10, and each mass was assigned a normal distribution with a μ_m of 1.0 and σ_m of 0.05, yielding coefficients of variation of 0.05 for all the system input “primitive” rv’s. As discussed previously, since this initial numerical simulation is performed to represent measurements of the dynamic characteristics of a physical population, the distribution of the underlying primitive variables is not critical; normal distributions were therefore chosen for convenience. The MC random vectors were then used to create the mass and stiffness matrices for the substructures (5,000 for each) and a modal analysis run on each substructure to obtain sample sets for their eigenvalues $\{\lambda\}^m$ and eigenvector matrix $[\Phi]^m$, $m=a,b$. This analysis was performed using FORTRAN and a set of matrix solution subroutines FORMA.⁴⁶

Even if maximum accuracy is desired, only three of the four modes for each substructure can be “kept” for the analysis; since the interface locations are modeled in the free condition, this introduces an extra mode for each substructure, which if kept, would cause the model to be overspecified. Instead of measuring the boundary partition of the 4×4 residual flexibility matrix $[G]^m$ using drive point frequency response measurements, as would be performed for the actual application of this method, it was analytically calculated directly from the modes that had been chosen to be truncated as discussed by Martinez:⁴⁷

$$[G] = \sum_{i=k+1}^N \left[\frac{\{\phi\}_i \{\phi\}_i^T}{\lambda_i} \right], \quad (111)$$

where, in this case, $k=3$ and $N=4$. It was later discovered that if equation (111) is chosen as the method used to obtain G , substantial error results if all of the deleted modes are not used; this necessitates the use of other methods for realistic structures, as will be discussed in chapter 5.

Proper treatment of the rigid body mode of substructure “b” is also important for the test case. Since the first mode is a zero frequency mode by definition, the first eigenvalue is not actually an rv. To

handle this in the coding, a mean and standard deviation of zero was manually attached to the variable so it could be easily kept as part of the rv set. It is important to note that the mode shape for this mode is random; it is a function of the random mass input. By imposing this random condition on the masses, complete generality of the problem was maintained. If only stiffness was chosen to be random, as has been the case for many other analyses of probabilistic systems, such as with bladed disks, the entire effect of the variable rigid body mode shape would be lost. The statistics on the dynamic characteristics of each substructure $\{\lambda\}^a$, $\{\lambda\}^b$, $[\Phi]^a$, $[\Phi]^b$, $[G]^a$, and $[G]^b$ and the correlation matrix were then calculated. These statistics are listed in table 2.

Table 2. Statistics of dynamic characteristics.

Substructure A			Substructure B		
Eigenvalues	Mean	Standard Deviation	Eigenvalues	Mean	Standard Deviation
1	30.431	1.2702	1	0	0
2	246.74	10.336	2	150.51	6.706
3	552.89	23.014	3	489.03	21.916
Eigenvectors, boundary location only			Eigenvectors, boundary location only		
Eigenvector	Mean	Standard Deviation	Eigenvector	Mean	Standard Deviation
1	0.7073	0.01155	1	0.53466	6.9105E-03
2	-0.70725	0.028546	2	0.75592	2.1945E-02
3	0.70688	0.058827	3	-0.55443	7.4042E-02
Residual Flexibility (one boundary point only)			Residual Flexibility (one boundary point only)		
Location	Mean	Standard Deviation	Location	Mean	Standard Deviation
1	6.46E-04	1.6159E-04	1	6.46E-04	1.5347E-04

The listed quantities comprise the vectors $\{x\}^a$ and $\{x\}^b$ as described in equation (103). A distribution characterization procedure was also applied to the distributions to verify the normal distribution assumption.⁴⁸ Partial results of the distribution characterization routine for one of the rv's are shown in table 3. The “W” statistic is a goodness-of-fit test developed by Wirshing and Carlson, where a smaller number indicates a closer fit. The results show that the data are well represented by both normal and lognormal distributions, with the lognormal being slightly better. The CDF values for each distribution, however, indicate that the curves for the two distributions predict almost exactly the same value, which can be the case for a particular set of lognormal parameters. The assumption of normality was therefore deemed to be accurate.

Table 3. Partial results of distribution types routine.

Substructure B, Eigenvalue 2	
W statistics (all types included)	
Normal:	0.00948
Exponential:	0.30339
Weibull:	0.04448
EVD:	0.04323
Lognormal:	0.00934
Normal Distribution Parameters	
Sample mean = 150.61, sample std. dev. = 6.502	
Normal Distribution CDF fit to data	
Response Value	CDF Value
143	0.1210
147	0.2895
150	0.4628
155	0.7503
Lognormal Parameters, base e	
mu = 5.014,	sigma = 0.43201
Lognormal Distribution CDF fit to data	
Response Value	CDF Value
143	0.1193
147	0.2947
150	0.4713
155	0.7540

These rv's were then grouped together for transformation, with the ordering as follows: substructure "a," boundary eigenvectors, eigenvalues, and residual flexibility term; then substructure "b" boundary eigenvectors, eigenvalues, and residual flexibility term. A matrix composed of cases of $\{u\}$ vectors was generated and multiplied by the correlation Cholesky decomposition matrix $[L]_C$ to obtain $\{X^I\}$, the set of correlated standard normal rv's. These were then converted to their nonstandard normal distributions and used in the residual flexibility substructure stiffness matrix. The substructures were then coupled together and a modal analysis was performed on the system matrices. The first system eigenvalue for each case along with its load case, $\{u\}$, was then input to the NESSUS/FPI routine. For this test case, it was erroneously assumed that the variance of the independent rv's $\{u\}$ were equal to one instead of the eigenvalues of the correlation matrix; this may have caused some error, although Mahadevan has theorized that it may not be significant because of the rapid dropoff of the response probability surface away from the mean values of these normalized rv's.⁴⁹

The FORM solution of λ_{sys}^1 from this routine is then used to plot an initial estimate of the CDF. The MPP's for each requested limit state were recorrelated and transformed back, following the AMV approach, into the original set $\{x\}^m$; this was used to create new substructure stiffness matrices, which were coupled to form the global system matrices for eigenanalysis. One of the most probable points is

shown in table 4. The updated system fundamental eigenvalues (one for each MPP) were plotted to form a new CDF. The comparison of these two CDF's is shown in figure 11.

Table 4. Sample MPP output.

Fundamental eigenvalue response value = 8.101
 $P(\lambda_{\text{sys}}^{-1}) < 8.101 = 0.01$

Most Probable Point			
Substructure A rv	Value	Substructure B rv	Value
u1	-0.4863	u1	-1.5205
u2	-0.1692	u2	0.2641
u3	-0.05685	u3	-0.2361
u4	-1.5807	u4	0.0
u5	-0.1221	u5	-0.3057
u6	-0.0269	u6	-0.0473
u7	0.211	u7	0.2267

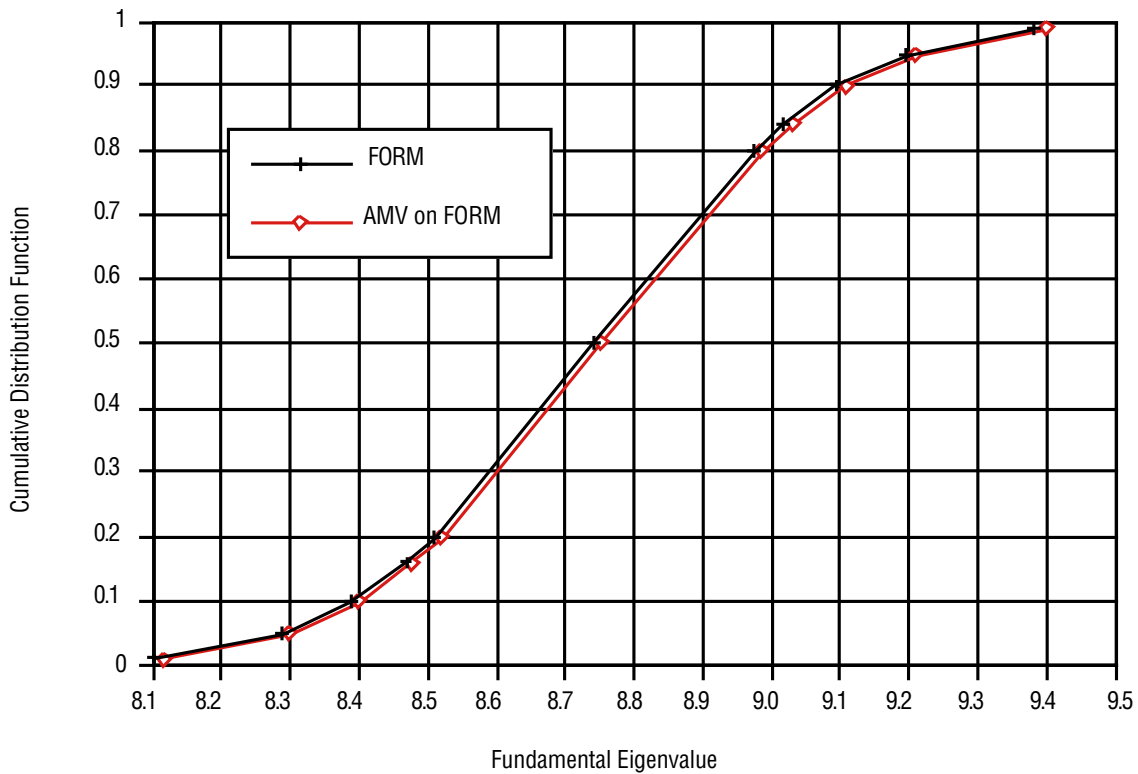


Figure 11. Comparison of PDS FORM and AMV with CDF's for seven spring/mass test case.

There are several choices for verification of the PDS method. For this case, the baseline chosen was an MC analysis performed on the same nondeterministic spring-mass system but using the original primitive rv's of mass and stiffness. The system eigenvalue is obtained directly from each

unsubstructured sample. This is the full model approach; it yields the closest available approximation to the exact solution, but it does not isolate the various approximations used in the PDS method. To isolate the effect of substructuring, for instance, it may be more illustrative to perform an MC simulation of the two substructures individually and then couple them together to obtain the system eigenvalues. These various applications of MC are examined in later sections of this thesis.

For comparison, the CDF for the full model is superimposed on the previous CDF's from the PDS method in figure 12. A very small amount of error is indicated graphically. To identify the error quantitatively, the amount of variation of the fundamental eigenvalue from its mean value at selected CDF probability values for the PDS method was compared to the spread for the full model. The result, shown in table 5, indicates that the deviations from the mean as computed by the AMV and MC methods agree to within 5 percent. In addition, the mean value of the fundamental eigenvalue computed by the AMV method is 8.751, which is only 0.5 percent higher than that computed using MC of 8.707, and the AMV standard deviation is 0.276, which is only 1.8 percent less than the MC standard deviation of 0.281. These results were considered acceptable based upon the measure of error used.

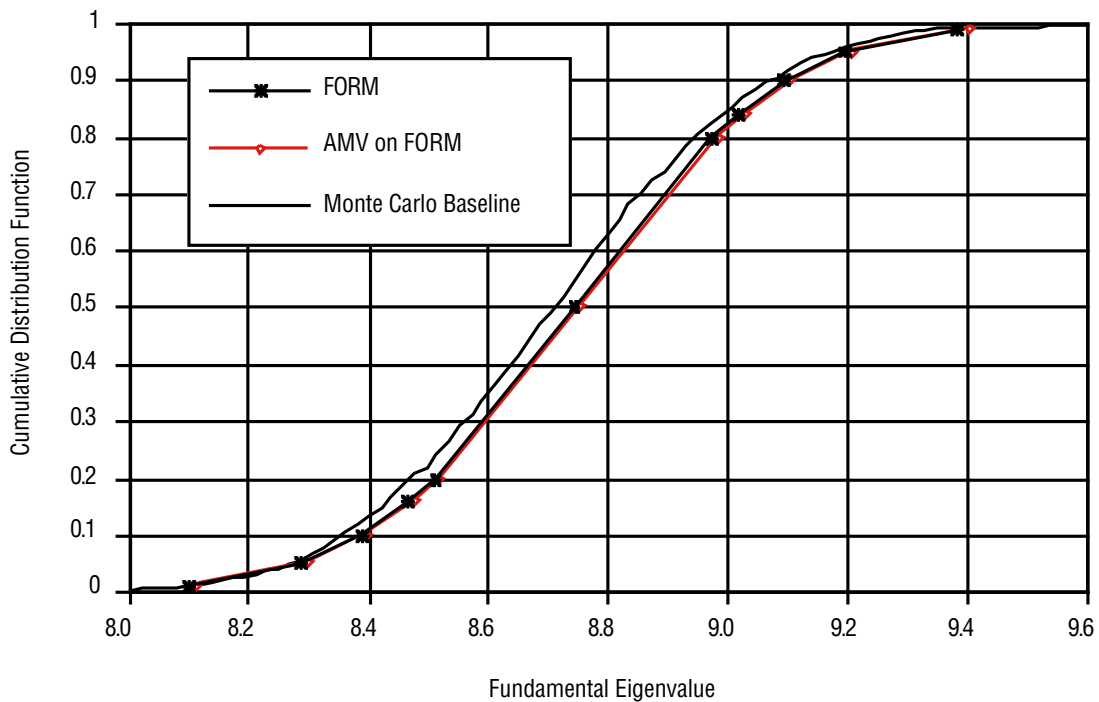


Figure 12. Comparison of CDF's using PDS FORM and AMV with MC.

Table 5. Dispersion error of PDS versus full MC model.

CDF Value	AMV	Delta From AMV Mean	Monte Carlo	Delta From MC Mean	% Error of Deltas
0.010	8.116	-0.635	8.094	-0.613	-3.46
0.050	8.300	-0.451	8.266	-0.441	-2.23
0.100	8.399	-0.352	8.352	-0.355	0.87
0.159	8.476	-0.275	8.426	-0.281	2.22
0.200	8.520	-0.232	8.467	-0.240	3.62
0.500	8.751	0.000	8.707	0.000	Not applicable
0.800	8.985	0.234	8.944	0.237	1.44
0.841	9.029	0.278	8.987	0.280	0.74
0.900	9.108	0.357	9.072	0.365	2.25
0.950	9.210	0.459	9.169	0.462	0.65
0.990	9.403	0.652	9.344	0.637	-2.28

4.3 Additional Studies of Seven Mass/Spring Problem

To gain a deeper understanding of the variety of methods available and the approximations and errors involved, a variety of additional analyses using this system were then performed using larger cov of the input rv's. It was anticipated that the high cov levels would prove more difficult for the FORM. Examination of equation (46) shows that the error in approximating g as a linear function is directly related to the size of the second (and higher) order terms in the expansion of g . The size of the second order terms is governed by the second partial derivatives of g and by the coefficients of these terms, which have the form $(x - \mu_x)^2$, a measure of the size of the cov. Therefore, any small nonlinearity that does exist will be magnified by a large cov. First, an examination of the linearity of the system as a function of the independent rv's $\{u\}$ was performed numerically. The system fundamental eigenvalue was calculated and plotted in figure 13 as an independent function of each independent rv. The range for the abscissa is between -2 and $+2$ times the standard deviation of each rv, which was calculated for this examination as the square root of the eigenvalue of the correlation matrix. The legend on the plot of the rv's $s1u1, \dots, s1u7, s2u1, \dots, s2u7$ refer to the original order in which the 14 dynamic rv's were placed, with $s1$ designating substructure 1 and $s2$ designating substructure 2. This graph shows that the limit state is somewhat nonlinear with respect to several of the rv's, in particular the first rv for each substructure, $s1u1$ and $s2u1$, and to $s2u4$.

To examine the effect of this nonlinearity, the analysis described in section 4.2 was repeated for cov's of 10 percent for each primitive rv. As expected, the results were found to be slightly worse than those obtained for the smaller cov case when using FORM. As with the previous system, the AMV update procedure was applied to the most probable points output from the NESSUS/FPI run. The results from this did not show any improvement, which may indicate that the AMV method is primarily a method of improving the results of nonlinear problems with small cov's. Further data presented later in this section support this hypothesis. Figure 14 compares the results using FORM and the AMV/FORM update with the MC baseline analysis for this case. There is some skew at the mean value using the PDS reliability methods, but the actual error is only 2 percent.

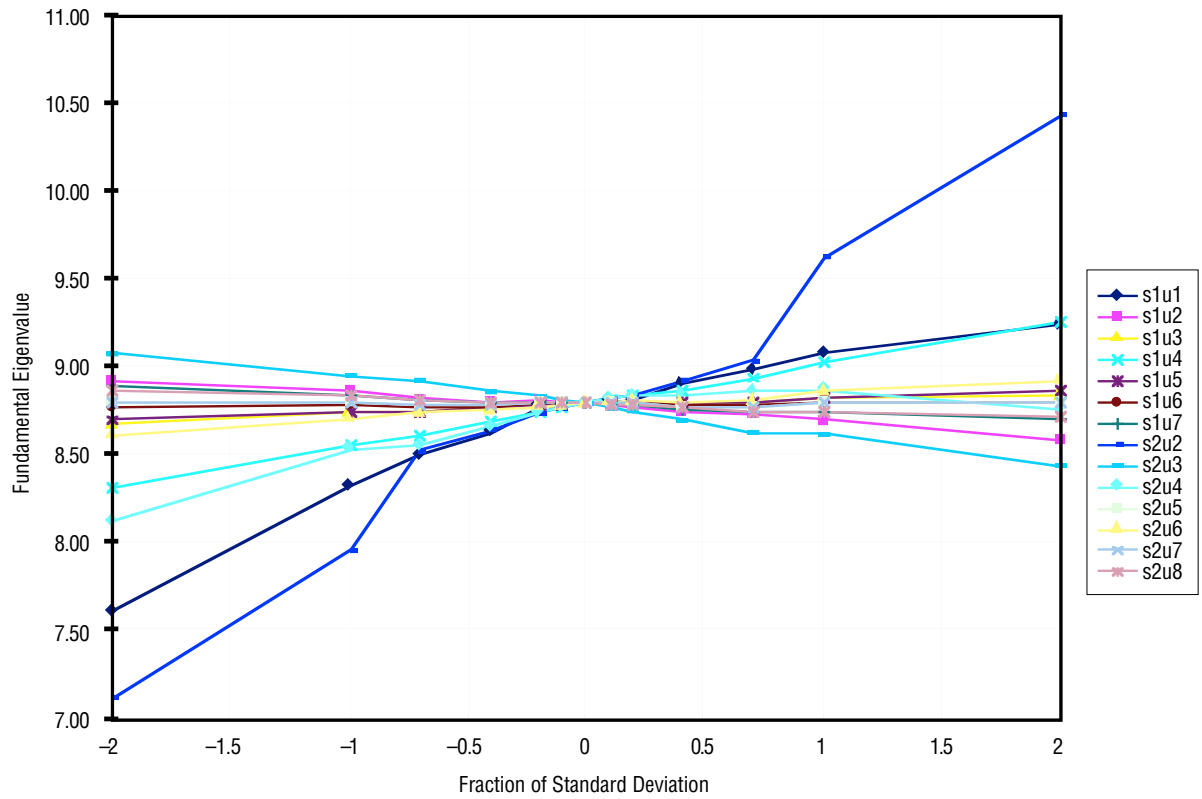


Figure 13. Linearity of fundamental eigenvalue w.r.t. independent rv's.

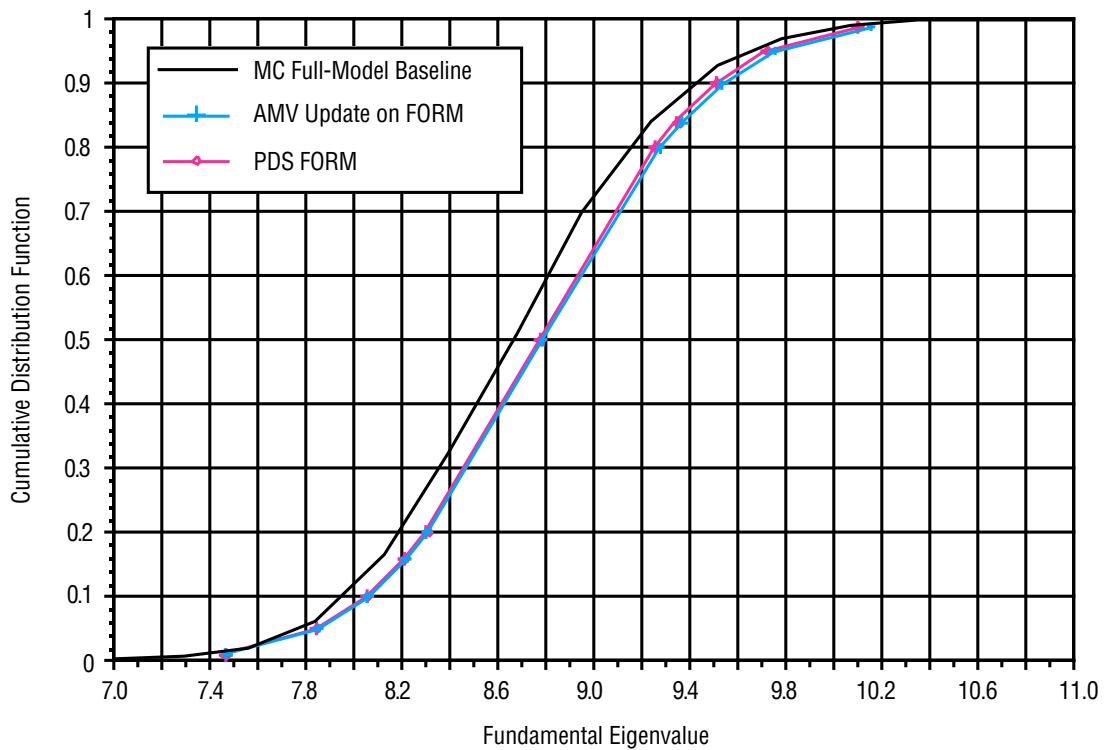


Figure 14. FORM and AMV CDFs versus MC; cov=10 percent.

The AFORM method described in section 3.3, which performs a higher order expansion of the limit state function, was implemented to try to incorporate the nonlinearities of the system which become important for the $\text{cov} = 0.10$ case. This required the creation of a minimum of two datapoints of variation of each rv in $\{u\}$ in addition to the value of the mean in order to perform a quadratic curve fit. Although only three total points are required, in this case four other variations were obtained using the following “load” sets, which are placed into a single matrix $[U]$, with the number of rows equaling the total number of rv’s in the entire structure $N_{\text{sys}} = N_1 + N_2$, and the number of columns equaling $4 N_{\text{sys}} + 1$ for the mean value set:

$$[u] = \begin{bmatrix} -0.2 & -0.1 & 0.1 & 0.2 & 0 & \cdots & 0 \\ 0 & 0 & 0 & 0 & -0.2 & \cdots & 0 \\ \vdots & \vdots & \vdots & \vdots & \vdots & \vdots & \vdots \\ 0 & 0 & 0 & 0 & 0 & \cdots & 0 \end{bmatrix}. \quad (112)$$

As with the linear methods, this set is re-correlated and back-transformed to a set of original rv’s $\{x\}$ which are used to generate an eigensolution. Each column of $[u]$ and its resulting response variable λ_{sys}^1 is then input into NESSUS and the “quadratic” g-function option is chosen. This quadratic g-function allows the AFORM methodology to be implemented. The results using the quadratic approximation of the g-function were noticeably better than for FORM (fig. 15), with an error at the median reduced to 0.7 percent. The AMV method was also applied to the most probable points output from this quadratic run, but the results show almost no improvement over the AFORM results. This may indicate that AFORM accounts well for the entire higher-order term in equation (46), including the coefficient, while AMV only accounts for excessive nonlinearities expressed by the second partial derivative of g with respect to the rv’s. This hypothesis is also supported at the conclusion of this section.

Since there were approximations and/or possible errors from several different sources for this analysis, some attempt at isolation of these sources was made. The first was to run an MC simulation, isolating the effect of the reliability methods from the CMS procedure by generating the response variable using a model generated with the residual flexibility CMS method instead of from a full model, as discussed in the last section. As shown in figure 16, which compares the two MC approaches, this resulted in a small error from the mean of the full MC of -0.1 percent, indicating that error from the above methods is due mostly to the probabilistic approximations involved, not the CMS approximation. This was anticipated, since all possible modes were used in the substructure formulation. In addition, an MC analysis was run on the full system entirely within NESSUS, as described below, and this solution matched very well with that obtained using the FORTRAN codes developed earlier.

Verification of the reliability methods as implemented in NESSUS was also performed to isolate possible sources of error. This was accomplished by directly inputting the full model directly into NESSUS using its user-defined FORTRAN subroutine capability, and using the built-in AFORM methodology to perturb the primitive system parameters (mass and springs), generate the quadratic g-function, and obtain a CDF. The results are shown in figure 17, and indicate that the AFORM methodology itself performs adequately compared with the MC simulation of the full model. The CDF resulting from applying AFORM with the PDS method is shown for reference as well.

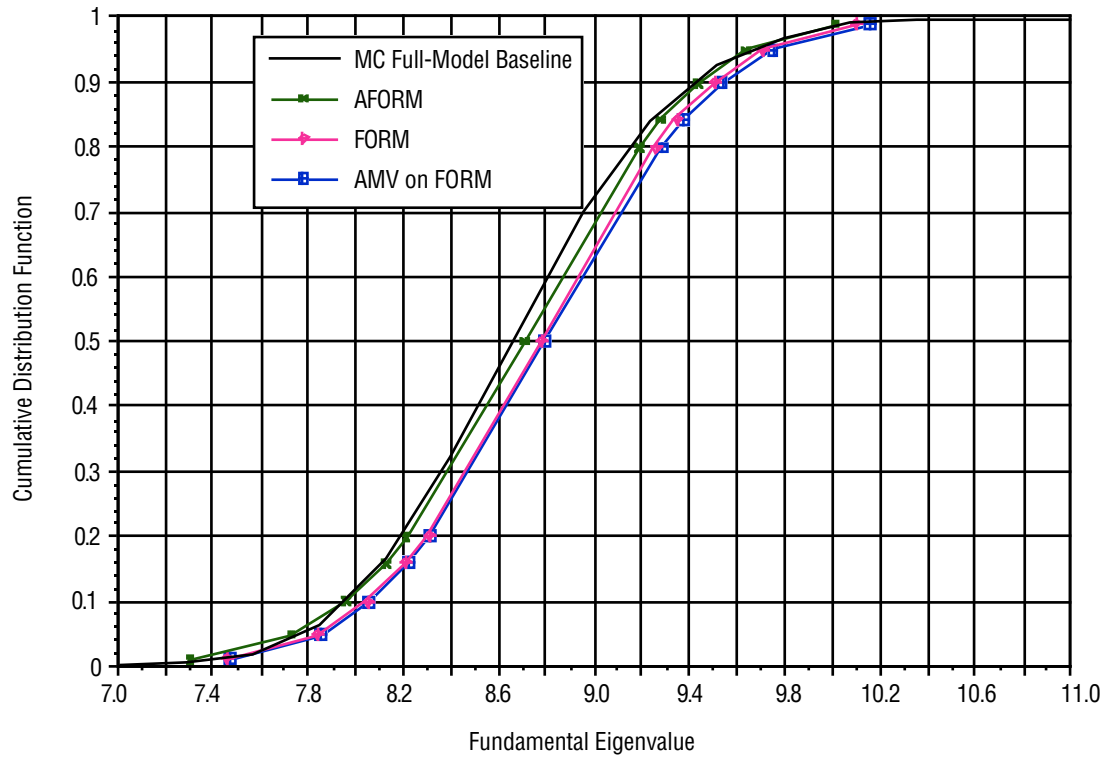


Figure 15. Comparison of AFORM with FORM, AMV; cov=10 percent.

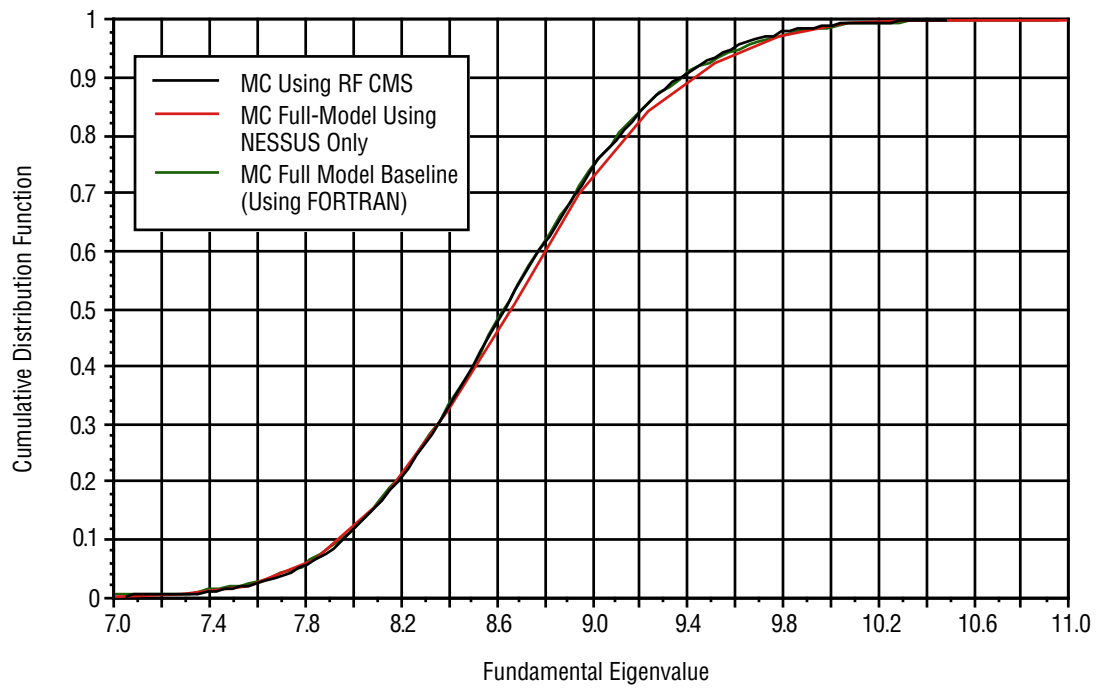


Figure 16. Comparison of CDF's for different MC approaches; cov=10 percent.

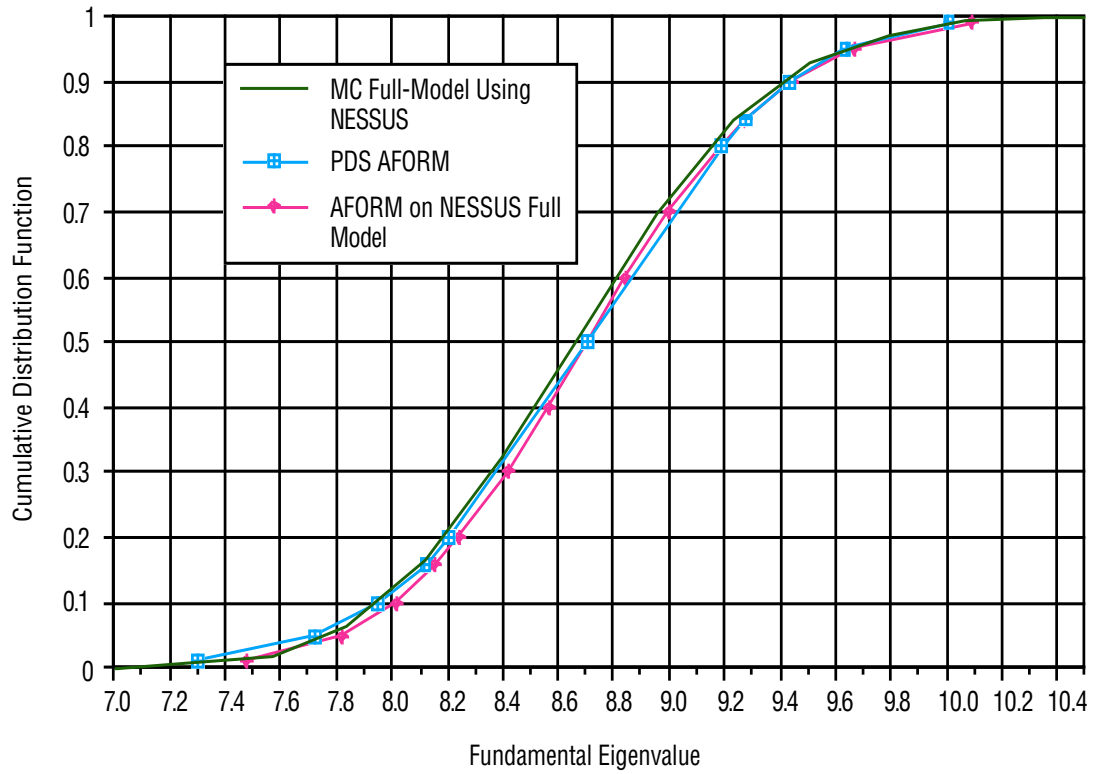


Figure 17. Verification of NESSUS/FPI AFORM.

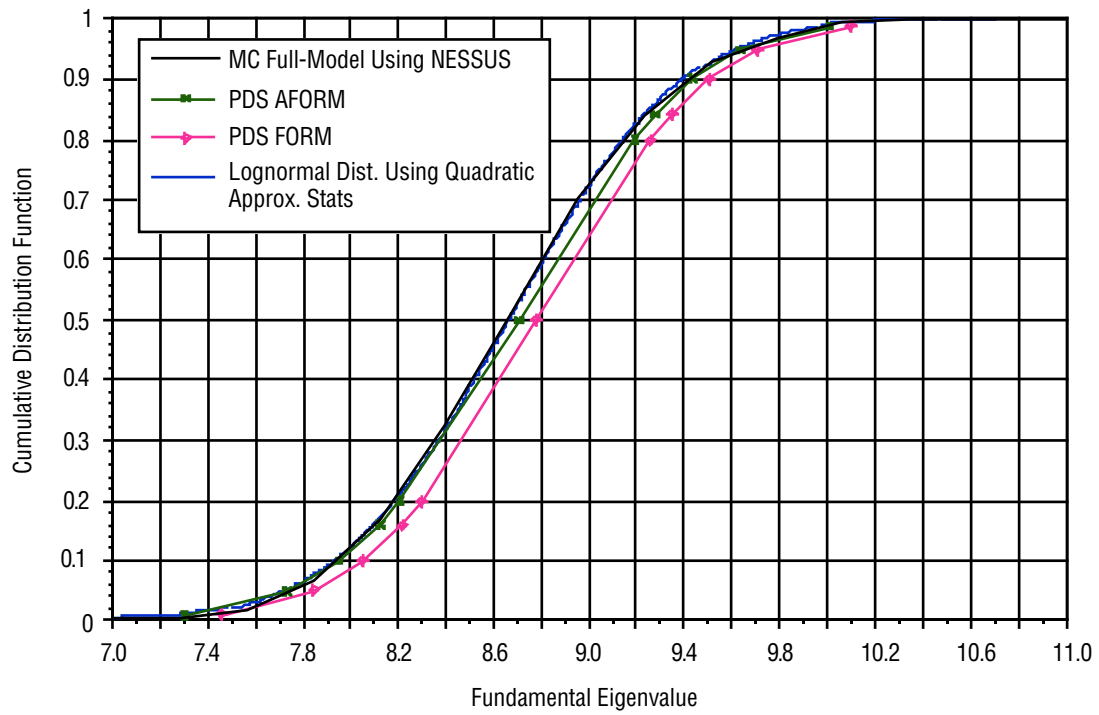


Figure 18. CDF using quadratic "approx. stats;" cov=10 percent.

Using the quadratic option also instructs NESSUS to generate the approximate mean, median, and standard deviation using the partial quadratic terms from equations (47) and (48) as discussed in chapter 3. These parameters are used to create a CDF using an assumed lognormal distribution which actually turns out to be closer to the MC results than the AFORM, FORM, or AMV results. The approximate statistics result is combined with the NESSUS/FORM and AFORM results in figure 18.

As seen in figure 15, the AFORM method shows an improvement over the FORM while the AMV update of the FORM does not. This difference in performance can be explained by the mechanism for inclusion of higher order effects for each method. The AMV partially includes the second order information by reassociating values of the CDF with updated response value solutions using the iteratively obtained MPP's. Since the limit state is expanded about the mean, the MPP for that value is not altered but instead stays at {0}, so an update is not possible. The FORM and AMV value at the mean is equal to the value of the limit state at the means of the input rv's ($g(X=\mu_X)$). Examining equation (47), reprinted below for clarity, shows that the error in this value is equal to a term that is directly related to the size of the cov times the second partial derivative of g with respect to the input rv, which is only nonzero for a nonlinear function:

$$\begin{aligned} \mu_g = g(\mu_x, \mu_y) + \frac{1}{2} \left(\frac{\partial^2 g(\mu_x, \mu_y)}{\partial x^2} [E(x^2) - \mu_x^2] + \frac{\partial^2 g(\mu_x, \mu_y)}{\partial y^2} [E(y^2) - \mu_y^2] \right) \\ + 2 \frac{\partial^2 g}{\partial x \partial y} E[(x - \mu_x)(y - \mu_y)] + \dots \end{aligned}$$

Even for a function with a small amount of nonlinearity, therefore, the error in the mean can be substantial if the cov is high, and this error will skew the entire CDF with respect to the MC CDF. Since the AMV corrects the value of the response for a given probability, it is therefore most effective in correcting the shape of the CDF, which is quantified by the standard deviation, rather than a skew, as quantified by the mean. The AFORM, on the other hand, uses an approximation of the entire second order term in equation (47), so it is able to improve both the original response and probability values. Errors in both the skew and shape of the CDF can therefore be corrected.

These studies were also performed on a system with a cov of 0.15. Similar results were obtained, and are shown in figure 19. The size of the errors measured at the mean are small, ranging from 1.6 percent for the PDS AFORM case to about 3 percent for the AMV case, but as seen in the previous case, the AFORM is a noticeable improvement.

Both increased computational speed and increased accuracy of input rv's are among the goals of the development of the PDS method. For completeness, comparisons of the speed of the models used in the preceding analysis will be presented, but it must be noted that these are not truly direct "apples-to-apples" speed comparisons. The bulk of the computational effort in the PDS method was used to convert the simulated dynamic data to a set of independent rv's and then to create the datapoints used to create the probability response surface for input to NESSUS. The MC case, on the other hand, was extremely useful as an accurate "baseline" case, but directly uses the "primitive" rv's and so does not have to

perform the CPU-intensive step of response surface datapoint generation. In addition, the purpose of this test case was to develop the PDS method and to examine the various methods available for obtaining accurate statistics of the response variable, not to prove that the method would be faster. Therefore, the FORTRAN runstreams developed were not optimized for efficiency and the advantages in the PDS method due to the use of the residual flexibility method of CMS were completely nullified by using as many dof's in the substructures as are present in the full model to ensure accuracy.

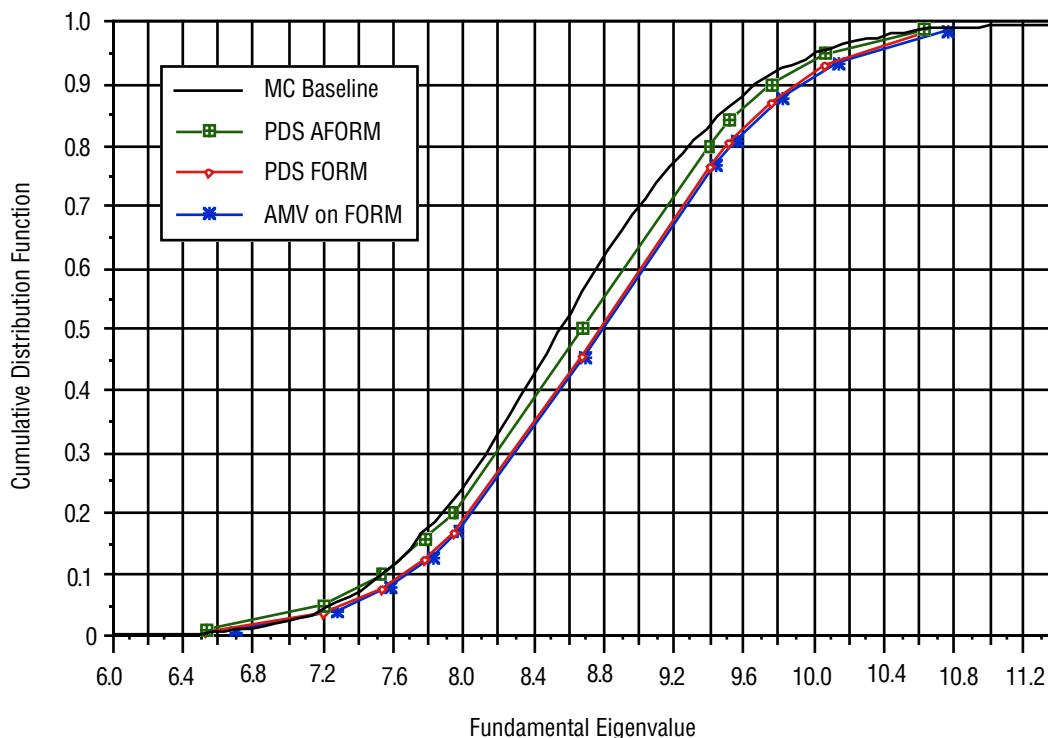


Figure 19. Comparison of CDF's of seven mass/spring system; cov=15 percent.

Nevertheless, the speed comparisons show the PDS method as applied takes the same order of magnitude of time to run as the MC procedure. The PDS method uses two main programs—a FORTRAN code “quad” to create the sample sets of the *primitive* rv's, create the load cases, and generate the datasets; and a NESSUS/FPI runstream that uses the datasets to create the CDF. The FORTRAN code took 80.144 sec of CPU time and 249 sec of wallclock time on a CRAY T/90 supercomputer. The NESSUS run took about 1 sec on an SGI workstation. The 10,000-sample MC simulation of the system performed entirely in FORTRAN took 24.8 sec of CPU time and 90.2 seconds of wallclock time. These values were in line with expectations based on the reasons stated above.

In conclusion, for a simple system, even with high values of cov, the PDS method can produce good approximations of the CDF using the partial higher order limit state approximation techniques. These results were successful enough to verify that the PDS methodology would provide a useful new technique for analyzing systems with nondeterministic substructures whose dynamic properties can be statistically characterized. It was anticipated, though, that implementation of the methodology on a more realistic system would illuminate many more theoretical as well as practical issues that would require resolution before PDS could be fully developed. The next chapter, therefore, examines a three-substructure system modeled using the finite element technique that brings these issues to light.

5. FREE- AND FORCED-RESPONSE ANALYSIS OF REALISTIC SYSTEM

This chapter describes the analysis of a realistic three-substructure probabilistic system using the PDS method. The purpose of this analysis is to identify and resolve problems associated with implementation of the method on a realistic engineering structure. Section 5.1 defines the problem motivating the dynamic analysis for a nondeterministic structure undergoing dynamic excitation. This definition is used to identify a metric for evaluation of the probabilistic methods applied in section 5.2. The deterministic and stochastic geometric and material properties of the structure are then described in section 5.3. The numerical simulation of the modal testing of the probabilistic substructures, which is the first step of the PDS process, is explained in section 5.4. Section 5.5 applies the methodology to obtain the partial free-response solution of the structure, which is a CDF of the third eigenvalue of the system. Finally, the forced response solution in the frequency domain is presented in sections 5.6 and 5.7.

5.1 Problem Definition

It is important to define the problem that is faced by designers and analysts of structures undergoing dynamic excitation. Frequently, the approach used in industry is to design structures initially to avoid resonance with potential harmonic excitation mechanisms, and then if that resonance cannot be avoided, to perform a forced-response analysis to evaluate the level of response. The problem statement therefore is divided into a free-response and a forced-response stage. For the free-response stage, standard practice has been to impose a rather arbitrary 5- or 10-percent band around the natural frequencies. This may have some basis in modal testing of the structure (e.g., modal testing of individual turbine blades), but it is not accurate if there is coupling between substructures nor is it tied quantitatively to a probability value.

The probabilistic approach to the free-response problem is to determine the actual “3- σ ” range of the structural natural frequencies about the mean and design the excitation to avoid that range. This entails calculating the CDF for each mode and using the natural frequencies at 0.14 percent and 99.86 percent (a $\pm 3\text{-}\sigma$ range for a normal distribution) as bounds. Therefore, a probabilistic method should be evaluated by its ability to yield the correct natural frequency for these given CDF values. In this research, 1 percent and 99 percent values were the closest probabilities to these 3- σ values that were obtained and so will be used instead.

If this frequency range cannot be avoided by the excitation, which is a frequent condition, then the forced response problem must be solved. In this case, standard practice has been to perform a deterministic analysis using the nominal geometry of the structure to obtain a maximum displacement or stress, and then to impose a “safety factor” on the result. This factor is purely experience-based since there is no current methodology in use by industry to evaluate the statistical variation of the response. The probabilistic approach for the problem is to determine the stress CDF of the maximum responding location and to design the structure to withstand the positive 3- σ response value. For the forced-response problem, therefore, a probabilistic method should be evaluated by its ability to obtain an accurate response value for a CDF value of 99.86 percent.

5.2 System Description

In order to examine the applicability of the PDS method for a realistic design problem, a structural system had to be chosen that met several criteria. First, the structure had to be modeled using standard methodology. This was satisfied by using the most widely used commercial finite element code, NASTRAN. Next, since tying CMS together with probabilistic methods is an important goal of this research, the size of the model had to be large enough to be able to realize a substantial reduction in computer time due to dynamic reduction. This requirement is satisfied by using a structural system composed of a “disk,” which is made up of 630 quad4 plate elements and constrained at the center, and two “blades,” which are each composed of 24 quad4 plate elements (see fig. 20). For ease of analysis, the standard assumption that in-plane translation and rotations are small has been applied by constraining out these dof’s, thereby halving the size of the model from 4,142 dof’s to 2,076 dof’s. To pave the way for the detailed bladed-disk analysis presented in chapter 6, the disk was assumed to be deterministic and the blades nondeterministic. To make the structure somewhat generic, a different mean thickness was defined for each of the blades. An additional goal requiring a model of this size is that it necessitates the use of model reduction techniques for coupling large, realistic substructures that are not needed for very small models like the one used in chapter 4.

Finally, the structure had to possess a “generic” level of randomness not easily defined by a single variation in a material or geometric property. A single rv would not be able to capture variations in mode shapes that are independent of variations of natural frequency, for instance. To achieve this goal, each blade was separated into three sections, with two of the sections having a thickness set to be an independent primitive rv. In addition, the density of each blade across all three sections was defined as an independent rv, thus giving each blade three independent rv’s. The different section properties for the two-bladed disk are shown in figure 20, and details on the geometry and other properties of the system model are shown in table 6. This level of randomness is similar to imposing a random field,⁵⁰ which is a methodology for imposing a correlated random spatial field along a structure. The use of this discipline is beyond the scope of this thesis.

Table 6. Three-substructure system (“two-bladed disk”) information.

Disk Substructure—Deterministic	
Number elements:	630
Number nodes:	631
Number dof's:	1,893
Number unconstrained dof's:	1,884
Boundary conditions:	Fixed at center and two adjacent nodes off center, node 2 and 12
Material:	Steel, Young's Modulus $E = 3.0 \times 10^7$, Poisson's Ratio $\nu = 0.29$, Density $\rho = 0.000769$ lb-sec ² /in.
Geometry:	Diameter = 2.51 in. Thickness $t = 0.1$ in.
Blade A	
Number elements:	24
Number nodes:	36
Number dof's:	108
Boundary conditions:	Free-Free
Material:	Steel, $E = 3.0 \times 10^7$, $\nu = 0.29$ $\rho \sim N(7.69 \times 10^{-4} \text{ lb-sec}^2/\text{in.}, 7.69 \times 10^{-5} \text{ lb-sec}^2/\text{in.})$ —independent rv
Geometry:	Length = 2 in. Thickness: Section 2: $t = 0.1$ in. (deterministic) Section 3: $t \sim N(0.1 \text{ in.}, 0.01 \text{ in.})$ —independent rv Section 4: $t \sim N(0.1 \text{ in.}, 0.01 \text{ in.})$ —independent rv
Blade B	
Number elements:	24
Number nodes:	36
Number dof's:	108
Boundary conditions:	Free-Free
Material :	Steel, $E = 3.0 \times 10^7$, $\nu = 0.29$ $\rho \sim N(7.69 \times 10^{-4} \text{ lb-sec}^2/\text{in.}, 7.69 \times 10^{-5} \text{ lb-sec}^2/\text{in.})$ —independent rv
Geometry:	Length = 2 inches Thickness: Section 5: $t = 0.2$ in. (deterministic) Section 6: $t \sim N(0.2 \text{ in.}, 0.02 \text{ in.})$ —independent rv Section 7: $t \sim N(0.2 \text{ in.}, 0.02 \text{ in.})$ —independent rv
Unsubstructured System	
Number elements:	678
Number nodes:	695
Number dof's:	2,085
Number unconstrained dof's:	2,076
Boundary conditions:	Fixed at center and two adjacent nodes off center, node 2 and 12
Other properties	same as above; all rv's independent

5.3 Monte Carlo Analysis

To provide a measure against which to measure the accuracy of the methodologies developed in this thesis, a baseline had to be generated. As in chapter 4, an MC analysis of the original system with its primitive rv's was chosen to be this baseline. In addition, MC analysis was required in this research to simulate the modal testing phase of the PDS methodology to obtain the statistics of the dynamic rv's. However, probabilistic analysis of structures with this level of detail and randomness has not been reported in the literature, even using MC, and is one of the unique aspects of this research. One of the reasons that so little research and analysis has been done with this type of realistic structure is that the

tools have essentially been unavailable. The finite element code contained within NESSUS was capable of modeling a structure similar to that described; however, the accuracy of the elements was suspect, and the code was developed with very basic research in mind and so was lacking many capabilities required for PDS, such as mass normalization of modes. In 1995–1996, NASA/Marshall Space Flight Center contracted Southwest Research Institute to develop an interface with NASTRAN.⁵¹ This interface allows any geometric or material property to be specified as an rv with a given distribution type and associated descriptive parameters (mean, standard deviation, etc.). The finite element model is read directly into NESSUS where the probabilistic algorithms described in chapter 3, including MC, FORM, and AFORM, can be performed. In addition, an extensive user-defined interface is available, allowing implementation of user-created FORTRAN or C subroutines. The PDS analysis of the three-substructure model described above was essentially a “beta” test for the NESSUS/NASTRAN interface, requiring the resolution of a number of bugs and software usability issues. The interface has now been made a standard part of the NESSUS code, which is commercially available. In addition to the unavailability of a code for performing the analysis, the supercomputing capability required to run several hundred (at a minimum) sequential finite element runs has not been available until the last several years. The runs performed for this analysis took up to 27 hr on a CRAY T-90, one of the most modern supercomputers available.

The new NESSUS/NASTRAN interface manages the simulation, both by creating the random vector set for the given input rv’s and by automatically submitting the jobs. The actual implementation of this automatic submission, however, required the solution of many network and software problems, as this was the first real test case for the code. Reliable solutions were eventually obtained, however, for use in the research.

The MC simulation is extremely time consuming, so a much smaller number of runs was used for the two-bladed disk system than for the test case discussed in chapter 4. Applying equation (45), a confidence level of 98.2 percent is obtained for the 0.01 probability level using 400 samples, which therefore should be sufficiently accurate. For verification, 1,000 sample cases were also run, and the resulting CDF’s matched the 400 sample cases almost identically. The results using 1,000 samples were used for the analysis of the two-bladed disk, but based upon this agreement, only 400 samples were used for the larger bladed disk analyzed in chapter 6.

5.4 PDS Methodology—Simulation of Statistics from Modal Test

As with the simple system described in chapter 4, the first step in the analysis is to perform MC simulations of the nondeterministic substructures to produce the dynamic rv sample set. This sample set, if actually measured from a population of substructures, would be significantly more accurate in representing the random substructures than using a set of assumed primitive rv’s. One of the first new issues that arose for this realistic system was producing a statistically consistent set of rigid body modes for the two free-free blades. Since there are 3 dof’s per node that are free, each blade will have three unique, zero-frequency rigid body modes. In general though, the shape of the modes (i.e., the combination of rigid-body translation and rotation) and the order that these modes are produced by a numerical procedure is arbitrary, since they are all at the same frequency. The PDS method requires that statistics be taken on the mass-normalized mode shape, so a method of producing consistent, reproducible output was necessary.

Because of this requirement, it was seen early in the analysis that the finite element capability built into NESSUS itself was unacceptable since it would not be able to provide this information directly. Fortunately, detailed study into NASTRAN capabilities resulted in the discovery that the use of the SUPORT card with the modified Householder method of eigenvalue extraction would yield exactly what was needed. This solution would produce rigid body modes parallel to the unconstrained coordinate frame, and the order of these modes would be consistent for the random perturbations in the model resulting from the probabilistic analysis. Sample sets for these mode shapes could therefore be obtained where, for example, the first mode would always be a translation parallel to the global z axis, the second mode would be a pure rotation about the x-axis, and the third mode would be a pure rotation about the y-axis. This enabled the generation of dynamic rv's from these modes with consistent means and standard deviations that could be used in PDS.

Another aspect of numerical eigenvalue extraction methods is that the signs of the modes are arbitrary and can be reversed for slight variations of the model. Since gathering the statistics of the modes require that they all be of one sign, a subroutine was written to compare the sign of the modes for the second and later samples with that of the first, and, if it was different, to multiply all the values in the mode by -1 .

Calculation of the residual flexibility matrix from the modal data, which was performed using FORTRAN subroutines linked to the NESSUS run, was also different than for the simple case. More detailed research and some test runs indicated that significant error would result if all of the truncated modes were not used in the calculation using equation (111). Since obtaining all the modes is generally not realistic, alternate methods for obtaining the residual flexibility had to be obtained. For the constrained deterministic disk, the system stiffness matrix is first inverted to create the total system flexibility matrix, as expressed in equation (16), and the residual flexibility is then obtained by subtracting the flexibility of the retained modes, which are, in general, much smaller in number than the truncated modes, from the total flexibility according to equation (22).

For the free-free probabilistic blades, the system is unconstrained so the stiffness matrix will be singular. The "inertia-relief" method, initially developed by Craig,⁵² is therefore used to obtain the residual flexibility. First define the transformation matrix P according to:

$$P = I - M\Phi_R\Phi_R^T, \quad (113)$$

where Φ_R contains the rigid body modes and M is the substructure mass matrix. Now choose any statically determinate subset (in this case, of size three), denoted E, from the boundary dof's, and partition the stiffness matrix accordingly into the E set and the other set, denoted by a subscript O:

$$[K] = \begin{bmatrix} K_{EE} & K_{EO} \\ K_{OE} & K_{OO} \end{bmatrix}. \quad (114)$$

Next, consider a flexibility matrix composed of only the inverse of the K_{EE} partition and defined as G^S :

$$G^S = \begin{bmatrix} K_{EE}^{-1} & 0 \\ 0 & 0 \end{bmatrix} . \quad (115)$$

In terms of P and G^S , Craig shows that the flexibility matrix for the elastic modes is given by

$$G^{\text{elastic}} = P^T G^S P . \quad (116)$$

Equation (22) is now applied to obtain the residual flexibility:

$$G^{\text{residual}} = G^{\text{elastic}} - G^{\text{retained}} = G^e - [\Phi_N][\Lambda_N]^{-1}[\Phi_N]^T , \quad (117)$$

where Φ_N are the retained elastic modes. The calculation of these residual flexibility values were calculated for each sample during the MC run, and saved so that the statistics could later be generated.

During this formulation of the analysis, it became evident that the size of the dynamic rv set would become intractable for a realistic problem. For this problem, which has only two probabilistic substructures and where 20 modes were chosen to be retained (out of a possible 108) per substructure, the number of dynamic rv's would be obtained as follows:

$$\begin{aligned} \text{Number dynamic rv's} &= 2 \text{ substructures} * \{ 17 \text{ elastic eigenvalues} \\ &+ (4 \text{ boundary nodes}) * (3 \text{ dof's/node}) * (20 \text{ retained modes}) \\ &+ [(4 \text{ boundary nodes}) * (3 \text{ residual flexibility dof's/node})]^2 \} = 802 \end{aligned}$$

It is evident that this size is highly dependent on the number of retained modes. Standard practice is to include up to the mode that has twice the natural frequency as the frequency of interest. In this case, the twentieth mode for the disk is at 7,596 Hz, and the blades are both above 50 khz. The frequency of interest, which was chosen for the third system mode, is only 456 hz, so the chosen modal representation should be sufficient. This rule of thumb can be inaccurate in certain cases. Exploring its applicability to this case is an avenue of future research.

Some attempt was made to incorporate this large number of rv's in the problem, which requires alteration of the NESSUS code as well as massive matrix storage issues. Rather than continue along this course of action, several assumptions were made to drastically reduce the number of dynamic rv's. The first was to assume that the limit state function was insensitive to the variation in the rotational dof's in the modes. This reduced the size of eigenvector rv's from 240 to 80 per substructure. The second was to assume the limit state was insensitive to not only the rotational dof's but also to the off-diagonal terms in the boundary residual flexibility matrix, which reduces the size of that contribution from 144 to 4 per substructure. These assumptions do not remove these variables from the formulation of the substructure stiffness matrices; instead, it allows the use of the mean value of those variables (or median, as will be discussed later). Admire and Tinker⁵³ examined the effect of completely removing the off-diagonal G elements, and calculated a natural frequency error of less than <5 percent between the exact value and the value obtained using the RF formulation.

After the entire sample set for the dynamic rv's was created, the program is then directed to a subroutine to calculate the correlation matrix for the blades. Recall from section 4.1 that the Cholesky decomposition technique is used to decorrelate the rv's. For this problem, the Cholesky decomposition broke down because the correlation matrix was positive semidefinite; for reasons discussed below, many of the eigenvalues were almost equal to zero. Due to the ill-conditioning of the correlation matrix, an alternate procedure, which used the eigenvalues $\{\lambda_c\}$ and eigenvectors $[\Phi_c]$ of the correlation matrix was implemented. The matrix of eigenvectors $[\Phi_c]$ was used to construct an orthogonal transformation from the independent rv "load set" $\{u\}$ to the standard normal variables $\{x^l\}$, which are obtained from the original vector of dynamic rv's $\{x\}$ using the mean and standard deviations of the elements, as performed for the benchmark case. This transformation is shown as follows:

$$\{x^l\} = [\Phi_c] \{u\} . \quad (118)$$

The set $\{u\}$ consists of independent rv's whose variances (square of the standard deviation) are elements in $\{\lambda_c\}$.

To verify that the calculation of the correlation was done correctly, in this case the back transformation of equation (118) was performed immediately to create $\{u\}$ and the correlation between these rv's was then calculated. If the elements of $\{u\}$ were uncorrelated, the correlation matrix would be an identity matrix. The result was somewhat different, but was very illuminating. For the rows/columns of the new correlation matrix $[C_u]$ that corresponded to eigenvalues on the order of one, the diagonal term was equal to 1.0 and the other elements in the associated row/column were very small. However, many of the eigenvalues turned out to be very small and the analogous rows and columns in $[C_u]$ were not diagonal; the diagonal values were 1.0 but the other terms in the row/column were all on the order of one (between zero and one) instead of being close to zero. This can be explained by realizing that the actual number of independent rv's in the system is equal to the original number of independent primitive rv's, not the number of dynamic rv's. Therefore, the rv's associated with the small λ_c values are actually insignificant and the magnitudes of these values are mainly due to numerical roundoff. The high off-diagonal values in the new correlation matrix in these rows/columns therefore indicates a large amount of correlation between these numerical artifact "rv's."

The above result can be used to further decrease the size of the rv set $\{u\}$. A sum of the eigenvalues of the correlation matrix was calculated, and any eigenvalue < 3 percent of the sum was deemed insignificant and the associated rv in $\{u\}$ was neglected. The value of 3 percent was reached by starting at 5 percent and decreasing the cutoff value (thereby including more rv's) until the final result stabilized. This reduced the eigenvalue set from 101 to 11. It is unclear why this value did not actually reduce to three, which is the number of primitive rv's per blade, but nevertheless, this reduction greatly facilitated the analysis.

5.5 Use of Dynamic Random Variables for PDS

As described in chapter 1, one the main goals of this research is to use the statistics of the dynamic characteristics of the substructures as the rv's in a probabilistic analysis rather than primitive rv's. These dynamic rv's can be applied either using an MC approach or using the reliability method approach. The MC should provide more accurate answers, while the reliability method will be more computationally efficient.

5.5.1 MC Using Dynamic Random Variables (PDS MC)

Using the assumption that the dynamic rv's followed a normal distribution, a vector of each rv was created using the data obtained in section 5.4 to generate the matrix $[u]$, where the number of rows equals the number of reduced independent rv's ($2*11/\text{blade}=22$) and the number of columns is equal to the number of samples. This matrix is transformed to the correlated standard normal variable matrix $[x^*]$ (of dimension equal to number of dynamic rv's by number of samples) by using a reduced matrix $[\Phi_c]$ (of dimension equal to number of dynamic rv's in $[x^*]$ by number of reduced independent rv's). Equation (118) therefore becomes

$$[x^*] = [\Phi_c][u] \quad . \quad (119)$$

As before, the statistics from the simulated modal testing are then used to transform $[x^*]$ to $[x]$, the set of original dynamic rv's for each substructure. Instead of using the mean values for the transformation from standard normal rv's to the original rv's, the median was used. This is explained in the next section. The matrix $[x]$ is then used to create the substructure stiffness matrices which are coupled together with the deterministic disk substructure to create a system stiffness matrix for each sample for eigenanalysis. The procedure used was essentially the same as for the benchmark case except that the complexity was considerably greater. This increased complexity was first evident in the ordering procedure used to rearrange the substructures into internal and boundary dof's and in the method used to tie the boundary dof's of adjacent substructures together. These procedures required the use of integer vector "maps," which label each substructure dof with its total structural dof. This methodology is used widely throughout industry for coupled loads analysis.

A modal analysis is then performed on each of these sample systems to generate CDF's for any particular free-response characteristic. For the purpose of this study, the third natural frequency of the combined system was selected. The comparison with the MC baseline is shown in figure 21. The results are mixed; from the design problem approach, the errors as seen in the tabular portion of figure 21 for the .01 and .99 CDF levels are < 2 percent, so the values could be used with confidence. From a theoretical standpoint, the curves do not line up extremely well; this is indicated by the error in the standard deviation of about 20 percent. Based on the results of chapter 4, it was anticipated that the performance of this method would be better. The potential sources of error are as follows:

- (1) Transformation error of the statistics of the original primitive rv's due to inaccuracy of the MC simulation of the dynamic rv's (possibly insufficient number of samples).
- (2) Transformation error in the statistics and recorrelation of the rv's due to their assumed normality.
- (3) Error due to truncation of the number of independent rv's.
- (4) Truncation error due to using the RF formulation of CMS.
- (5) Programming error.

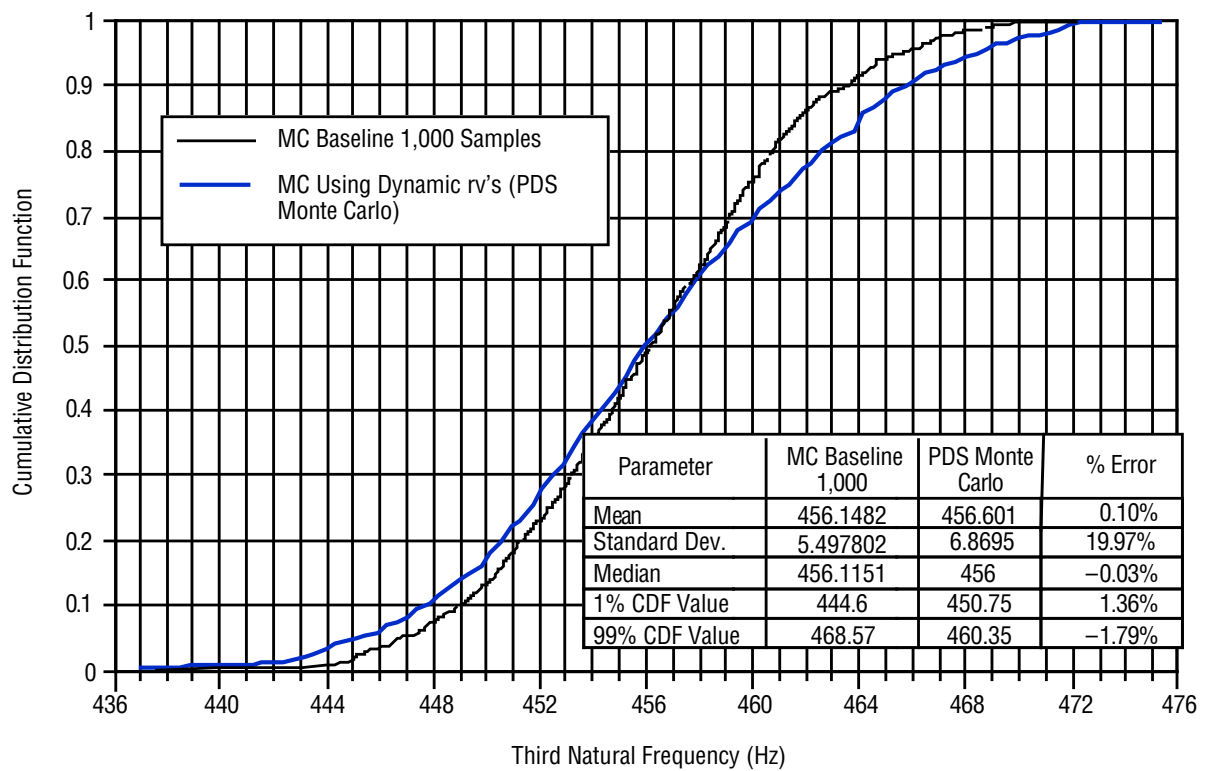


Figure 21. Two-bladed disk, mode 3 natural frequency; comparison of PDS MC with MC baseline.

5.5.2 Using Dynamic Random Variables in Reliability Approach (PDS Reliability)

The data obtained in section 5.4 are now used to generate the different “load” cases of $[u]$ for use in the reliability method of probabilistic analysis as opposed to for an MC simulation. Matrix $[u]$ is created in this approach by varying each of its elements by ± 0.3 of a standard deviation, which for that rv is the square root of the correlation matrix eigenvalue, as described in section 5.4. The number of rows in $[u]$ is equal to the number of probabilistic substructures times the reduced number of indepen-

dent rv's, and the number of columns is equal to this number times two, plus one additional column for the mean value set. The superscripts $j=1,2$ on the matrix variables below refer to the number of the probabilistic substructure, and the subscript $i=1,\dots,11$ refers to the number of the independent rv:

$$[u] = \begin{bmatrix} -0.3 * \sigma_{u_1^1} & 0.3 * \sigma_{u_1^1} & 0 & 0 & 0 & 0 \\ 0 & 0 & \ddots & 0 & 0 & 0 \\ 0 & 0 & 0 & -0.3 * \sigma_{u_i^j} & 0.3 * \sigma_{u_i^j} & 0 \end{bmatrix}. \quad (120)$$

The response value of interest, the third eigenvalue in this case, was then appended to each column of $[u]$ from equation (120) to create a NESSUS/FPI "datapoint."

With these datapoints, the AFORM quadratic solution method can be applied by NESSUS. By simply changing the first variation in the above approximation to a value very close to zero times the standard deviation, the three points can also be used to create a FORM linear approximation. The quadratic and linear methods yielded virtually identical CDF's. This implies that the system is very linear and that the coefficient of variation of 10 percent is not large enough to magnify the small nonlinearities. The linear (FORM) CDF is plotted along with the MC baseline solution of the total system in figure 22. Because of the large difference in the CDF's as seen visually and as indicated by the size of the standard deviation, sources of error not previously examined were investigated.

One subtle but important error found was in the application of the transformation to standard normal variables. For the MC baseline solution, the results are obtained by creating a normal distribution about the mean values of the primitive rv's; this distribution is symmetric, so the median is equal to the mean. Since the finite element solution is slightly nonlinear as a function of the input rv's, the mean of the solution will not equal the median (see equation (47)), but the median solution will result from using the mean (equal to median) primitive rv's.

As PDS is implemented for these analytical simulations, there is an intermediate step that introduces error. Symmetric Gaussian MC distributions are created about the means of the dynamic rv's, which will not be the medians since a slightly nonlinear eigensolution has been performed to obtain them. This results in a skew of the entire CDF curve since the method assumes that the dynamic rv's do in fact follow a symmetric distribution. The median of the results (indicated by the response value at a CDF level of 0.5) should result from the median of the input rv's. However, the deterministic value for mode three obtained for the medians of the primitive input rv's using the RF CMS method is equal to 455.3 Hz, which is 1.4 Hz less than the median value obtained using AFORM of 456.7 Hz.

It should be noted at this point that the RF CMS method was used for this deterministic calculation to provide a consistent basis for comparison with the reliability methods, which also use the RF CMS method. This calculation can also serve as a checkout of the RF CMS method itself by comparing it with the deterministic value obtained using the original NASTRAN unreduced model using the medians of the input primitive rv's. The NASTRAN value of 456.035 is only 0.735 Hz, or 0.16 percent, greater than the RF CMS deterministic value. These values are also shown in figure 23.

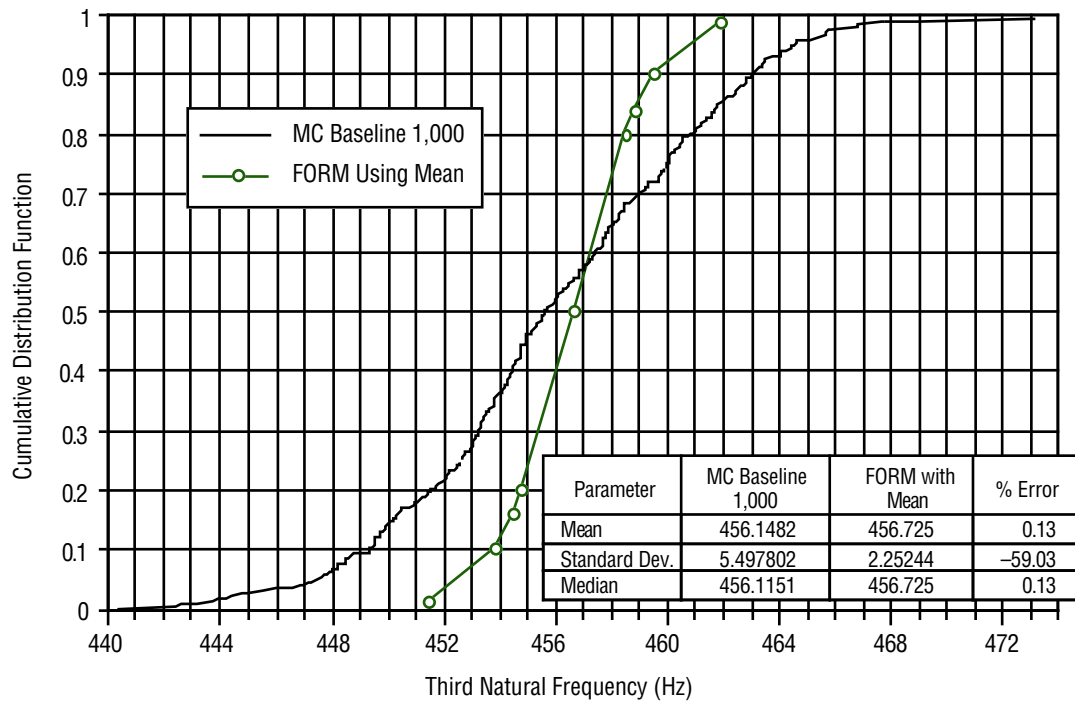
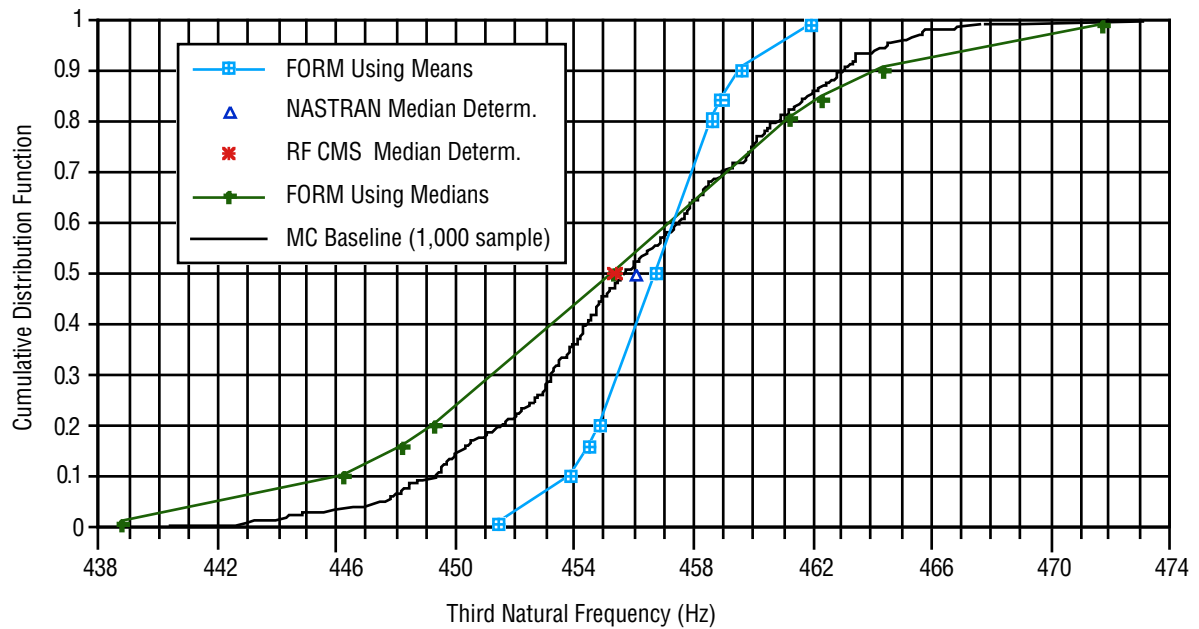


Figure 22. Two-bladed disk, mode 3 natural frequency comparison of MC baseline with PDS FORM with mean.



Parameter	MC Baseline 1,000	FORM Using Mean	% Error	FORM Using Median	% Error
Mean	456.1482	456.725	0.13	455.297	-0.19
Standard Dev.	5.497802	2.25244	-59.03	7.08748	28.91
Median	456.1151	456.725	0.13	455.297	-0.18

Figure 23. Two-bladed disk mode 3 natural frequency comparing FORM using median versus mean.

The error resulting from using the means can be corrected by simply ensuring that the median primitive values are carried through the procedure to generate the median results. This is accomplished by using the medians \tilde{x} of the calculated dynamic rv's as the "mean" in the transformation to standard normal coordinates:

$$\{x\} = \{x^*\} \sigma + \tilde{x} \quad . \quad (121)$$

Although there is still some error inherent in the normal assumption, this correction allows for a direct "apples-to-apples" comparison with MC baseline simulations. The results for this correction are shown in figure 23 and are clearly better.

One unexpected benefit from using this correction was the vast improvement not only in the skew of the CDF curves at the median, but also in the standard deviation. This change can be understood by examining the variation of the response variable to the input rv's when the expansion is performed about the medians instead of the means. The expansion is shifted to an entirely new location in the hyper-dimensional response surface space, and the curvature is different. This is indicated by looking at the variation of the response variable with respect to a single independent rv, u_{16} , for an expansion about the median and about the mean. As seen in figure 24, the sensitivity curve is much steeper when the expansion is about the median than the mean. This indicates a higher standard deviation, or spread in the CDF curve, since the same variation in the input rv will yield a larger change in the response variable. This increased standard deviation is seen in the final comparison of results in figure 25, which shows a much better fit with the MC. The results are discussed in more detail in section 5.5.3. The higher order reliability methods were also applied to this problem using the medians instead of the means of the dynamic rv's. Neither the AMV or the AFORM showed any improvement over the linear case; this may be due to the very small nonlinearity of the limit state.

In addition to the methods discussed above, the approximate statistics generated as a first step of the AFORM solution can be used to create a CDF, as mentioned in chapter 4. Using the mean and standard deviation from the FORM solution with an assumed Gaussian distribution yields a CDF identical to the FORM solution, as expected. Since the AFORM solution approximate statistics yield a different value for the median and mean (since a partial quadratic calculation of the mean is used), it is more appropriate to use these in an assumed lognormal distribution. The resulting CDF was also virtually identical to the linear solution, indicating a strong degree of linearity in the system.

5.5.3 Results Using PDS Methods

The results using the PDS MC, PDS reliability, and PDS "approximate statistics" methods are compared with the MC baseline CDF in figure 25. The graph can be used to visually compare the total match of the CDF's, while the table should be used to evaluate the errors for the locations of interest in the design problem. As with the PDS MC, the actual error for the design values is very small when using the PDS reliability methods, so they could be used with confidence, but the discrepancy in the shapes of the CDF's, as indicated by the errors in the standard deviations as well as visually, suggest that further improvements could be made. The potential sources of error for the reliability methods are the same as

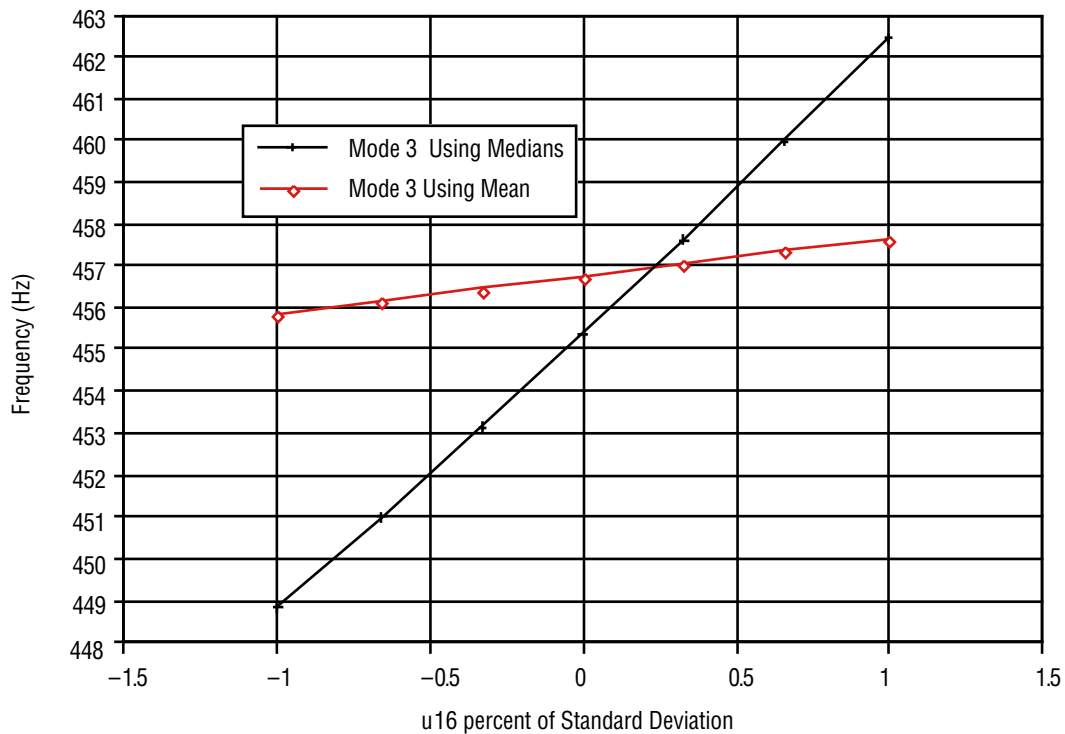
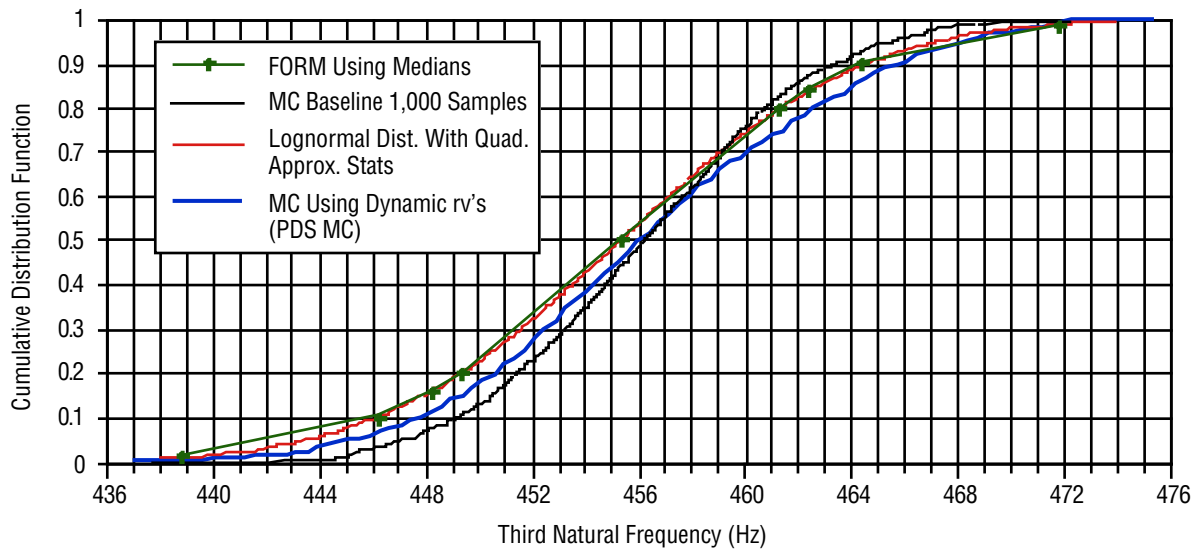


Figure 24. Two-bladed disk, mode 3 frequency as a function of u16, using medians and mean values of dynamic rv's.



Parameter	MC Baseline 1,000	FORM Using Medians	% Error	PDS Monte Carlo	% Error	Lognormal Dist.	% Error
Mean	456.1482	455.297	-0.19	456.601	0.10	458.747	0.57
Standard Dev.	5.497802	7.08748	28.91	6.8695	19.97	7.231	23.97
Median	456.1151	455.297	-0.18	456	-0.03	455.296	-0.18
1% CDF Value	444.6	438.81	-1.30	450.75	1.36	438.95	-1.29
99% CDF Value	468.57	471.79	0.69	460.35	-1.79	472.35	0.80

Figure 25. Two-bladed disk, mode 3 natural frequency comparing MC with PDS.

for the PDS MC method with the addition of other inaccuracies as discussed in chapter 3.

It is interesting to compare computational times at this point. All the analyses were performed on a CRAY T-90 supercomputer. The MC baseline analysis took 2,527 CPU sec and 20.3 hr of wallclock time to run. PDS MC took 389.5 sec of CPU time and 1,112.3 sec (18.5 min) wallclock time, a drastic reduction enabled by the continuous generation, storage, and analysis of modally reduced system matrices rather than the complete model generation and analysis necessary for each of the MC baseline samples. The FORM method took only 20.1 sec of CPU and 64.2 sec of wallclock to create the datapoints for input to NESSUS/FPI, and about 30 sec wallclock to run FPI to perform the FORM solution. This further reduction is due to the substantial decrease in the number of solutions generated. As anticipated, both the use of CMS and probabilistic methods drastically decreased the amount of time necessary to run the analysis, which, especially for a more detailed model, could be a prerequisite for use in design.

5.6 Forced Response—Deterministic Case

The use of PDS was now expanded to forced response. In particular, a frequency response solution of the system was derived since this type of excitation would prove most applicable to the bladed-disk problem. This requires a rederivation of the basic equations derived in chapter 2 for the RF CMS method. Initially, the dof's of a substructure are partitioned into three sections: x_o , which are internal dof's with no external load applied; x_i , internal dof's with an external load applied; and x_b , boundary dof's which may or may not have external load applied. The equation of motion is therefore

$$[M] \begin{Bmatrix} \ddot{x}_o \\ \ddot{x}_i \\ \ddot{x}_b \end{Bmatrix} + [C] \begin{Bmatrix} \dot{x}_o \\ \dot{x}_i \\ \dot{x}_b \end{Bmatrix} + [K] \begin{Bmatrix} x_o \\ x_i \\ x_b \end{Bmatrix} = \begin{Bmatrix} f_o \\ f_i \\ f_b \end{Bmatrix} . \quad (122)$$

The RF transformation matrix $[T]$ defined in equation (29) is altered slightly for this method of partitioning:

$$\begin{Bmatrix} x_o \\ x_i \\ x_b \end{Bmatrix} = \begin{bmatrix} \phi_i - G_{res-ob} G_{res-bb}^{-1} \phi_b & 0 & G_{resob} G_{res-bb}^{-1} \\ 0 & \phi_i - G_{res-ib} G_{res-bb}^{-1} \phi_b & G_{res-ib} G_{res-bb}^{-1} \\ 0 & 0 & I \end{bmatrix} \begin{Bmatrix} q_o \\ q_i \\ q_b \end{Bmatrix} = [T] \{q\}_1 \quad (123)$$

and is used to convert the above equation into new coordinates $\{q\}_1$:

$$[M]_1 \begin{Bmatrix} \ddot{q}_o \\ \ddot{q}_i \\ \ddot{q}_b \end{Bmatrix}_1 + [C]_1 \begin{Bmatrix} \dot{q}_o \\ \dot{q}_i \\ \dot{q}_b \end{Bmatrix}_1 + [K]_1 \begin{Bmatrix} q_o \\ q_i \\ q_b \end{Bmatrix}_1 = [T]^T \begin{Bmatrix} f_o \\ f_i \\ f_b \end{Bmatrix} , \text{ where} \quad (124)$$

$$[M]_1 = [T]^T [M] [T] , \quad [C]_1 = [T]^T [C] [T] , \text{ and } [K]_1 = [T]^T [K] [T] .$$

The transformed mass and stiffness matrices will be identical to those obtained for the free response shown in equations (31) and (32). Rather than carry out the multiplication of the righthand side of equation (124) to determine an expression, the transformation matrix and the original load vector are both carried throughout the analysis until the generalized force is needed, at which time the matrix multiplication is carried out. To actually perform the forced-response analysis, the coupled system above is transformed to an uncoupled system using a set of truncated mass normalized system eigenvectors $[\Phi]_1$ resulting from a free-response solution of equation (124).

$$\{q\}_1 = [\Phi]_1 \{q\}_2 \quad . \quad (125)$$

The uncoupled system is in the form

$$[I]\{\ddot{q}\}_2 + [C]_2\{\dot{q}\}_2 + [\Lambda]_1\{q\}_2 = [\Phi]_1^T [T]^T \{f\} \quad , \quad (126)$$

where $[\Lambda]_1$ is the diagonal matrix of the eigenvalues of the transformed system. The standard (viscous) modal damping assumption is used for $[C]_2$:

$$[C]_2 = 2.0(\zeta)[\Lambda]_1^{\frac{1}{2}} \quad . \quad (127)$$

In this analysis, ζ is assumed to be constant for all the modes, and the input force is phased with a structural mode to simulate bladed-disk excitation. There are standard techniques available for obtaining the frequency-response solution for this set of uncoupled single dof systems. Because of the series of linear transformations performed on the solution, a complex quantity for the solution is desired rather than one in terms of magnitude and phase, as is commonly derived in texts on the subject and which cannot be easily transformed.

To this end, first express the element of the original excitation vector $\{f\}$ acting on the n 'th dof as follows:

$$f_n = p_n e^{i(\Omega t - \alpha_n)} = p_n e^{i\Omega t} e^{-i\alpha_n} = p_n e^{i\Omega t} (\cos \alpha_n - i \sin \alpha_n) = F_n e^{i\Omega t} \quad , \quad (128)$$

where p_n is the amplitude, Ω is the frequency of excitation, α_n is the relative phase of the excitation force, and F_n is a complex number defined as shown. The righthand side of equation (126) is defined to be the generalized force $\{f_{gen}\}$, which can be calculated directly as

$$\{f_{gen}\} = \{F_{gen}\} e^{i\Omega t} = [\Phi]_1^T [T]^T \{F\} e^{i\Omega t} \quad . \quad (129)$$

It should be noted that this step now requires more information for the RF transformation matrix $[T]$ than the free response does. As seen in equation (123), the columns of the transposed matrix $[T]^T$ corre-

sponding to the new forces applied at the internal dof's f_i are needed for the matrix multiplication to calculate the generalized force. In addition, for final recovery of displacement locations not at the boundaries, the same information will be needed. Therefore, additional elements of the modal matrix $[\Phi]_1$ and of the residual flexibility matrix $[G_{ib}]$ must be saved from the eigensolution and residual flexibility calculation and used to create a partial $[T]$ matrix using equation (123). Only the partition of $[T]$ corresponding to the internal dof's where load is applied, internal dof's where final displacements are recovered (if different), and the boundary partitions are actually needed for the calculation of $\{f_{gen}\}$ using equation (129).

Now, it is assumed that the solution q_2 has a harmonic solution of the form

$$q_{2j} = v_j e^{i(\Omega t - \Psi_j)} = v_j e^{i\Omega t} e^{-i\Psi_j}, \quad (130)$$

where $j=1, \dots, p$ is the number of modes retained in $[\Phi]_1$ and Ψ_j is the output phase of the j 'th generalized dof. Substitution of equation (130) into (125) yields the following expression for the j 'th generalized coordinate:

$$-v_j \Omega^2 e^{-i\Psi_j} e^{i\Omega t} + (2\zeta \omega_j) v_j i \Omega e^{-i\Psi_j} e^{i\Omega t} + \lambda_j v_j e^{-i\Psi_j} e^{i\Omega t} = F_{gen j} e^{i\Omega t} \quad (131)$$

or

$$\left(-\Omega^2 + 2\zeta \omega_j \Omega i + \lambda_j\right) v e^{-i\Psi_j} e^{i\Omega t} = F_{gen j} e^{i\Omega t}, \quad (132)$$

where ω_j is the j 'th natural frequency (square root of the eigenvalue λ_j). Solving for v yields

$$v_j = \frac{F_{gen j}}{\omega_j^2 \left[1 - \left(\frac{\Omega}{\omega_j} \right)^2 + \left(2\zeta \frac{\Omega}{\omega_j} \right) i \right]} e^{i\Psi_j}. \quad (133)$$

Now, substituting (133) into (130), applying the definition of F_j as described in (128) and f_{gen} as described in (129), and canceling out terms in the exponent yields the solution for the generalized coordinate q_2 :

$$q_2 = \frac{f_{gen j}}{\omega_j^2 \left(1 - \left(\frac{\Omega}{\omega_j} \right)^2 + i \left(2\zeta \frac{\Omega}{\omega_j} \right) \right)}. \quad (134)$$

The complex vector $\{q\}_2$ can now be transformed back to the original coordinates $\{x\}$ using equations (29) and (124):

$$\{x\} = [T][\Phi]_1\{q\}_2 \quad (135)$$

The absolute values of this complex vector are then calculated to obtain the physical displacement vector.

This solution procedure was applied to the deterministic two-bladed disk as a test case. A system of four harmonic loads, each of amplitude 1 lb and applied to be in-phase with a peak displacement location of mode 3, shown in figure 26, was considered. A range of excitation frequencies ± 5 Hz from the mode 3 deterministic natural frequency of 455.35 Hz was applied, and an equivalent viscous damping value ζ of 2 percent was used in all modes. The maximum resulting response was 0.044558 in. for node 640 (at the tip of blade A), occurring at the natural frequency, as expected. The deterministic solution procedure was verified by performing the same analysis in NASTRAN for the full-up model, using a frequency range of ± 5 Hz from the NASTRAN mode 3 frequency of 456.035 Hz; this run resulted in a value of 0.044832 in. for the same node, an error of only 0.6 percent.

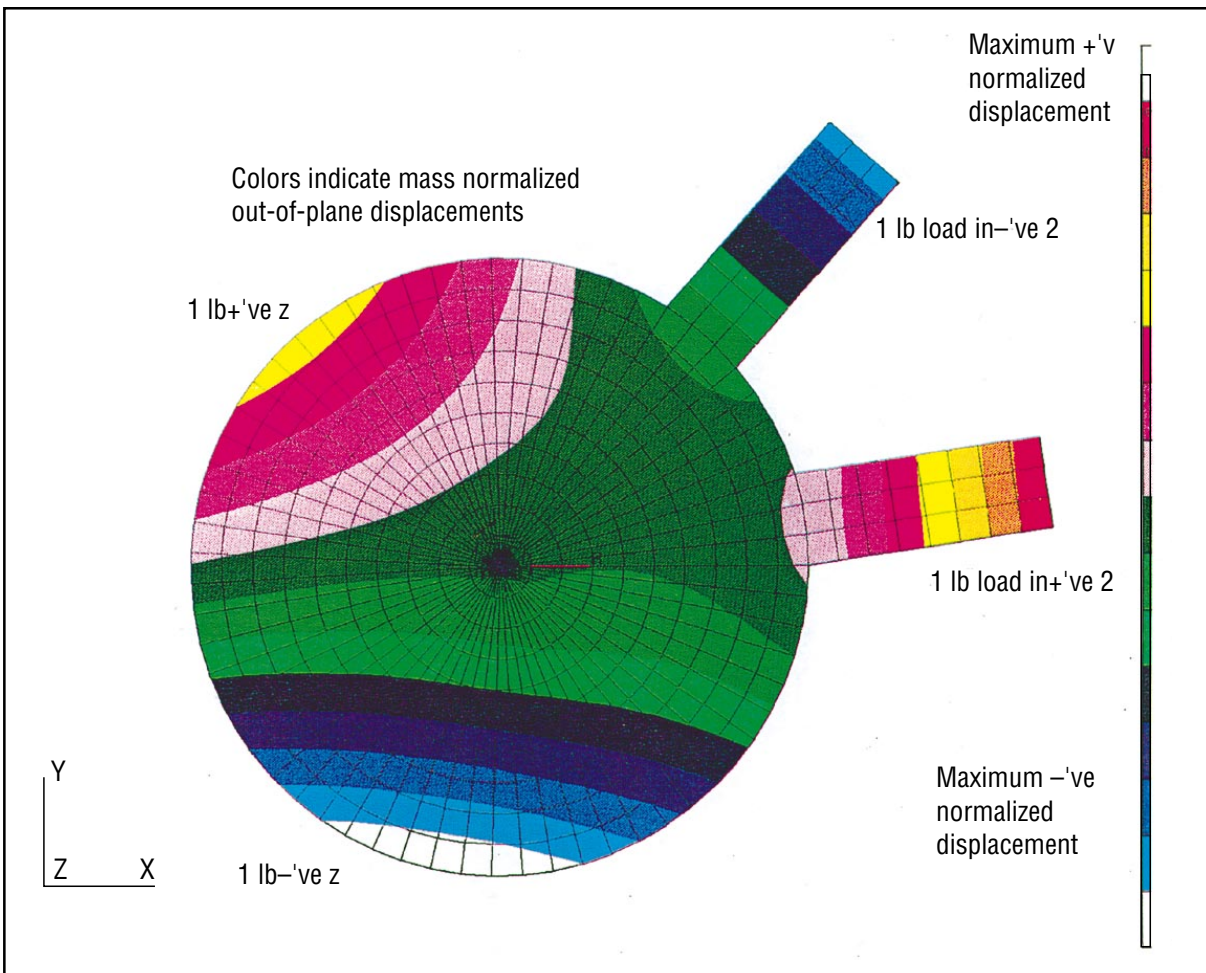


Figure 26. Two-bladed disk, mode 3 at 456 Hz.

It should be mentioned that an alternative, more direct method to solve for the vector $\{q\}_1$ could also have been applied. In this method, the matrices $[M]_1$, $[C]_1$, and $[K]_1$, are not transformed into modal coordinates but are rather combined in a system matrix $[Z]_1$ as shown below:

$$[Z]_1\{q(\Omega)\}_1 = \{f(\Omega)\}_1, \quad (136)$$

where

$$[Z]_1 = \left[-\Omega^2[M]_1 + i\Omega[C]_1 + [K]_1 \right] \quad (137)$$

and $f(\omega)$ is a complex quantity representing the magnitude and phase of excitation as shown in the derivation of the modal superposition method. The response vector $\{q(\Omega)\}_1$ is obtained by premultiplying $f(\Omega)$ by the inverse of $[Z]_1$ at each excitation frequency of interest. This approach is preferred if there is no modal truncation performed, which is the case for the solution of $\{q\}_2$ after equation (126) is formulated. Since it is more direct, this method is recommended for future research.

5.7 Forced Response—Probabilistic Case Using PDS

As discussed above, applying the forced-response solution requires more information from the modal data and the residual flexibility matrices. This increases the number of dynamic rv's necessary to solve the problem, which increases the complexity of the problem in several aspects. More statistical calculations, a larger correlation matrix, and more dimensions for the solution of the AFORM algorithm are all required. To minimize this number, it is important to decide a-priori which internal dof's will either have external load applied or require a displacement recovery. Although the entire modal matrix and residual flexibility matrix are calculated, only those partitions of the modal matrix and the residual flexibility matrix, along with the boundary dof's, are stored. In addition, only the correlations with these additional dof's are generated. Note that one might also include the measured modal damping ratios of each substructure in the set of dynamic rv's for the forced-response problem. Given the variability in measured damping properties, the incorporation of statistics on the modal damping value could be an important avenue for future research.

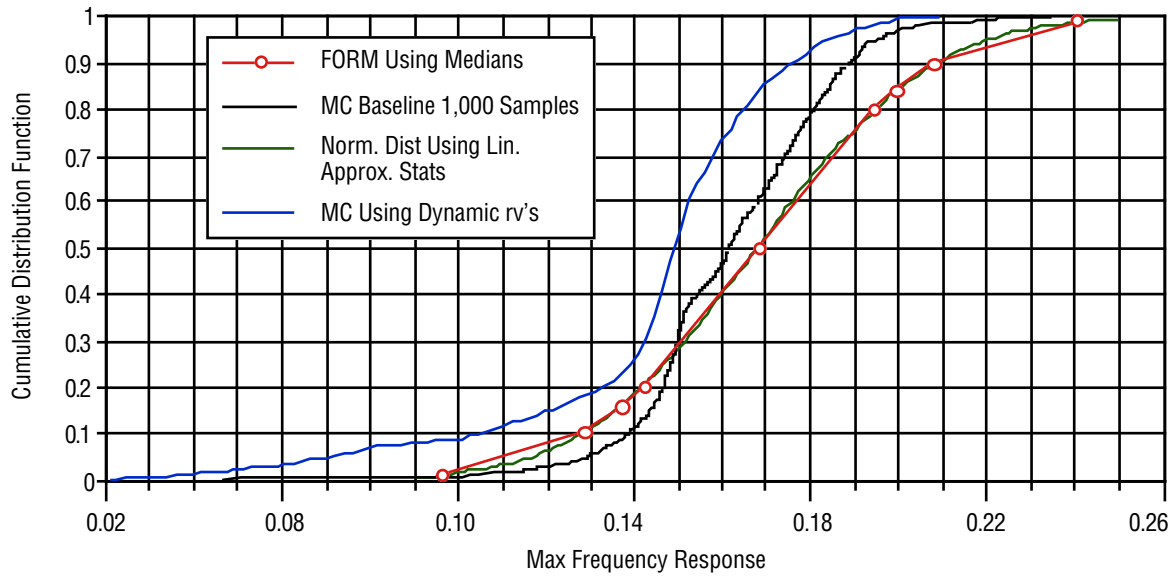
To address the design problem defined earlier, the response variable for the forced-response analysis was chosen to be the maximum response for all dof's in the structure. Initially, the excitation was applied at only a single frequency, but this was changed to a wide excitation bandwidth since the maximum response occurs at the damped natural frequency of the mode shape being excited, and this mode shape can occur over a range of frequencies for a probabilistic structure. It is assumed that the actual excitation mechanism could also vary in frequency by this amount, which is generally the case in engine turbomachinery, for instance. Using the maximum over some frequency range also helps to reduce the extreme variability in response which can be observed at any particular excitation frequency.⁵⁴ This variability, which is largest near peaks and zeros in frequency response functions, would introduce substantial nonlinearities in the response limit state surface. A range of ± 10 Hz about the deterministic natural frequency of 458 Hz was used in this case. This value is probably inadequate, since the free-response case shows that the actual range is between 438 and 472 Hz, so this may be a source of error in the final results.

The MC baseline frequency-response solution required extensive alteration of the MSCPOST subroutine within the NESSUS code. This subroutine reads the NASTRAN dataset OUGV1, which contains any displacement data obtained during the NASTRAN run. The frequency response solution for the baseline full-up model was run using the NESSUS/NASTRAN MC solution sequence, as with previous cases, but the entire displacement set for each sample was then read and a sorting routine performed to find the maximum value. The value was then fed back into the NESSUS main program for statistical calculations. This MC baseline solution sequence was extremely computer intensive, so only a limited sample size was run.

The PDS procedure using both the MC and reliability approaches for the frequency-response problem is similar to the free-response problem. The main additions are the subroutines necessary for calculation of the different $[T]$ matrices for each substructure and the complex solution algorithm detailed in the deterministic case. Because the value of the largest responding dof is no longer at a frequency known a-priori (since the third natural frequency and third natural mode will vary for each statistical sample), a sorting algorithm to find the maximum value was used that scanned the response values for all the selected dof's for all the frequencies in the bandwidth chosen. The dof's selected were those at the blade tips, which were assumed to contain the maximum responding dof for the entire structure with the chosen excitation. This value was then used as the NESSUS response variable, and input along with the corresponding load set. Also, to magnify the response a bit from the deterministic case, a modal damping ratio value of 0.5 percent was used. PDS MC and FORM cases were run as well as a normal distribution using the linear "approximate statistics." The PDS quadratic AFORM method using the medians was also attempted, but the AFORM algorithm in NESSUS/FPI never converged to a solution. Several different attempts were made using different sizes of the variation of the input rv, but answers were not generated. The reason for this problem is unknown at this point, and is an issue for future research.

The CDF results for the PDS methods are plotted along with a 1,000-sample MC baseline simulation in figure 27. The MC baseline CDF is extremely unsymmetric, so this clearly causes a problem for the reliability methods. It is also noted that there is fair agreement between the MC baseline result and that obtained from MC using dynamic rv's. The errors for the design point at 99 percent are still around 10 percent for both PDS methods, which is within reason especially when one considers that at present, there are no alternative methods for obtaining this maximum value. As with the free-response analysis, the significant error in the standard deviation and the lack of coincidence of the curves indicated visually signifies that there is still error present in the methods. An additional source of error in the reliability methods for this analysis is the extent to which the maximum responding dof does not have a smooth dependence on the rv's. Possible discontinuities in this dependence would cause errors in the response surface generation created using numerical differentiation, as discussed in chapter 3.

An examination of the computer run times shows that the MC baseline took 728 sec of CPU time and 27.3 hr of wallclock (which was much faster than normal due to low computer usage during the entire run), the PDS MC took 389 CPU-sec and 1,112 wallclock sec (the free- and forced-response were actually performed simultaneously), and the PDS FORM took 20.35 CPU sec, 60.6 wallclock sec, and less than 30 sec for the NESSUS/FPI run. Because these results showed an acceptable level of error from the design perspective and because the main goals of the method were achieved, an analysis of a realistic bladed-disk system was pursued and is discussed in the next chapter.



Parameter	MC Baseline Using 1,000 Sample	FORM With Medians	% Error	MC Using Dyn. rv's	% Error
Mean	0.1612384	0.168355	4.23	0.1455	-10.81
Median	0.1595526	0.168355	5.23	0.1500	-6.37
Standard Dev.	0.02350084	0.031058	24.33	0.0314	25.06
99% CDF	0.21584	0.243983	11.53	0.1970	-9.56

Figure 27. Two-bladed disk frequency response; MC versus PDS.

6. FREE- AND FORCED-RESPONSE ANALYSIS OF REALISTIC BLADED-DISK SYSTEM

6.1 Introduction and Literature Survey

The development of the PDS method discussed in the previous chapters is now complete enough for it to be applied to the dynamic analysis of rocket engine or gas turbine disks with turbine blades attached. Because of finite manufacturing capabilities, which cause the geometry of the blades to be uncertain, and because of variability in the material properties, each of the blades typically have slightly different modal characteristics when considered independently; each of the dynamic characteristics can therefore be characterized by a distribution type, mean, standard deviation, and other statistical parameters. An example of this variation is the first three measured cantilever modes of the turbine blades used on a first stage disk in the new Pratt & Whitney Space Shuttle Main Engine (SSME) high pressure fuel turbopump, shown in figure 28. The cov's of these distributions are around 1 percent, and the same distribution fitting program as used in the benchmark problem was run on the first mode, yielding a close fit with either the lognormal or normal distributions. The blade-to-blade variations in dynamic characteristics result in the combined bladed-disk system being mistuned with respect to an ideal system having identical, evenly-spaced blades. It is known that the dynamic response of the structure becomes irregular and difficult to predict. Two of the main results of this irregularity are localization, which is the concentration of the response at a certain blade within the set; and amplification, which is the magnification of the response of the maximum-responding blade in a mistuned bladed disk over the maximum-responding blade (or blades) in a tuned disk.

The mistuning phenomena has been examined in detail by researchers since D.J. Ewins described the problem in 1968.⁵⁵ Generally, two approaches have been taken for examining the problem. The first one is the deterministic approach, which uses both analytical and numerical techniques for deterministically defined mistuned disks. A general review of the research by Leissa in 1981 summarizes some of the analytical methods used, such as the receptance method, in which elements of an impedance matrix relating force applied to the disk to response at the blade and vice versa are determined by using closed-form partial differential equations.⁵⁶ Ewins applied this method to the study of packeting of blades on a disc, where blades are split into groups with identical blade frequencies within the group.⁵⁷ MacBain used impedance to determine the approximate level of response for any particular level of mistuning, or level of spread of blade natural frequencies about the mean value, for a set of blades.⁵⁸ Afolabi used these methods to define the localization and amplification phenomena seen in mistuned bladed disks.⁵⁹

One of the major deterministic methods of examining these systems is to use a lumped mass model composed of N single-degree-of-freedom (sdof) spring-mass systems each grounded but connected to each other with a coupling spring to represent the bladed-disk system. These lumped masses can be used to generate sets of simultaneous equations for matrix solution. One of the first papers to identify localization in structures was published by Pierre and Dowell in 1987, who generalized a geometrically periodic structure with lumped masses; they also incorporated perturbation techniques to analytically model the mistuning level rather than use a given set of mistuned frequencies.⁶⁰ Pierre and Wei continued

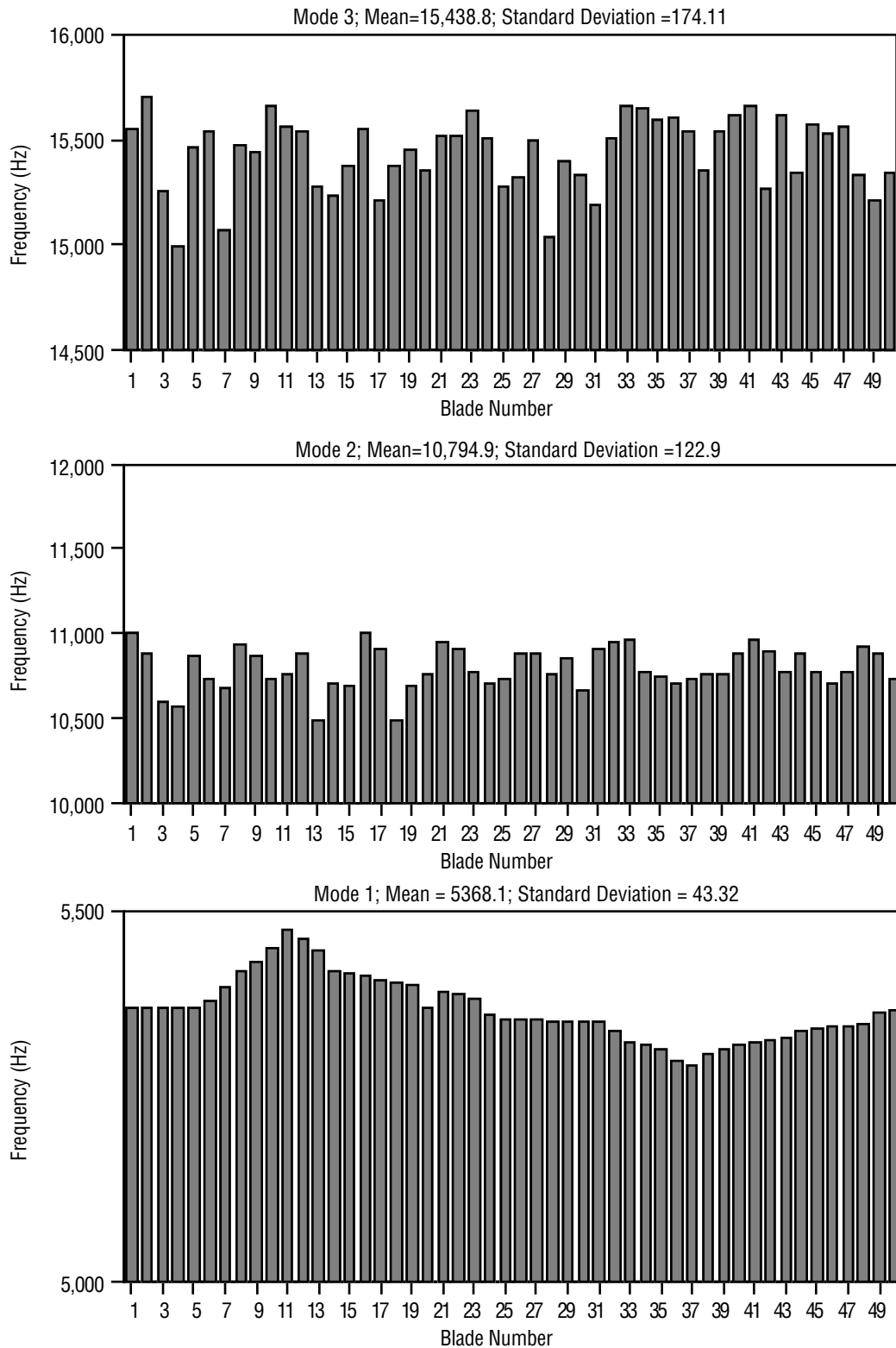


Figure 28. Variation of first three first-stage turbine blade frequencies for P&W SSME fuel pump.

this localization work and examined the relationship with structural coupling.⁶¹ They used a deterministic, closed-form solution for the eigenvalues and eigenvectors as a function of a single coupling parameter R and the “mistuning strength” of each sdof “blade,” which was defined simply as the variation of that blade’s natural frequency from the mean, Δf_i . The deterministic cases examined were generated by using a random number generator to determine the $N \Delta f_i$ values. Only two complete mistuned systems were able to be examined for amplification and localization using this method. In addition to the lumped mass method, some finite element studies have been performed to examine deterministic mistuned bladed disks. Irretier created a simple deterministic finite element model of a mistuned bladed disk, similar to that described in the last chapter, and proved that CMS methods could be used to accurately reduce the size of the model and maintain the localization behavior of the system.⁶²

The second major approach to examining mistuning phenomena is to apply statistical techniques. As with the deterministic approach, both analytical and numerical methods have been used. Generally, the perturbation method, as described in chapter 3, has been used to obtain the statistical properties of the response variable in the analytical approach. A closed-form expression for the variation of the elements of the system matrix A , as expressed in equation (88), in terms of the input rv’s is obtained directly. This is possible if the variation in the system matrix is kept extremely simple, as is the case when the system is composed of sdof “blades” and the only rv is the stiffness of each “blade.”

One of the first statistical examinations was performed by Huang in 1982, who approximated the system as a continuous disk with statistically characterized randomly varying circumferential parameters.⁶³ A partial differential equation was developed for this continuous system, which was then solved by applying the perturbation method. The result was analytical expressions for the stochastic dynamic characteristics of the structure. Sinha and Chen built upon this work in 1989 by applying it to discretely modeled bladed disks using the sdof per blade approximation.⁶⁴ The perturbation method was used to create an analytical expression for the maximum responding blade of the structure, which could then be represented by a power series. The statistics of this series were then used to obtain probability density functions of the response. The expressions obtained in this paper are extremely confusing, and direct integration of the joint pdf is required to obtain the CDF, which limits the applicability to simple functions with a small number of rv’s, as discussed in chapter 3. Purely numerical statistical work has also been performed on the problem, notably by Griffin and Hoosac in 1983, who characterized the response of large lumped-mass systems by using an MC simulation to run multiple eigensolutions rather than determining an explicit expression for the response variable.⁶⁵

Towards the beginning of the 1990’s, it became better recognized that a statistical approach was required for mistuning analysis because the blade population is large enough to require its characterization as an rv. In 1989, Pierre and Wei pointed out that the mean and standard deviation of the largest amplitude response experienced by a bladed disk cannot be generated by analytical techniques.⁶⁶ In this paper, they combined analytical techniques with MC simulations to understand the effects of mistuning. In a paper the next year, Pierre notes that only two studies of localization using statistical methods had been performed to that date.⁶⁷ In the same year, Hamade and Nickolaidis presented the first application of the reliability method of probabilistic analysis to the localization problem. They applied the FORM and the Rackwitz-Fiessler most probable point search algorithm to obtain the statistics on a dynamics of a simple two-span beam problem. Chamis and Shah in 1990 applied NESSUS to the bladed-disk prob-

lem, modeling the system with simple lumped masses with Young's Modulus as the single rv. This study was just a cursory look at the problem as an application of NESSUS. In 1993 Mignolet and Lin expanded upon the closed-form expressions developed by Sinha, and made comparisons between mistuned analysis methods.⁶⁸ The comparison of the various curves were performed on a qualitative, visual basis.

In 1995, Pierre and Kruse starting working on methods that would examine the statistics of more realistic mistuned bladed disks, realizing that the lumped-mass parametric studies previously performed are "difficult to relate to more descriptive finite element models."⁶⁹ They emphasized that the use of MC simulations is "critical" in calculating the maximum response of bladed disks although it is "prohibitively" expensive. Therefore, along with Ottarson in 1995,⁷⁰ they developed a "reduced-order method" (ROM), a finite element reduction method similar to CMS that is aimed directly at bladed disks by modeling only one sector of the disk. Only the Young's Modulus of each blade is set as an rv in this method, thereby allowing the natural frequencies of the blades to be directly mistuned. A deterministic tuned bladed-disk test case resulted in errors of 7 percent and 13 percent for the maximum blade response and system natural frequencies, respectively, between the "reduced-order" model and the full-up model where the size of the reduced-order model was 1/40 of that for the full-up model. A 1,000-sample MC simulation using a mistuned reduced-order model was performed to generate plots of the mean mistuned response normalized to the tuned response and a mean $+3\text{-}\sigma$ mistuned response normalized in the same way. Using this information, the researchers were able to identify important characteristics for mistuned bladed disks, in particular that "moderately weak" blade coupling is required for significant amplification. Yang, Griffin, and Kiefling simultaneously developed a very similar reduced-order approach, but did not perform any statistical analyses.⁷¹

6.2 Comparison of Previous Techniques for Mistuning Analysis With PDS

The extensive literature survey summarized above clearly identifies the importance and uniqueness of the PDS technique, not only for probabilistic substructures in general, but in particular to the analysis of mistuned bladed disks. One of the biggest drawbacks to most of the studies is that they concentrated on very simple systems. The SSME turbine blade, for instance, is a doubly curved, hollow structure with 25 modes in the excitation range; a typical finite element model, shown in figure 29, contains over 30,000 dof's. Representing this structure with an sdof spring-mass system clearly is inadequate for most analyses. For this reason, while the analytical, closed-form solutions as developed by Sinha and Mignolet are important for understanding some of the physical phenomena of the problem, they are impractical for realistic analysis. At this point in time, practical analysis is vitally needed by industry. Rocketdyne, the manufacturer of the standard set of turbopumps for the SSME, performed a quick analysis of their second stage liquid oxygen pump and showed that considerable amplification did exist for a system model as compared with a single blade approach.⁷² They reported in 1989 that they and other bladed-disk manufacturers are not using any kind of mistuning in their production analysis because the research in the field has been too unrealistic. In addition to this practical need, the analysis of realistic structures is important to capture the true characteristics of the mistuning phenomena, which can be lost using simplified models.

The work performed recently by Pierre, Griffin, and their co-workers does attempt to move towards realistic analysis methods. However, because of their reliance on the perturbation method, which is only practical for blades represented by sdof structures where the partial differential of the

elements of the system matrix $[A]$ with respect to each rv can be represented by closed-form equations (as discussed in section 3.5), these investigators have not taken advantage of the tremendous advances made in probabilistic analysis using reliability methods. They therefore still model the variations in the blades by a single rv , which is clearly overly restrictive. Sinha briefly referenced the FORM in the mid-1980's, but quickly dismissed it and has not examined it since. Hamade and Nickolaidis used the method for localization, but have not done any work since then, extending it to bladed disks; and Chamis touched on the subject, but has not performed any additional work.

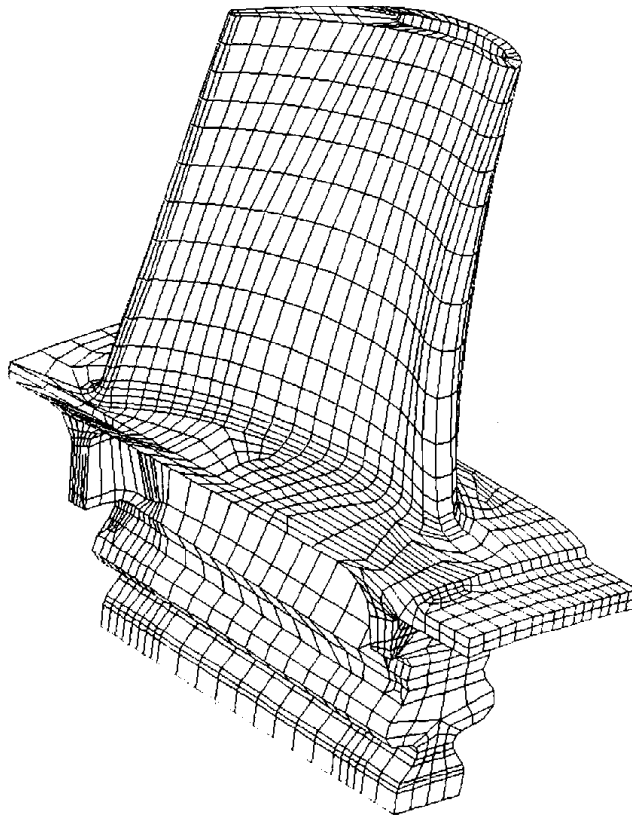


Figure 29. Finite element model of SSME turbine blade.

The PDS method has a number of advantages over the methods discussed in the preceding survey. First, realistic finite element models can be used for two reasons: the size of the model can be reduced tremendously using component mode synthesis, and each blade on the disk, which can number up to a 100, does not have to be modeled separately since the statistical characteristics of each blade are identical. A second advantage is that assigning the dynamic characteristics of the structures to be the rv 's makes no assumptions regarding the origin of the random characteristics of the blades; all of the preceding research assumes all of the randomness is in the natural frequency or elastic modulus of the blade, and completely ignores variability in the mass, geometry, etc. which may only show up in the mode shapes or residual flexibility. Using a realistic model also allows actual values of mistuning and coupling to be inherent in the system model rather than having to specify a "mistuning" or "coupling" parameter. Finally, applying the approximate reliability techniques to obtain the response statistical density functions is an order of magnitude faster than MC, which is imperative for the completion of parametric studies necessary for understanding these types of complex systems.

6.3 Application of PDS for Nine-Bladed Disk

6.3.1 Model Definition, Baseline Analysis

The application of PDS on a realistic nine-bladed-disk system, shown in figure 30, can now be attempted. A great deal of parametric investigation is necessary for a complete mistuning analysis; the goal here is to obtain some basic results that illustrate the applicability of PDS to the problem, thereby laying the groundwork and methodology for future studies of realistic systems. The disk and blade “A” of the model are identical to the system described in chapter 5, and the other eight blades possess identical yet independent statistical parameters to blade “A.” Therefore, the construction of only one blade model is required and rotation transformations can be applied to this model to create the bladed-disk system model. Compared to some other methods of modeling mistuned bladed disks in which each slightly different blade is modeled separately, these rotations are a tremendous savings in effort and computer time since the substructure has already been reduced using CMS.

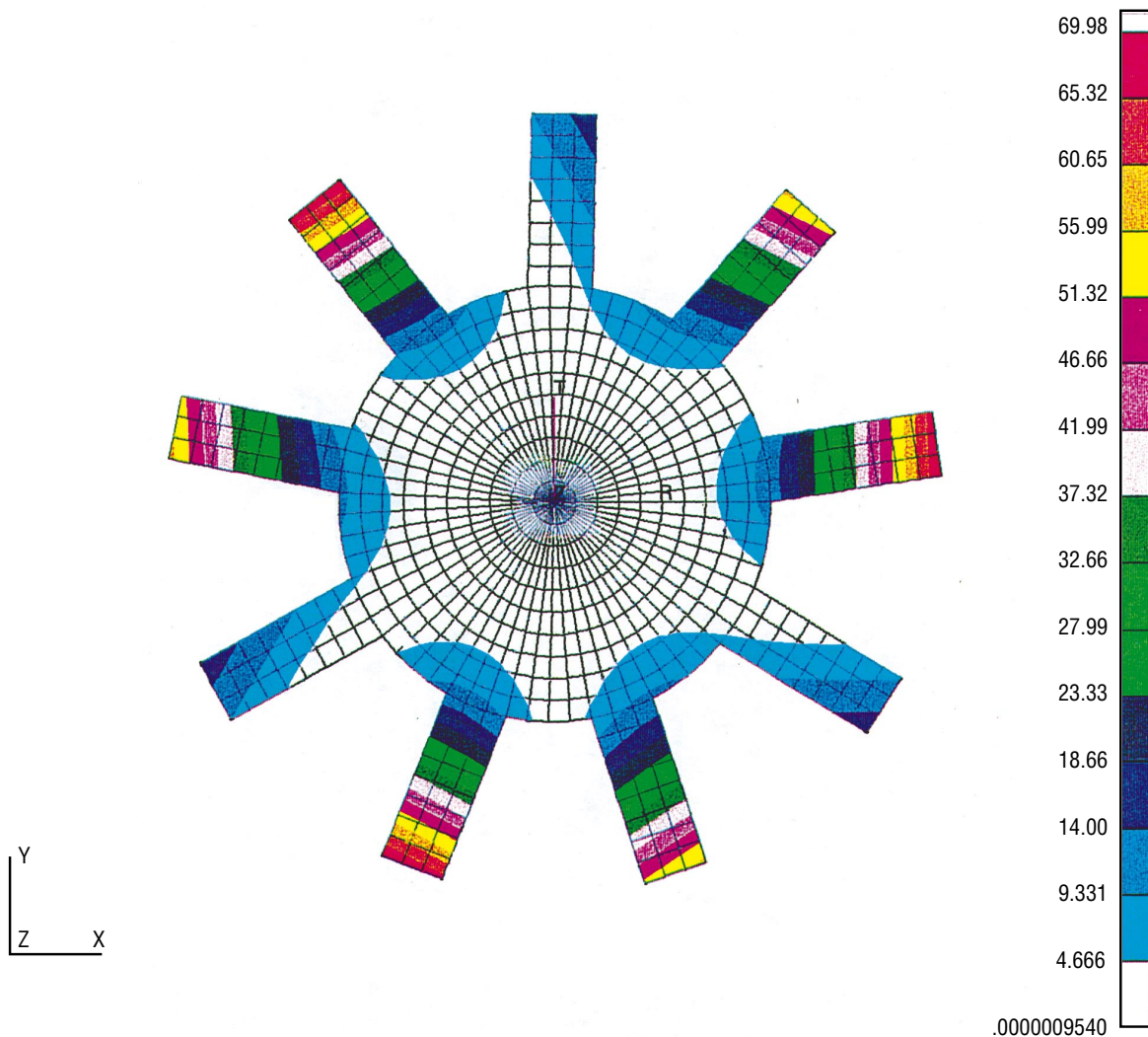


Figure 30. Nine-bladed disk, mode 6 at 444.6 Hz (using CMS).

The first step in the analysis is to produce baseline results for comparison. This was accomplished using the same free- and forced-response procedures as described in chapter 5. Based upon the close agreement in CDF's between the 400- and 1,000-sample cases for the two-bladed-disk system, 400 samples were used for this larger system to save computer time. The assumption that this number of samples is sufficient may not be valid and could be a source of error. As discussed in the previous chapter, this will be the first publication of an MC analysis of a realistic bladed-disk system modeled to this degree of detail in both modeling representation and level of stochasticity.

Following the PDS procedure, an MC simulation using NESSUS/ NASTRAN to obtain the statistics of the first blade was then performed. The mean and standard deviation of the resulting distributions for the dynamic rv's and the correlation matrix were then used to create independent "load cases" used for creating the substructure stiffness matrices for coupling with the system. Only those uncorrelated rv's whose correlation matrix eigenvalues were greater than 3 percent of the sum of the all values were actually used as dynamic rv's in NESSUS, as previously discussed. This approach was taken to eliminate eigenvalues which did not contribute to the total randomness in the system, as represented by the sum. Rather than creating an enormous load case matrix [u] containing independent variations of each rv for each blade, a matrix [u] for the first blade only was created and reused for all the blades. This was accomplished by coupling each variation case for blade $i=1,...,9$ with the mean value case (a column of all zeroes) for all the other blades. A rigid body transformation matrix

$$R = \begin{bmatrix} \cos \theta_z & \sin \theta_z & 0 \\ -\sin \theta_z & \cos \theta_z & 0 \\ 0 & 0 & 1 \end{bmatrix} \quad (138)$$

was created, where θ_z is the angle about the z axis of the original blade from the transformed blade. In degrees, the blade angles are:

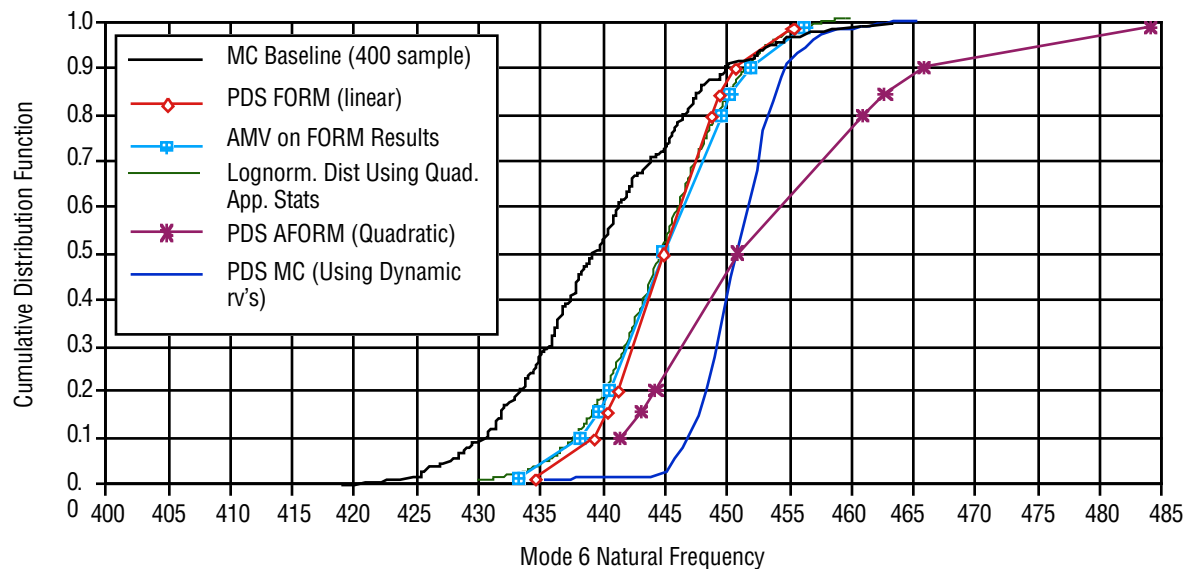
$$\theta_z = 0, -40, -80, -120, -160, -200, -240, -280, -320 \text{ .} \quad (139)$$

These rotation angles were then used on each node in the eigenvectors and the residual flexibility matrix by placing [R] into partitions along a diagonal band in a global transformation matrix. The eigenvalues are the same for each blade, and the correlation matrix is the same also because only the z translational displacement elements of the above matrices are used as dynamic rv's, and the rotation about the z axis will not affect these rv's. The substructure matrices resulting from applying the RF CMS method using this information was then coupled into the system using a map identifying the location in the system matrices of the boundary dof's, the dof's whose displacements were chosen to be recovered, and the generalized dof's.

6.3.2 Free-Response Analysis

An analysis to obtain the CDF of mode 6 (see fig. 30) was performed on this nine-bladed disk. This mode was chosen because it was used as the excitation mode for the frequency response analysis performed subsequently. Both PDS MC and PDS reliability methods were applied. As described in the

last chapter, the medians of the dynamic rv's were substituted for the means in the variable transformations. The results are shown in figure 31, with the figure indicating the degree to which the CDF curves match the baseline and the table quantitatively expressing the error using the various measures described in chapter 5. In general, the AMV update of the linear FORM method yielded the best results, with a skew at the mean of only 1.2 percent, and errors at the CDF values of interest for design (0.01 and 0.99) of 2.5 and 0.6 percent, respectively. The shape of the CDF does show some error as indicated visually and by the standard deviation error of 48 percent; this average standard deviation value for comparative purposes was calculated by taking the difference in the response values at $\pm 1\sigma$ (0.8414 and 0.1586) and dividing by 2. The PDS MC results actually show worse results in both the shape of the CDF and in the error measurements. This result was unexpected since, as described in the previous chapter, there are fewer sources of error in the MC methodology than the PDS reliability methodology. For both the free- and forced-response analyses, it should be noted that statistical outliers (values beyond $\pm 4\sigma$) generated in the PDS MC analyses were deleted from the sample to not falsely exaggerate the standard deviation. The AFORM method yields the worst results. A possible reason for these results is discussed in the next section. However, the approximate statistics generated by the partial quadratic formulation of the limit state in the AFORM solution was used to create a CDF by assuming a lognormal distribution. This CDF actually matches the AMV results almost exactly. These results are consistent with a conclusion that the function is nonlinear without having a large coefficient of variation.



Parameter	MC Baseline	PDS FORM	% Error	AMV/ FORM	% Error	PDS Quad Approx.	% Error	AFORM	% Error	PDS MC	% Error
Mean	439.65	444.87	1.17	444.87	1.17	460.650	4.78			451.21524	2.56
Median	439.58	444.87	1.19	444.87	1.19	444.86	1.20	450.86	2.50	450.7	2.47
Std. Dev	7.89	4.457	-77.04	5.333	-47.96	5.596	-29.08	9.829	19.72	3.31281996	-138.19
1% CDF Value	422.20	434.49	2.83	433.23	2.55	432.45	2.43			437.8	3.56
99% CDF Value	459.00	455.24	-0.83	456.29	-0.59	457.6	-0.31	484.11	5.19	461.4	0.52

Figure 31. Nine-bladed disk, mode 6 PDS evaluation.

Examining the run times shows the MC baseline using 400 samples took 1,527 sec of CPU time and 23.2 hr wallclock, the PDS MC using 500 samples took 3,867 CPU-sec and 4.8 hr wallclock, and the PDS FORM took 778 CPU sec, 2,849 sec (0.79 hr) wallclock, and < 30 sec for the NESSUS/FPI run. As expected, the PDS methods result in a tremendous savings in overall computer time.

There are several interesting points to note in the results of the free-response analysis that could explain some of the errors. As with the two-bladed-disk system, a deterministic NASTRAN analysis of the system was run using the means of the primitive rv's as well as a deterministic RF CMS analysis using the medians of the dynamic rv's. The NASTRAN deterministic analysis yielded values of 445.6 Hz for both modes 6 and 7, and examination of the mode shapes verified that their only difference is a rotation about the center of the disk. However, the median of the MC baseline run for mode 6 was 439.6 Hz, a decrease of 6 Hz. For a tuned system, the NASTRAN deterministic result would be almost identical to the MC median value (for enough samples), but because of the mistuning, the double mode at 445.6 hz bifurcates into a low mode (number 6) and a high mode (number 7), and since the lower mode is being sampled, the CDF will be skewed lower. The RF CMS deterministic analysis using the dynamic rv's, on the other hand, results in mode 6 at 444.87 Hz and mode 7 at 451.2 Hz. Apparently, some aspect of the reductions in the RF CMS methodology, which would be expected to stiffen the system, actually slightly mistuned the system, causing the double mode to split for this median case. The median (CDF = 0.5) value for the FORM analysis is also defined to be this value, so the skew between the FORM CDF and the NASTRAN MC baseline CDF at the median can be explained by the reduction of the baseline due to the bifurcation. The increase in the median value for the PDS MC results compared to the RF CMS deterministic value, on the other hand, cannot be explained using this reasoning and is not understood at this time.

6.3.3 Forced-Response Analysis

A frequency-response solution for the maximum responding blade tip dof in response to an excitation wave in the three nodal diameter shape of mode 6 and 7 at a deterministic mode 6 frequency of 444.6 Hz was then run using the synthesized systems. This solution yields a more general evaluation of the PDS technique than the analysis of mode 6 only because, as described in chapter 5, a modal superposition method is used so the effect of the variation in all the modes is included, although the most important ones are modes 6 and 7. A 2-percent modal damping value was used in the analysis. After several iterations, a frequency band of 50 Hz was determined to be required for the accurate determination of the peak response since the mistuned system can resonate at both modes 6 and 7, which are split by the mistuning. The maximum value of the response was obtained by sorting through the responses of all the blade tips at all analyzed frequencies. For every "load case," the dof and frequency of the maximum response was output. As expected, this spatial and spectral location varies significantly, both due to the variation in the mode 6 and 7 frequencies and the mistuning localization effects.

The reliability methods applied for the free-response analysis were applied in this case as well. In addition, the AMV+ method, which is a further update method in which the limit state is expanded about each most probable point, was used. However, none of the higher order methods achieved reasonable results, and so are not included in the summary chart, which is shown in figure 32. Note that there is good agreement between the shape of the MC baseline and MC PDS results, although the median values differ by about 5 percent. The fact that the curve for the PDS MC is shifted to lower levels of response can partially be explained by the stiffening that accompanied the RF CMS model reduction, which was also

seen by the higher frequencies of modes 6 and 7 in the previous section. The relatively good agreement in median values predicted by the PDS MC and PDS FORM methods is also reassuring since both utilize the same reduced models. The response levels at a CDF value of 0.99, which is of significant importance in the design process, show that the FORM has an error of 6.25 percent and the PDS MC an error of 14.13 percent. Examining the run times shows the MC baseline using 400 samples took 780 sec of CPU time and 23.0 hr wallclock, the PDS MC using 500 samples took 14,627 CPU sec and 4.16 hr wallclock (the wallclock time for this run was unusually close to the CPU time because it took place over a period of very low computer usage), and the PDS FORM took 3,088 CPU sec, 2.19 wallclock hr, and < 30 sec for the NESSUS/FPI run. These results indicate that the PDS methodologies can provide the designer with a legitimate tool for generating previously unobtainable maximum response values for a mistuned bladed disk in a reasonable amount of time.

To determine whether the mistuned system analyzed actually does display amplification effects as described in the bladed-disk literature, an analysis of a tuned system was also performed. To obtain a true “apples-to-apples” comparison, this analysis must also be probabilistic, but the values of the rv’s within each blade must be identical to those values in the other blades for the disk to be tuned. An MC baseline run was therefore performed on a full-up model with only three independent rv’s for the whole system, which are the same rv’s as for the mistuned system but set to be the same for all the blades. As alluded to previously, the deterministic response of the system using the median values of all the input rv’s would be for a tuned, (not mistuned) system; a median mistuned system is difficult to quantify other than with a probabilistic analysis. Figure 33 compares the tuned and mistuned MC CDF plots. Also shown is the response amplitude for the deterministic case (small circle). This plot clearly shows an amplification of the response, indicating that the model successfully represents a mistuned system.

6.3.4 Discussion of Error and Conclusions

A possible reason for the problems with the approximate high order methods for both the free- and forced-response solutions is the extreme nonlinearity of the response away from the mean value. This nonlinearity is determined by isolating the response as a function of the two independent rv’s that NESSUS indicated were the most important to the response under its “sensitivity” column, which is part of its standard output. The response to these two variables, which turned out to be numbers 23 and 89 out of 99 total independent rv’s for the system (the first rv’s for the third and ninth blade), was calculated for a range of -2 times the standard deviation to $+2$. Plots of the value of the mode 6 natural frequency and of the maximum blade response versus these variables is shown in figure 34. The maximum blade response is jagged, which may be due to its possible discontinuities as a function of the input rv’s, as discussed in chapter 5. It is apparent that the function cannot be approximated by a quadratic; a linear approximation about the mean may actually be a better fit of the response surface. For the mode 6 frequency response, the minimum inflection point appears to be somewhat less than the mean, so a quadratic approximation about the mean would also not be very accurate. It must be remembered that the independent rv’s are not tied to a specific primitive rv; therefore, it should not be surprising that the curve is nonmonotonic. It may be noted that expanding the limit state about a value equal to -0.3 times the standard deviation might give good results for a quadratic approximation technique. It is recommended that studies along this line be pursued in future research.

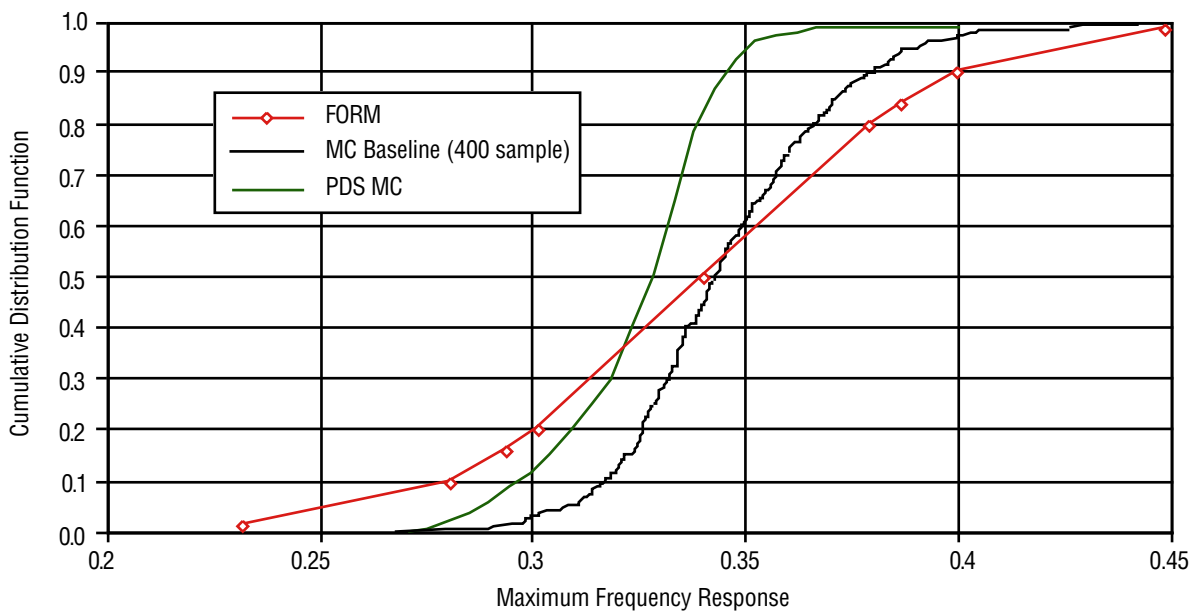


Figure 32. Maximum frequency response using PDS and MC.

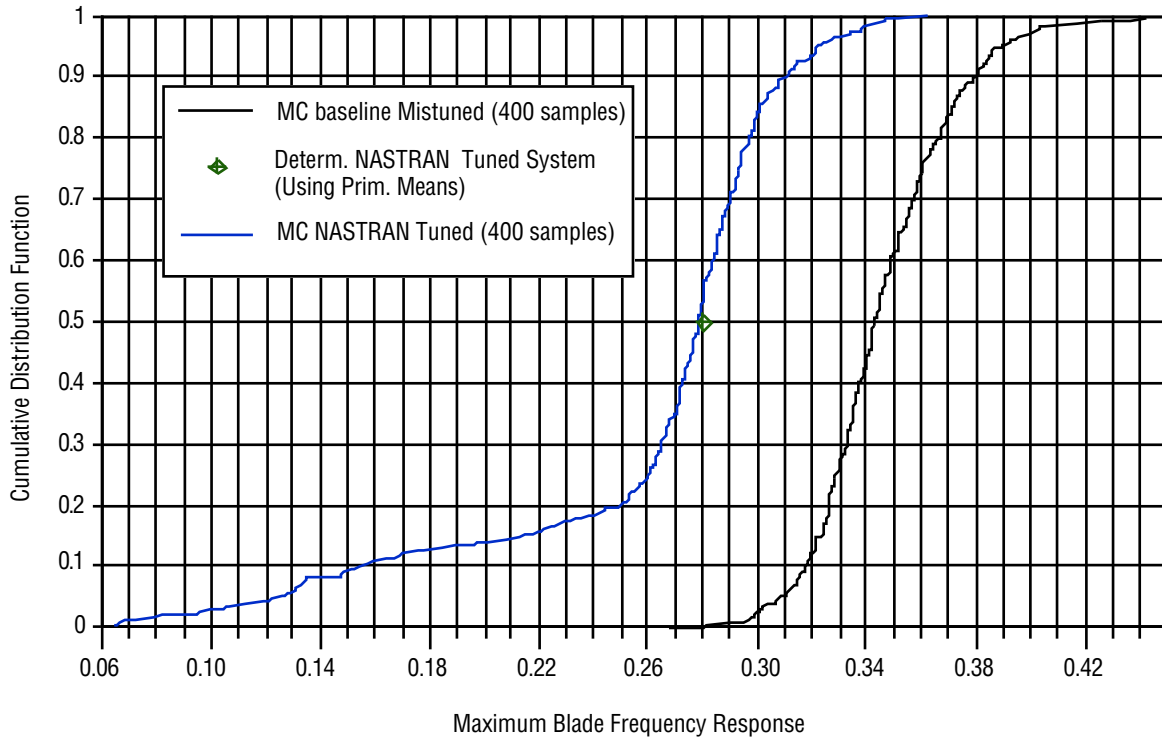


Figure 33. Frequency response of maximum blade to 3ND input for 50 Hz frequency range at mode 6 of median system; comparison of tuned system variation versus mistuned system.

Because of the unusual phenomena of closely spaced natural frequencies, localization, and amplification, it was not known if a reasonable result using the PDS methodology would be possible for the analysis of a mistuned bladed disk. The results shown in this chapter do show significant discrepancies with MC baseline runs, but they are promising enough to be a valuable tool for analyzing realistic bladed disks in new engine designs. This is especially true if one considers the accuracy, availability, and computational intensity of other analysis techniques. Further refinement of the method may be necessary to use it for exploration of the whole range of mistuning issues.

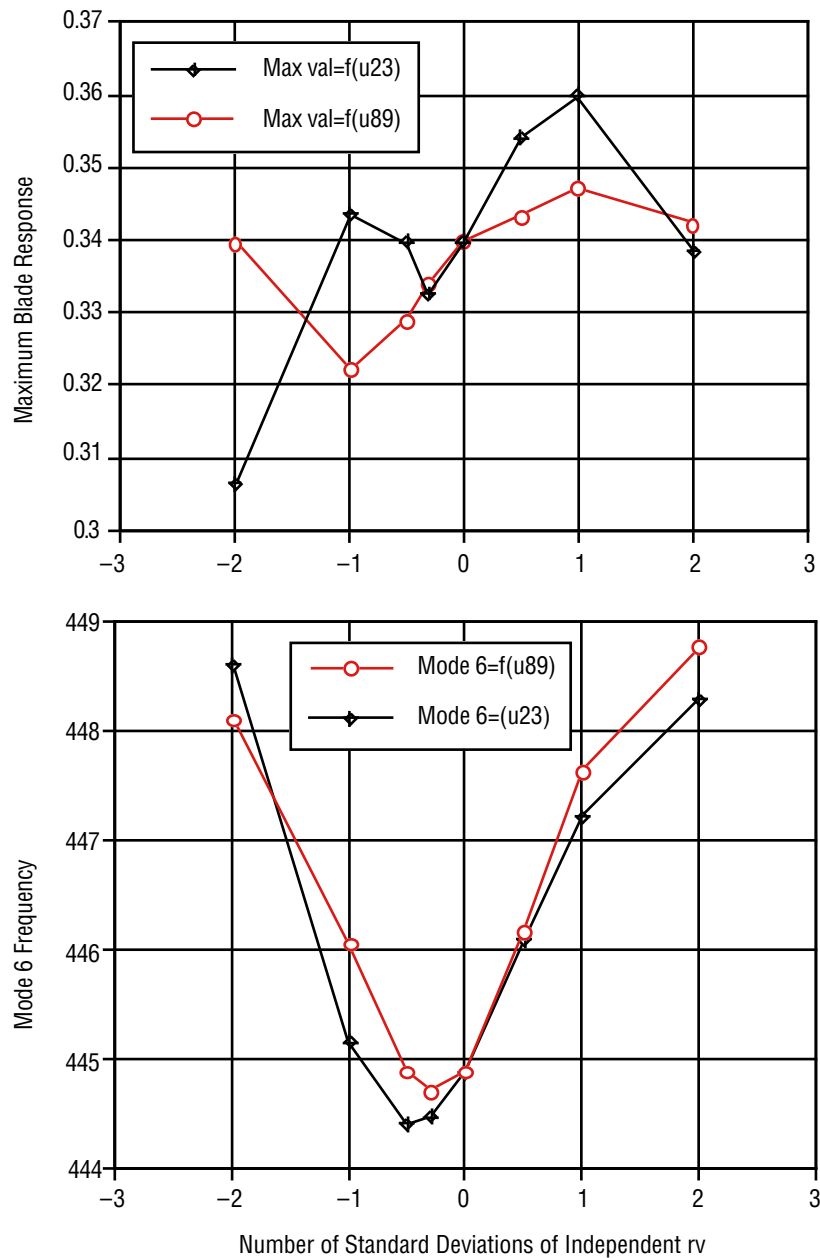


Figure 34. Nonlinear dependence of mode 6 and maximum response as a function of independent rv's 23 and 89.

7. CONCLUSIONS AND FUTURE RESEARCH

7.1 Conclusions

A methodology has been developed in this thesis to perform probabilistic analysis of structural systems composed of substructures whose dynamic characteristics can be characterized statistically. This method, entitled probabilistic dynamic synthesis, has been created using new developments in probabilistic analysis and the residual flexibility method of component mode synthesis. It enables the use of realistic, comprehensive statistics obtained from modal testing of substructures rather than much less complete statistics for primitive rv's such as geometry variation. These statistics can be applied either using the well-tested but computationally intensive method of MC simulation, or by using new reliability methods, which can significantly reduce the computational effort. Additionally, the use of component mode synthesis to couple these substructures provides for a considerable savings of computer resources through a reduction in the size of the analytical model of the structural system.

The development of this methodology initially required the examination of the many methods available for component mode synthesis. Investigations into the final makeup of the system matrices resulted in the conclusion that the residual flexibility method was the only one that solely required information that could be obtained from test. This allowed the complete statistical variability of the substructure population to be accounted for in the subsequent analysis.

An evolution of the major developments in probabilistic methods was then presented to identify and understand how best to apply these methods. The approximate "reliability" methods were found to be able to incorporate realistic structural analysis techniques such as the finite element method, and can provide accurate CDF's using an order of magnitude less calculations than MC simulations. Methods using both first order and partial second order approximations of the limit state function were found to be applicable to the PDS method. In addition, a detailed comparison was made between the perturbation method, which is an analytical method used frequently in the study of periodic disordered systems, and the reliability methods. Essentially, the perturbation method was found to be equivalent to the FORM but much less applicable to realistically sized systems.

A simple benchmark test problem consisting of two probabilistic substructures was then analyzed. Many of the details involved in applying the PDS method to a structure were developed using this test problem, and a variety of reliability methods were applied to obtain statistics of the system fundamental frequency. A procedure was developed that used MC numerical analysis to simulate the modal testing that would actually be used in PDS to determine the statistics of the substructure eigenvalues, eigenvectors, and residual flexibility matrix elements. These statistics were then used for the generation of "load" cases for a derived set of independent, uncorrelated rv's that were used to obtain the desired response variable in terms of variation of each of the independent rv's. These "datasets" defining the response surface were then input into a newly available probabilistic code NESSUS which uses reliability methods to determine the CDF of the response variable. For this simple case, a linear approximation

of the limit state using the first order reliability method provided results that matched well with a comparison to an MC simulation of the full, unstructured system. For larger coefficients of variation (10–15 percent), the partial higher order advanced first order reliability method resulted in better answers. The advanced mean value method was also applied, and it was found that this method is better suited to problems where the limit state itself is more nonlinear.

The PDS method was then applied to a realistic finite element model of a three-substructure system. The baseline structure was modeled with a sufficient number of independent primitive rv's to accurately represent the random variation in realistic structures, which had not been done by other researchers. A great many practical issues necessary for actual use of the method were discovered and resolved, including developing the ability to perform an accurate baseline MC analysis of a realistic structural system, reducing the number of independent rv's by examining the relative size of the eigenvalues of the correlation matrix, and using the medians, rather than the means, of the samples of the dynamic rv set for the transformation to the independent rv set. These dynamic rv's were applied using both the MC method and the linear and higher order reliability methods. The accuracy of the results was sufficient for design purposes and showed a tremendous savings in computer time, but there were discrepancies in the CDF's that should be investigated further.

In addition to the solution for a selected eigenvalue, the statistics of the forced, frequency-response solution for the system were obtained. This required the derivation of a methodology for applying phased excitation in the frequency domain and implementation to the residual flexibility method of CMS. The errors for the PDS methods were larger than the free-response case, and there were substantial differences in the shapes of the CDF's from the baseline case. From a design viewpoint, however, the errors were within the acceptable range. Considering the lack of alternatives for probabilistic forced-response analysis and the tremendous savings in computer time, the PDS method was concluded to be an important new tool for analyzing these types of systems.

The PDS method is particularly suited for the mistuned blade-disk problem because of the random nature of the substructure blades, so it was then applied to this problem. An extensive literature survey was performed that clearly identified the advantages of the method over other techniques used, such as the perturbation method. The motivation for analyzing realistic disks, both because of the practical nature of the problem and to gain a better insight into mistuning, was also presented. A disk with nine statistically identical but independent blades was modeled, and the previously developed procedure applied to obtain the free- and forced-response solution. Although a high degree of nonlinearity was associated with the problem because of the mistuning phenomena, answers similar to those obtained for the simpler three-substructure system were obtained for this larger bladed disk .

In conclusion, the PDS method was shown to be an important new method for the determination of the statistical response of nondeterministic structures. Acceptable results for a variety of structures have been shown, and the details of the procedure have been examined. In particular, application of PDS to the mistuning problem should prove extremely beneficial for both an increased understanding of the phenomena and for actual design of bladed disks by industry.

7.2 Directions for Future Research and Application

A great many avenues of research lie ahead for the application of this research and for its continued development. To help serve as a roadmap for this research, table 7 is presented to clarify the methodologies examined and developed in this thesis, and to compare their benefits and limitations. This table also can be used to identify the options available to an engineer when designing a bladed disk or other structure with a significant probabilistic component.

Several of the techniques developed in this thesis are of immediate benefit for the analysis of general probabilistic structures and bladed disks in particular. An immediate application of these methods will be for the bladed disk presently being developed by NASA/MSFC for the turbopump of the new X-33 reusable launch vehicle. This information will be extremely important for design of the blades, which have been assumed to be tuned until now, as is standard practice in industry, with various safety factors applied to account for large responses. The use of the techniques and computer codes developed in this thesis can quantify the statistical distribution of the actual response values, providing much more accurate information for engineering design and analysis.

While the PDS method is being applied to the above engineering problem, several options should be explored to increase its accuracy. One major source of improvement to the PDS reliability methods may be obtained by more direct integration of the FORTRAN codes written for this development with the automated features of the NESSUS code. This may eliminate some programming error and would allow use of more advanced reliability techniques, such as the AMV+ method, convolution method, Latin Hypercube sampling, and the FFT method.⁷³ Other improvements may be possible by reducing the other sources of error discussed in this thesis, such as using a larger sample size for the MC analysis of the original primitive rv's, expanding the limit state about more suitable points than the mean, and incorporation of more modes in the reduced model of the bladed disk to ensure the calculation of double modes. Finally, a significant source of error for the forced response problem can be addressed by examining only an sdof, rather than the maximum responding dof. This should increase the smoothness of the limit state and the accuracy of the reliability methods. A greater understanding of these errors may be obtained by generating the PDF of the results in addition to the CDF. The PDF would highlight the shape of the distribution, which has been shown to be the main discrepancy between the MC baseline and PDS results.

Performing the PDS analysis on an engineering system may require some variation of the techniques developed in this dissertation to account for the unavailability of the data. Since residual flexibility measurements may be difficult to obtain in certain circumstances, a hybrid test/analytical PDS methodology could be developed which uses the analytical value of the residual flexibility and measured eigenvalues and eigenvectors. As mentioned in chapter 2, the measurements of these quantities themselves are not without error. Present testing methods actually require a statistical sampling of a single structure to generate an output value. The fact that the PDS method requires many samples, however, may actually mitigate this error because it uses the statistics of the measurements directly in the problem formulation, unlike a deterministic problem. An evaluation of the robustness of the statistics taken for PDS is an important subject for future research.

Table 7. Comparison of methods for analysis of structures with probabilistic substructures.

Method, Name, Users, Year	Model Size	Random Variable Description	Modeling Methodology	Probabilistic Methodology	Benefits	Limitations	Questions
"Lumped mass approach;" Sinha, Pierre, etc. 1980–1990	One lumped mass per substructure	One primitive rv/substructure	Closed-form equations	Perturbation—closed-form equations of [A] wrt. rv's	Quick	Inaccurate for real structures since neither 1 dof or 1 rv/ substructure are correct	
"Reduced order methods;" Pierre, Griffin, 1995	Finite element model	One primitive rv/substructure	Reduced order methods—similar to CMS	Monte Carlo	Representative structure	(1) Unrepresentative description of rv's; (2) Slow, CPU-intensive probabilistic calculations	
"Full model Monte Carlo" (MC baseline): in this thesis; previously unpublished	Finite element model	Multiple primitive rv's/substructure	Full model	NESSUS/ NASTRAN Monte Carlo	(1) Representative structure, more representative rv's (2) Accurate CDF for given rv's	(1) Rv's difficult to characterize accurately (2) Slow, CPU intensive	
"Full model—reliability;" immediate future work	Finite element model	Multiple primitive rv's/substructure	Full model	Reliability methods	(1) Representative structure (2) More representative rv's than above (3) Faster than "full-model MC"	(1) Rv's difficult to characterize accurately (2) Faster probabilistic method than "full-model MC"	May be less accurate CDF for given rv's
"PDS—Monte Carlo;" in thesis	Finite element model	Complete set of dynamic rv's from test/substructure	Residual flexibility CMS	Monte Carlo (FORTRAN)	(1) Representative structure, most representative rv's (2) Accurate CDF for given rv's (3) Faster than "full-model MC" (more efficient modeling)	Slow, CPU-intensive probabilistic calculations	Results not as accurate as anticipated
"PDS—Reliability;" in this thesis	Finite element model	Complete set of dynamic rv's per substructure	Residual flexibility CMS	Reliability methods	(1) Representative structure, most representative rv's (2) Most efficient model representation and probabilistic methodology for speed	Less accurate CDF than "full model—Monte Carlo" for given rv's	Further improvements in accuracy req'd before use in general bladed-disk studies
"CMS only—reliability;" future work	Finite element model	Multiple primitive rv's/substructure	Craig-Bampton component mode synthesis	NESSUS/ NASTRAN reliability methods	(1) Representative structure, fairly representative rv's (2) Most efficient model representation and probabilistic methodology for speed	Rv's difficult to characterize accurately	

Another assumption requiring future investigation is accurate representation of the boundary connections. In a traditional bladed disk, the blades are inserted into slots in the disk and then held in place by a combination of centrifugal force and axial stops. In this case, the interface of the blade with the disk is difficult to model accurately. A study using the boundary connection as an independent, analytical rv may prove important for representing these structures. This problem is not as important for blisks, in which the blades are integrally machined with the disk. In these cases, the free-free modes would have to be obtained by either cutting the blades from the disk or by clamping the disk tightly and using the techniques developed by Han, Chen, and others for converting cantilevered modal test results to free-free results.

A similar extension of the PDS method might be in the determination of the statistics of the global damping value of a structural system as a function of the damping values of the substructures. Modal damping ratios are generally measured during modal testing, so statistics could be compiled and the ratio used as a dynamic rv. These values could be used directly in the substructure forced response equations. Estimates of the global damping value for a particular mode could be obtained from the measured frequency response functions using, for example, the half-power method. This global value could then be used as the desired output variable of interest and a CDF obtained.

In addition to the actual application of the PDS method to an engineering problem, it would be illustrative to quantify the gain in accuracy in PDS enabled by the use of the dynamic rv's. These rv's allow a very general degree of randomness in the structure compared to other methods that can only use a single rv per substructure, like Young's Modulus. This could be accomplished by comparing the results of the MC baseline analysis presented in this thesis with MC results obtained for an identical bladed disk, but with only a single rv represented. The inherent inaccuracy of primitive rv's has not been recognized in the literature, and the use of dynamic rv's to model more representative random structures is one of the major achievements of this research.

Finally, the PDS method can be used to examine the mistuning phenomena in greater detail. To this end, the variety of new tools and techniques developed and tested during this research, as shown in table 7, can be applied. The first of these to be applied would be the "full-model MC," "full-model reliability," and "CMS only—reliability" methods, which use full-up or substructured analyses of purely analytical mistuned bladed disks modeled with primitive rv's and which use either the MC or reliability methodologies to obtain the desired statistical response. These analytical results would be used for parametric studies and then compared with results from using the "PDS MC" and "PDS reliability" methods, which are more applicable for an actual bladed disk. The most recent work by Ottarson and Pierre⁷⁴ has identified several important relationships concerning the amount of amplification as a function of damping, coupling, and mistuning strength, and these results could be verified for the more complex structures now able to be analyzed with these new tools. These results could help conclusively define the effects of mistuning for realistic bladed disks, which will be of great importance to both the industrial and academic communities.

REFERENCES

1. Melchers, R.E.: "Structural Reliability Analysis and Prediction," John Wiley & Sons, New York, p. 90, 1987.
2. Wirshing, P.: "A Seminar and Workshop on Reliability Methods in Mechanical and Structural Design," University of Arizona, Tucson, Arizona, Jan. 20–24, 1992.
3. Wu, Y.T: "FPI Theoretical Manual, NESSUS Reference Manual," Southwest Research Institute, Version 1.0, July 1991.
4. Ottarsson, G.; Castanier, M.; and Pierre, C.: "A Reduced-Order Modeling Technique for Mistuned Bladed Disks," Proceedings of the 35th Structures, Structural Dynamics, and Materials Conference, pp. 2552–2562, 1994.
5. Hurty, W. C.: "Dynamic Analysis of Structural Systems Using Component Modes," AIAA Journal, Vol. 3, No. 4, pp. 678–685, April 1965.
6. Craig, R.; and Bampton, M.: "Coupling of Substructures for Dynamic Analysis," AIAA Journal, Vol. 6, No. 7, pp. 1313–1319, July 1968.
7. MacNeal, R.H.: "Hybrid Method of Component Mode Synthesis," Computers and Structures, Vol. 1, pp. 581–601, 1971.
8. Martinez, D.R.; Carne, T.G.; and Miller, A.K.: "Combined Experimental/Analytical Modeling Using Component Mode Synthesis," Proceeding of the 25th Structures, Structural Dynamics and Materials Conference, pp. 140–152, May 1984.
9. Craig, R.: "Structural Dynamics: An Introduction to Computer Methods," John Wiley & Sons, New York, p. 470, 1981.
10. Craig, R.: "Structural Dynamics: An Introduction to Computer Methods," John Wiley & Sons, New York, p. 476, 1981.
11. Admire, J.R.; Tinker, M.L.; and Ivey, E.W.: "Residual Flexibility Test Method for Verification of Constrained Structural Models," AIAA Journal, Vol. 32, No. 1, pp. 170–175, January 1994.
12. Martinez, D.R.; Carne, T.G.; and Miller, A.K.: "Combined Experimental/Analytical Modeling Using Component Mode Synthesis," Proceeding of the 25th Structures, Structural Dynamics and Materials Conference, p. 143, May 1984.
13. Admire, J.R.; Tinker, M.L.; and Ivey, E.W.: "Residual Flexibility Test Method for Verification of Constrained Structural Models," AIAA Journal, Vol. 32, No. 1, p. 173, January 1994.

14. Han, W.Z.; Chen, S.-H.; and Guo, Y.G.: "Improved Method for Determining Free-Free Modes Using Constrained Test Data," *AIAA Journal*, Vol. 35, No. 2, p. 400–403, year.
15. Sinapius, J.: "Identification of Free and Fixed Interface Normal Modes by Base Excitation," 14th International Modal Analysis Conference, Dearborn, Michigan, p. 23–30, 1996.
16. Bookout, P.: "Statistically Generated Weighted Curve Fit of Residual Functions for Modal Analysis of Structures," NASA Technical Memorandum 108481, February 1995.
17. Hines, W.H.; and Montgomery, D.C.: "Probability and Statistics in Engineering and Management Science," Second Edition, John Wiley & Sons, New York, p. 87, 1980.
18. Hines, W.H.; and Montgomery, D.C.: "Probability and Statistics in Engineering and Management Science," Second Edition, John Wiley & Sons, New York, p. 69, 1980.
19. Siddall, J.N.: "Probabilistic Engineering Design," Marcel Dekker, Inc., New York, p. 181, 1983.
20. Wirshing, P.: "A Seminar and Workshop on Reliability Methods in Mechanical and Structural Design," University of Arizona, Tucson, Arizona, p. 8–26, Jan. 20–24, 1992.
21. Melchers, R.E.: "Structural Reliability: Analysis and Prediction," Ellis Horwood, Ltd, Chichester, p. 94, 1987.
22. Siddall, J.N.: "Probabilistic Engineering Design," Marcel Dekker, Inc., New York, p. 204, 1983.
23. Wirshing, P.H.: "Truncation Errors in First-Order Reliability," *Journal of the Structural Division of the ASCE*, Vol. 101, No. ST11, p. 2482–2486, November 1975.
24. Cornell, C.A.: "A Probability-Based Structural Code," *Journal of the American Concrete Institute*, Vol. 66, No. 12, pp. 974–985, December 1969.
25. Hasofer, A.M.; and Lind, N.C.: "Exact and Invariant Second Moment Code Format," *Journal of the Engineering Mechanics Division, ASCE*, Vol. 100, No. EM1, pp. 111–121, 1974.
26. Wu, Y.T.: "FPI Theoretical Manual, NESSUS Reference Manual," Southwest Research Institute, Version 1.0, p. 11, July 1991.
27. Rackwitz, R.: "Practical Probabilistic Approach to Design," Bulletin No. 112, Comité Européen du Béton, Paris, France, 1976.
28. Rackwitz, R.; and Fiessler, B.: "Structural Reliability Under Combined Random Load Sequences," *Computer and Structures*, Vol. 9, No. 5, pp. 489–494, 1978.
29. Chen, X.; and Lind, N.C.: "Fast Probability Integration by Three-Parameter Normal Tail Approximation," *Structural Safety*, Vol. 1, pp. 269–276, 1983.
30. Rackwitz, R.; Fiessler, B.; and Neumann, H.J.: "Quadratic Limit States in Structural Reliability," *Journal of the Engineering Mechanics Division, ASCE*, Vol. 105, pp. 661–676, August 1979.

31. Wirshing, P.: "A Seminar and Workshop on Reliability Methods in Mechanical and Structural Design," University of Arizona, Tucson, Arizona, p. 924, Jan. 20–24, 1992.
32. Wu, Y.T.: "Demonstration of a New, Fast Probability Integration Method for Reliability Analysis," Journal of Engineering for Industry, ASME, Vol. 109, pp. 24–28, February 1987.
33. Wu, Y.T.: "FPI Theoretical Manual, NESSUS Reference Manual," Southwest Research Institute, Version 1.0, p. 11, p. 21, July 1991.
34. Wirshing, P.: "A Seminar and Workshop on Reliability Methods in Mechanical and Structural Design," University of Arizona, Tucson, Arizona, pp. 4–11, Jan. 20–24, 1992.
35. Wu, Y.-T.; and Wirsching, P.: "New Algorithm for Structural Reliability Estimation," Journal of Engineering Mechanics, ASCE, Vol. 113, No. 9, pp. 1319–1336, September 1987.
36. Mahadevan, S.: "Modern Structural Reliability Methods," unpublished report for NASA/Marshall Space Flight Center, p.77, October 1994.
37. Meirovitch, L.: Computational Methods in Structural Dynamics, Sijthoff & Noordhoff, Alphen aan den Rijn, The Netherlands, p. 102, 1980.
38. Collins, J.D.; and Thompson, W.T.: "The Eigenvalue Problem for Structural Systems with Statistical Properties," AIAA Journal, Vol. 7, No. 4, pp. 642–648, 1968.
39. Kiefling, L.: "Comment on 'The Eigenvalue Problem for Structural Systems with Statistical Properties,'" AIAA Journal, Vol. 8, No. 7, pp. 1371–1372, 1970.
40. Collins, J.D.; Kennedy, B.; and Hart, G.C.: "Prediction of the Uncertainty in Modal Characteristics Based on Uncertainty in Structural Characteristics," NASA Report No. N71–15195, CR 102974, 1970.
41. Hart, G.C.; and Hasselman, T.K.: "Modal Analysis of Random Structural Systems," Journal of the Engineering Mechanics Division, ASCE, pp. 561–579, June 1972.
42. Pierre, C.: "Analysis of Structural Systems with Parameter Uncertainties," Ph.D. Dissertation, Duke University, 1985.
43. Mahadevan, S.: "Modern Structural Reliability Methods," unpublished report for NASA/Marshall Space Flight Center, pp. 62–68, October 1994.
44. Brown, A.M.; and Ferri, A.A.: "Probabilistic Component Mode Synthesis of Nondeterministic Substructures," AIAA Journal, Vol. 34, No. 4, pp. 830–834, year.
45. Mahadevan, S.: "Modern Structural Reliability Methods," unpublished report for NASA/Marshall Space Flight Center, p. 68, October 1994.
46. Admire, J.R.; and McGhee, D.M.: "Fortran Matrix Algorithms," NASA/Marshall Space Flight Center, 1996.

47. Martinez, D.R.; Carne, T.G.; and Miller, A.K.: "Combined Experimental/Analytical Modeling Using Component Mode Synthesis," Proceeding of the 25th Structures, Structural Dynamics and Materials Conference, p. 142, May 1984.
48. Wirshing, P.H.; and Carlson, J.R.: "Model Identification for Engineering Variables," Journal of the Engineering Mechanics Division, ASCE, Vol. 103, No. EM1, pp. 125–138, February 1977.
49. Private Correspondence with S. Mahadevan, Vanderbilt University, September 1996.
50. Mahadevan, S.: "Modern Structural Reliability Methods," unpublished report for NASA/Marshall Space Flight Center, p. 203, October 1994.
51. Millwater, H.: "NESSUS/NASTRAN Interface," Southwest Research Institute Report, SwRI No. 06–7212, NASA Contract No. NAS8–39797, 1996.
52. Craig, R.: "Structural Dynamics: An Introduction to Computer Methods," John Wiley & Sons, New York, p. 483, 1981.
53. Admire, J.R.; Tinker, M.L.; and Ivey, E.W.: "Residual Flexibility Test Method for Verification of Constrained Structural Models," AIAA Journal, Vol. 32, No. 1, p. 174, January 1994.
54. Ginsberg, J.H.; and Pham, H.: "Forced Harmonic Response of a Continuous System Displaying Eigenvalue Veering Phenomena," ASME Journal of Vibration and Acoustics, Vol. 117, pp. 439–444, 1995.
55. Ewins, D.J.: "The Effects of Detuning upon the Forced Vibrations of Bladed Disks," Journal of Sound and Vibration, Vol. 9, No. 1, pp. 65–79, 1969,
56. Leissa, A.: "Vibrational Aspects of Rotating Turbomachinery Blades," Applied Mechanics Reviews, Vol. 34, No. 5, pp. 629–633, May 1981.
57. Ewins, D.J.: "Further Studies of Bladed Disc Vibration: Effects of Packeting," Vibrations in Rotating Machinery, I. Mech. Engineers, pp. 97–102, 1980.
58. MacBain, J.C.: "Maximum Resonant Response of Mistuned Bladed Disks," Vibrations of Bladed-Disk Assemblies, ASME, pp. 153–159, 1983.
59. Afolabi, D.: "A Note on the Rogue Failure of Turbine Blades," Journal of Sound and Vibration Vol. 122, No. 3, pp. 535–545, 1988.
60. Pierre, C.; and Dowell, E.H.: "Localization of Vibrations by Structural Irregularity," Journal of Sound and Vibration, Vol. 114, No. 3, 1987, pp. 549–564.
61. Pierre, C.; and Wei, S.T.: "Localization Phenomena in Mistuned Assemblies with Cyclic Symmetry—Part 1: Free Vibrations," Bladed Disk Assemblies, ASME, pp. 61–79, Sept. 1987.
62. Irretier, H.: "Spectral Analysis of Mistuned Bladed Disk Assemblies by Component Mode Synthesis," Vibrations of Bladed-Disk Assemblies, ASME, p. 115, 1983.

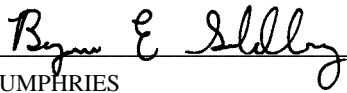
63. Huang, W.: "Vibration of Some Structures with Periodic Random Parameters," AIAA Journal, Vol. 20, No. 7, p. 1001, July 1982.
64. Sinha, A.: "A Higher Order Technique to Compute the Statistics of Forced Response of a Mistuned Bladed Disk Assembly," Journal of Sound & Vibration, No. 130(2), p. 207, 1989.
65. Griffin, J.; and Hoosac, T.M.: "Model Development and Statistical Investigation of Turbine Blade Mistuning," Vibration of Bladed-Disk Assemblies, pp. 105–113, 1983.
66. Pierre, C.; and Wei, S.T.: "A Statistical Analysis of the Effects of Mistuning on Forced Response of Cyclic Assemblies," 30th Structures, Structural Dynamics, and Materials Conference, pp. 1734–1748, 1989.
67. Pierre, C.: "Weak and Strong Vibration Localization in Disordered Structures: A Statistical Investigation," Journal of Sound and Vibration, Vol. 139, No. 1, p. 111–132, 1990.
68. Mignolet, M.P.; and Lin, C.C.: "The Combined Closed Form-Perturbation Approach to the Analysis of Mistuned Bladed Disks," Journal of Turbomachinery, Transactions of ASME, Vol. 115, p. 771–780, October 1993.
69. Pierre, C.; and Kruse, M.: "Forced Response of Mistuned Bladed Disks Using Reduced-Order Modeling," Unpublished Draft of paper presented at 1995 Consortium on Forced Response of Bladed Disks.
70. Ottarsson, G.; and Pierre, C.: "On the Effects of Interblade Coupling on the Statistics of Maximum Forced Response Amplitudes in Mistuned Bladed Disks," 36th Structures, Structural Dynamics, and Materials Conference, pp. 3070–3078, 1995.
71. Yang, M.T.; Griffin, J. H.; and Kiefling, L.: "Mistuned Vibration of Bladed Disk Assemblies: A Reduced Order Approach," Earth to Orbit Conference, Marshall Space Flight Center, pp. 451–455, May 1994.
72. "Rocketdyne Structural Dynamics Manual," Rocketdyne Corporation, Vol. 4, Sec. 2, p. 4.2–1, 4.2–28, 1989.
73. Wu, Y.T: "FPI Theoretical Manual," Southwest Research Institute, pp. 17–41, 1996.
74. Ottarsson, G.; and Pierre, C.: "On the Effects of Interblade Coupling on the Statistics of Maximum Forced Response Amplitudes in Mistuned Bladed Disks," 36th Structures, Structural Dynamics, and Materials Conference, pp. 3070–3078, 1995.

APPROVAL

DEVELOPMENT OF A PROBABILISTIC DYNAMIC SYNTHESIS METHOD FOR THE ANALYSIS OF NONDETERMINISTIC STRUCTURES

A.M. Brown

The information in this report has been reviewed for technical content. Review of any information concerning Department of Defense or nuclear energy activities or programs has been made by the MSFC Security Classification Officer. This report, in its entirety, has been determined to be unclassified.



W.R. HUMPHRIES
DIRECTOR, STRUCTURES AND DYNAMICS LABORATORY

REPORT DOCUMENTATION PAGE			Form Approved OMB No. 0704-0188	
Public reporting burden for this collection of information is estimated to average 1 hour per response, including the time for reviewing instructions, searching existing data sources, gathering and maintaining the data needed, and completing and reviewing the collection of information. Send comments regarding this burden estimate or any other aspect of this collection of information, including suggestions for reducing this burden, to Washington Headquarters Services, Directorate for Information Operation and Reports, 1215 Jefferson Davis Highway, Suite 1204, Arlington, VA 22202-4302, and to the Office of Management and Budget, Paperwork Reduction Project (0704-0188), Washington, DC 20503				
1. AGENCY USE ONLY (Leave Blank)		2. REPORT DATE June 1998		3. REPORT TYPE AND DATES COVERED Technical Memorandum
4. TITLE AND SUBTITLE Development of a Probabilistic Dynamic Synthesis Method for the Analysis of Nondeterministic Structures				5. FUNDING NUMBERS
6. AUTHORS A.M. Brown				
7. PERFORMING ORGANIZATION NAME(S) AND ADDRESS(ES) George C. Marshall Space Flight Center Marshall Space Flight Center, Alabama 35812				8. PERFORMING ORGANIZATION REPORT NUMBER M-874
9. SPONSORING/MONITORING AGENCY NAME(S) AND ADDRESS(ES) National Aeronautics and Space Administration Washington, DC 20546-0001				10. SPONSORING/MONITORING AGENCY REPORT NUMBER NASA/TM-1998-208473
11. SUPPLEMENTARY NOTES Prepared by the Structures and Dynamics Laboratory, Science and Engineering Directorate				
12a. DISTRIBUTION/AVAILABILITY STATEMENT Unclassified-Unlimited Subject Category 39 Nonstandard Distribution			12b. DISTRIBUTION CODE	
13. ABSTRACT (Maximum 200 words) Accounting for variability of structures in analysis has been a topic of considerable research, with one of the primary goals being able to determine quantifiable measures of statistical probability of a desired response variable to replace experience-based "safety factors." Several problems with the satisfactory application of this research to realistic structures, though, include accurate definition of the input random variables, the large size of finite element models, and accurate generation of the Cumulative Distribution Function (CDF) of the response variable. A new method called "probabilistic dynamic synthesis" (PDS) is presented here that addresses these problems. The PDS method uses dynamic characteristics of substructures measured from modal test as input random variables, which accurately account for the entire random character of the substructure, rather than "primitive" random variables representing material or geometric uncertainties. Using the residual flexibility method of component mode synthesis, these dynamic characteristics are used to generate reduced-size sample models of the substructures, which are then used in a Monte Carlo simulation or in the response surface reliability method to obtain the CDF. Both free and forced analyses have been performed, and the results indicate that the method produces usable and more representative solutions for the design of realistic structures with a substantial savings in computer time.				
14. SUBJECT TERMS probabilistic mechanics, structural dynamics, bladed disks, reliability methods			15. NUMBER OF PAGES 114	
			16. PRICE CODE A06	
17. SECURITY CLASSIFICATION OF REPORT Unclassified	18. SECURITY CLASSIFICATION OF THIS PAGE Unclassified	19. SECURITY CLASSIFICATION OF ABSTRACT Unclassified	20. LIMITATION OF ABSTRACT Unlimited	